

# Sheffield Hallam University

*Application of imaging MALDI-MS to the determination of hazardous compounds in skin.*

PRIDEAUX, Brendan.

Available from the Sheffield Hallam University Research Archive (SHURA) at:

<http://shura.shu.ac.uk/20249/>

## A Sheffield Hallam University thesis

This thesis is protected by copyright which belongs to the author.

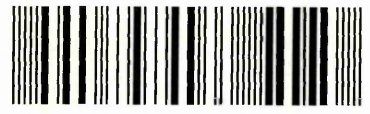
The content must not be changed in any way or sold commercially in any format or medium without the formal permission of the author.

When referring to this work, full bibliographic details including the author, title, awarding institution and date of the thesis must be given.

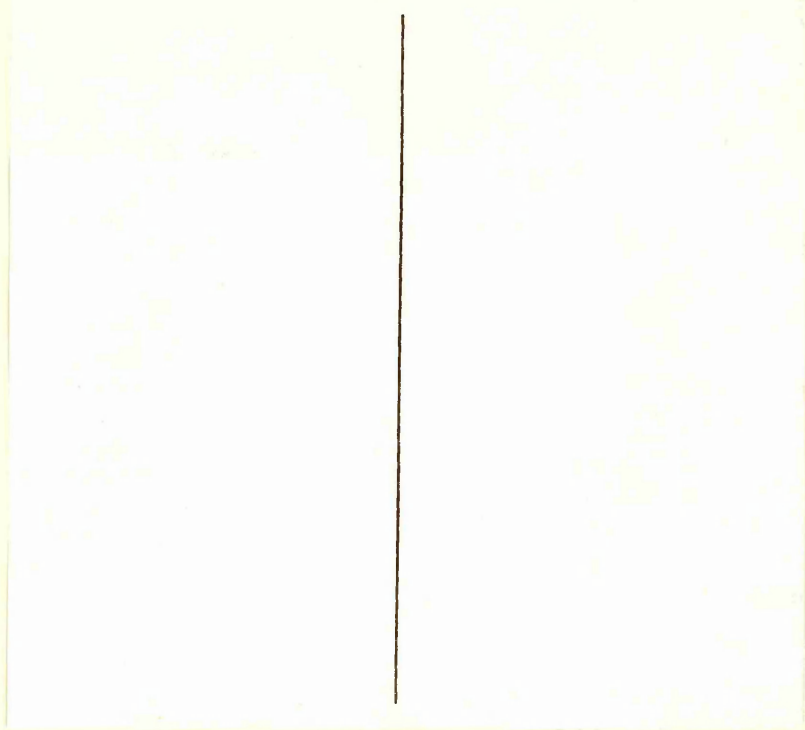
Please visit <http://shura.shu.ac.uk/20249/> and <http://shura.shu.ac.uk/information.html> for further details about copyright and re-use permissions.

Sheffield City Campus  
Sheffield S1 1WB

101 859 893 6



**Return to Learning Centre of issue**  
**Fines are charged at 50p per hour**



**REFERENCE**

ProQuest Number: 10700894

All rights reserved

INFORMATION TO ALL USERS

The quality of this reproduction is dependent upon the quality of the copy submitted.

In the unlikely event that the author did not send a complete manuscript and there are missing pages, these will be noted. Also, if material had to be removed, a note will indicate the deletion.



ProQuest 10700894

Published by ProQuest LLC (2017). Copyright of the Dissertation is held by the Author.

All rights reserved.

This work is protected against unauthorized copying under Title 17, United States Code  
Microform Edition © ProQuest LLC.

ProQuest LLC.  
789 East Eisenhower Parkway  
P.O. Box 1346  
Ann Arbor, MI 48106 – 1346

**Application of Imaging MALDI-MS to the Determination  
of Hazardous Compounds in Skin**

**By**

**Brendan Prideaux**

**A thesis submitted in partial fulfillment of the requirements of Sheffield  
Hallam University for the degree of Doctor of Philosophy**

**April 2007**

**Collaborating Organisation:  
The Health and Safety Laboratory, Buxton, UK**



## **Acknowledgements**

Thanks to Dr Malcolm Clench for help and guidance throughout the project.

Dr Jackie Morton for all her assistance and Kate Jones for helpful chemistry discussions (Health and Safety Laboratory).

Dr Angela Curtis and Dr Gareth S. Evans for cell biology sample preparation, advice and information (Health and Safety Laboratory).

Joan Hague for all her assistance in the lab.

Family and friends for support and coffee.

## **Abstract**

The overall aim of this work described in this thesis was to apply MALDI-MS and imaging MALDI-MS (MALDI-MSI) to the analysis of compounds of interest in occupational hygiene monitoring.

Isocyanates are highly reactive compounds with a wide variety of industrial uses. MALDI-MS and MS/MS were used to investigate diisocyanate stability and reactivity. A monoisocyanate intermediate product was observed from the hydrolysis of both an aromatic and also an aliphatic diisocyanate. The stability of this product was assessed over a 14 day experimental period. Ethanol was used to derivatise hexamethylene diisocyanate (HDI) and the resulting urethane was observed to be stable over 14 days. This derivatisation method was incorporated into a surface swab technique for sampling of HDI from work surfaces.

Industrial diisocyanates have been reported to penetrate through skin and to be excreted as diamine metabolites in urine. A LC-MS method for the determination of free toluene diamine (TDA) monomer formed by biotransformation of toluene diisocyanate (TDI) when applied to HaCaT cells was developed. In the two experiments performed, TDA was only observed at low levels after spiking with high concentrations of TDI. This appeared to be due to most of the isocyanate becoming conjugated to proteins within the cell and thus not being extracted during the extraction procedure.

A novel ethanol-saturated cellulose membrane blotting technique was developed for the extraction and ethanol-derivatisation of HDI from the surface of skin. However, not all of the HDI present on the membrane reacted with the ethanol. Increasing the amount of ethanol on the membrane did increase the amount of derivatised HDI monomer observed although this occurred at the expense of spatial information. The technique was also applied for analysis of the insecticide chlorpyrifos, for both skin surface sampling and permeation studies. From the images obtained, chlorpyrifos was observed to readily penetrate through the stratum corneum and reach a depth of 1.7mm. The highest amount was located in the dermis after the 1 hour exposure time.

The dermal absorption of HDI was monitored after 1 hour exposure by mapping HDI monoamine penetration through the skin via indirect blotting and novel direct skin analysis methods. Similar profiles were observed from both methods. Penetration depths of 2.3 and 2.6 mm were observed for the direct skin and indirect blotting methods respectively. The highest level of HDI monoamine was located in the dermis.

## Contents

<b>1.0 Introduction</b>	<b>1</b>
<b>1.1 Occupational Hygiene</b>	<b>2</b>
1.1.1 Exposure	3
1.1.2 Dermal Exposure	4
1.1.3 Contact Dermatitis	6
1.1.4 Legislation	7
<b>1.2 Dermal Absorption</b>	<b>9</b>
1.2.1 The Structure of Skin	9
1.2.2 Barrier Properties of the Stratum Corneum	12
1.2.3 Dermal Penetration	13
1.2.4 Skin Source and Storage for Dermal Absorption Studies	15
1.2.5 Absorption Compounds of Interest	16
<b>1.3 Dermal Absorption Measurement Techniques</b>	<b>17</b>
1.3.1 Autoradiography	17
1.3.2 Diffusion Cells	19
1.3.3 Tape Stripping	20
<b>1.4 Direct Spectrometric Analysis</b>	<b>22</b>
1.4.1 Attenuated Total Reflectance Fourier Transform Infra Red Spectroscopy (ATR-FTIR)	22

1.4.2	Remittance Spectroscopy	23
1.4.3	Fluorescence Spectroscopy	24
1.4.4	Photothermal Spectroscopy	25
1.5	Mass Spectrometry	25
1.5.1	Introduction to Mass Spectrometry	25
1.5.2	History of Mass Spectrometry	26
1.5.3	Time-of-Flight Mass Spectrometry (TOF-MS)	28
1.5.4	Quadrupole Time-of-Flight	32
1.5.5	Matrix Assisted Laser Desorption Ionisation (MALDI)	34
1.5.5.1	Ion Formation	36
1.5.5.2	Matrix	38
1.5.6	Secondary Ion Mass Spectrometry (SIMS)	39
1.6	Biological Imaging Mass Spectrometry	40
1.6.1	Imaging MALDI-MS (MALDI-MSI)	41
1.6.1.1	Instrumentation	42
1.6.1.1.1	Lasers	42
1.6.1.1.2	Oversampling	43
1.6.1.1.3	MALDI Mass Microscope	44
1.6.1.2	Sample Preparation	45
1.6.1.2.1	Matrix Application Methods	45
1.6.1.2.2	Membrane Blotting	46
1.6.1.2.3	MALDI-MS Analysis of Direct Tissue	48
1.6.1.3	Applications of MALDI MSI	50

1.6.1.3.1 Peptide and Protein Analysis	50
1.6.1.3.2 Analysis of Pharmaceutical Compounds	51
1.6.2 Desorption Electrospray Ionization (DESI) Mass Spectrometric Imaging	52
1.6.3 Laser Ablation ICP Imaging Mass Spectrometry	54
1.6.4 Imaging SIMS and NanoSIMS	55
1.6.5 Statistical Interpretation of MS Imaging Data Sets	57
1.7 Conclusion	57
1.8 References	60
<b>2.0 Applications of MALDI-MS to the Study of Diisocyanate Stability and Introduction of a Novel Ethanol-Derivatization Method for Extraction from Workplace Surfaces</b>	<b>77</b>
2.1 Introduction	78
2.1.1 Introduction to Isocyanates	78
2.1.2 Hexamethylene Diisocyanate and Pre-Polymers	80
2.1.3 Reactivity of Isocyanates	81
2.1.4 Potential for Isocyanate Exposure	83
2.1.5 Occupational Health	84
2.1.6 Monitoring Isocyanate Exposure	85
2.1.6.1 Airborne Isocyanate	85
2.1.6.2 Surface and PPE Sampling	87
2.1.7 Aims	89

2.2 Methods	89
2.2.1 Materials	89
2.2.2 MALDI-MS Analysis of TDI Using Suspension Matrices	90
2.2.3 Analysis of Ethanol-Derivatised HDI (HDI-Urethane)	90
2.2.4 HDI Stability in Acetone	90
2.2.5 Stability of Ethanol-Derivatised HDI	91
2.2.6 Ethanol Swab Method and extraction Efficiency	91
2.2.7 Mass Spectrometric Analysis	92
2.3 Results	92
2.3.1 Analysis of TDI Using Suspension Matrices	92
2.3.2 Tandem MS of Peak at m/z 148	93
2.3.3 Reactivity of HDI with Ethanol	96
2.3.4 Stability of HDI in Acetone	99
2.3.5 Stability of Ethanol-Derivatised HDI	105
2.3.6 Ethanol Swab Method and Extraction Efficiency	109
2.4 Conclusion	111
2.5 References	114
<b>3.0 Application of LC-MS to the Determination of the Biotransformation of TDI to TDA by a Human Keratinocyte (HaCaT) Cell Line</b>	<b>119</b>
3.1 Introduction	120
3.1.1 Introduction to High Performance Liquid Chromatography Mass Spectrometry (LC-MS)	120
3.1.1.1 Partition Phases	120

3.1.1.2 Columns	122
3.1.1.3 Elution Methods	124
3.1.2 Mass Spectrometry	125
3.1.2.1 Electrospray Ionization(ESI)	125
3.1.3 Metabolism of Diisocyanates	127
3.1.3.1 Application of Mass Spectrometry for Diisocyanate Metabolite Monitoring	129
3.1.4 Dermal Diisocyanate Exposure and Immune Response	130
3.1.5 Aim	131
3.2 Methods	132
3.2.1 Materials	132
3.2.2 Preparation of Cells	132
3.2.3 Preparation of Standards	133
3.2.4 Preparation of Samples	133
3.2.5 Improved TDI Extraction Method: Preparation of Standards	
3.2.6 Preparation of Samples	134
3.2.7 LC-MS Analysis	136
3.3 Results	137
3.3.1 Extraction of TDA from TDI-Spiked HaCaT Cells	137
3.3.1.1 Construction of Calibration Curves	137
3.3.1.2 Analysis of TDI-Spiked HaCaT Cells	138
3.3.2 Extraction of TDA from TDI Spiked HaCaT Cells Incorporating a Triple Rinse Extraction Procedure	143

3.4 Conclusion	148
3.5 References	150
<b>4.0 Sample Preparation and Data Interpretation Procedures for the Examination of Xenobiotic Compounds in Skin by Indirect Imaging MALDI-MS</b>	<b>154</b>
4.1 Introduction	155
4.1.1 Introduction to Chlorpyrifos	155
4.1.2 Exposure	156
4.1.3 Toxicity of Chlorpyrifos	157
4.1.4 Methods of Measuring Chlorpyrifos Exposure	158
4.1.5 Introduction to Isocyanates	159
4.1.5.1 Isocyanate Reactivity	159
4.1.6 Aims	160
4.2 Methods	160
4.2.1 Materials	160
4.2.2 Analysis of Chlorpyrifos on Porcine Epidermal Surface	160
4.2.3 Depth Profiling of Chlorpyrifos Absorption	161
4.2.4 Analysis of HDI-2MP on Porcine Epidermal Surface	161
4.2.5 On-Membrane Ethanol-Derivatisation of HDI	162
4.2.6 Mass Spectrometric Analysis	163
4.3 Results	163
4.3.1 MALDI-MS Spot Analysis of Chlorpyrifos Standard and	

Dursban 4	164
4.3.2 Profiling Chlorpyrifos Absorption on Skin Surface	165
4.3.3 Profiling Chlorpyrifos Absorption into Skin	169
4.3.4 Analysis of HDI-2MP on Porcine Epidermal Surface	173
4.3.5 On-Membrane Ethanol-Derivatisation of HDI	176
4.4 Conclusion	180
4.5 References	182
<b>5.0 Indirect Blotting and Direct Skin Analysis by Imaging MALDI-MS to Determine the Dermal Absorption of Hexamethylene Diisocyanate</b>	<b>185</b>
5.1 Introduction	186
5.1.1 Introduction to HDI	186
5.1.2 HDI Exposure	186
5.1.3 Dermal Toxicity of HDI	187
5.1.3.1 Irritation	187
5.1.3.2 Sensitization	188
5.1.3.3 Toxicity of HDI Pre-Polymers	190
5.1.4 Aim	191
5.2 Methods	192
5.2.1 Materials	192
5.2.2 Indirect Blotting Approach	192
5.2.3 Direct Tissue Analysis	193
5.2.4 Mass Spectrometric Analysis	193

5.3 Results	194
5.3.1 Indirect Blotting Approach to Profile the Dermal Absorption of HDI	194
5.3.2 Direct Skin Analysis to Profile the Dermal Absorption of HDI	195
5.3.3 Use of Gold Coating to Enhance Sensitivity of HDI Species from Tissue	203
5.4 Conclusion	207
5.5 References	209
<b>6.0 Conclusion and Future Work</b>	<b>212</b>
6.1 Conclusion and Future Work	213
6.2 References	218
<b>Appendix</b>	
Appendix 1	
Oral Presentations	219
Appendix 2	
Poster Presentations	220
Appendix 3	
Publications	221

## 1.1 Introduction to Occupational Hygiene

Occupational hygiene is concerned with the anticipation, recognition, evaluation and control of hazards and risks to health from activities conducted within the workplace. Such risk parameters include noise, vibration, heat, lighting and substances harmful to health (physical, chemical and biological).

Workers in a range of industries will be exposed to chemicals or reagents which may be described as hazardous or harmful. Exposure is defined as a function of the concentration of the toxin and its duration of interaction with the subject <sup>[1]</sup>. The effects may vary depending upon the nature of the exposure resulting in a chronic or acute effect.

Acute effects can be defined as singular or limited exposure to relatively high concentrations of a toxin such as may occur during spillage. A prolonged or repeated exposure to a hazardous compound may result in chronic toxicity. The severity of health effects observed in an individual will depend on the toxicity of the hazardous compound, the exact nature of the exposure circumstances and the general health of the individual prior to exposure.

Chronic exposure may occur without the individual's awareness and significant damage may have occurred before treatment is sought (sometimes many years

after initial exposure). Conditions associated with exposure to toxic materials include irritation, mutagenesis, carcinogenesis, reproductive constraints and multi organ damage <sup>[2]</sup>.

### **1.1.1 Routes of exposure**

Workers may be exposed to toxic chemicals through three main routes; dermal, respiratory or ingestion. Airborne particles that are swallowed are the most likely source of an ingested chemical. Accidental ingestion may occur with the consumption of food or liquids contaminated by a toxin. Oral ingestion is the least commonly reported route of exposure.

The main occupational exposure routes for hazardous compounds are via the respiratory tract or dermal contact. Substances such as gases, vapours, dusts, volatile solvents and liquids may be encountered during many common industrial processes. The effects exerted upon the body are determined by many factors which may be chemical or physiological including: the concentration of the toxin, duration of exposure, reactivity of the substance in various parts of the body, the rate of excretion from the body, the health of the individual <sup>[3]</sup> and possible genetic predeposition to occupationally induced disease such as cancers <sup>[4]</sup>.

Inhalation of toxins or irritant substances may have an acute or chronic health effect upon the individual. Acute inhalation of these substances may lead to

asphyxiation leading to a loss of consciousness and/or death. If inhaled in significant quantities, irritant substances such as 2,6-toluene diisocyanate cause pulmonary oedema resulting in fatality<sup>[5]</sup>. Chronic respiratory diseases are more commonly observed and of these the most frequently reported is occupationally induced asthma<sup>[6]</sup>. Occupational asthma (OA) is a disease characterised by variable obstruction of airflow and / or airway hyper-responsiveness attributable to factors associated with the workplace<sup>[7]</sup>. The disease may be pathogenically distinguished as allergen induced (resulting in hypersensitivity to a causative agent) or irritant / toxin induced, which occurs after repeated contact with the causative agent at low doses<sup>[8]</sup>.

### **1.1.2 Dermal Exposure**

This thesis is predominantly concerned with the dermal absorption of selected compounds of interest in occupational hygiene. Dermal absorption of compounds can be affected by chemical or physical properties of the analyte as well as the physical properties of the skin itself. The thickness of the skin as well as its natural coating of grease and sweat provides some limited protection against chemicals<sup>[9]</sup>. This natural protection may be bypassed through cuts, abrasions or punctures occurring through existing wounds or during penetrative chemical exposure, for example needle puncture accidents. Solvents degrease skin resulting in a reduction of the skins natural defense and thus enhancing dermal

penetration of toxins <sup>[10]</sup>. Humidity levels in the working environment can lead to under or over hydration of the barrier layer. This change in humidity of the stratum corneum can increase the individual's susceptibility to dermal penetration <sup>[11]</sup>.

Personal protective equipment (PPE) e.g. gloves forms a barrier which may greatly reduce direct contact between a chemical and the skin and thus dermal absorption (without necessarily completely preventing it). Topically applied barrier creams may be used independently or in conjunction with gloves to reduce or prevent chemicals from penetrating into the skin <sup>[12, 13]</sup>. However issues such as frequency of application and accurate determination of complete skin coverage must be addressed.

The most prevalent occupationally induced skin disease is dermatitis. Occupational dermatitis is defined as a skin disease of which occupational exposure is a major, casual or contributory factor <sup>[14]</sup>. The best estimate of the prevalence of work related skin disease comes from the self reported work related illness survey conducted 2001 / 2002. This provided an estimated prevalence of self reported work-related skin diseases of 39000 workers for the UK. Between the years 2000-2002 an estimated average of 3900 new cases of work related skin disease were diagnosed each year. Voluntary surveillance schemes organised by occupational physicians reporting activity (OPRA) and EPI-DERM reported an estimated average of 3900 new cases of work-related

skin disease each year between 2000 and 2002. Approximately 80% of these cases were clinically diagnosed as contact dermatitis <sup>[15]</sup>.

### **1.1.3 Contact Dermatitis**

There are three main types of contact dermatitis: irritant, urticarial and allergic. The most common form is irritant contact dermatitis (ICD) which is responsible for approximately 80% of cases <sup>[15]</sup>. It may be further sub-divided into acute or chronic forms. Acute irritant contact dermatitis may occur after a single exposure to a strong irritant. Skin damage may often be visible. Multiple exposures to weaker irritants over a prolonged period of several months or even years may result in a cumulative form of dermatitis known as chronic irritant contact dermatitis. Surveillance of occupationally induced chronic irritant contact dermatitis is frequently difficult due to the prolonged duration between exposure and the onset of symptoms <sup>[16]</sup>. ICD is caused by direct injury to the cells. The reaction with the irritant does not activate an immune cascade, but it is believed that direct damage to keratinocytes induces the inflammatory response <sup>[17]</sup>.

A less commonly observed dermatitis is contact urticaria. This form of contact dermatitis represents an immediate anaphylactoid-type IgE mediated response <sup>[18]</sup>.

Allergic contact dermatitis (ACD) results from a type 4 delayed hypersensitivity reaction, resulting from cumulative exposure to a skin sensitiser (allergen). Once the initial mechanism has been initiated it takes approximately seven days to complete the induction of sensitisation. Further skin contact with that particular sensitiser occurring after this period results in the onset of allergic contact dermatitis. The concentration of sensitiser on the skin required to initiate sensitisation (induction concentration) is higher than the concentration subsequently required to elicit allergic contact dermatitis (elicitation concentration), which may be extremely low <sup>[19]</sup>. Once sensitised to a compound, it may be impossible for an individual to work with the compound again. Although it only accounts for 20% of new incident cases, ACD may have a large economic and morbidity impact due to its relentless nature if the inciting allergen is not avoided <sup>[20]</sup>.

#### **1.1.4 Legislation and the Health and Safety Executive**

The health and safety at work act 1974 introduced wide ranging legal duties including duties for the control of chemical hazards <sup>[21]</sup>. More detailed obligations are contained in the control of substances hazardous to health (COSHH) regulations most recently updated in 2002 <sup>[22]</sup>, updated from 1988, 1994 and 1996 regulations. The notification of new substances (NONS) 1993 is a European wide system that requires chemicals suppliers to provide information

on substances that are new to the European market <sup>[23]</sup>. This information is used to decide the hazard severity of the chemical. The scheme is enforced by the Health and Safety Executive (HSE) together with the Environment Agency in the UK.

Suppliers of dangerous chemicals are governed by the Chemicals (Hazard Information and Packaging for Supply) (CHIP) Regulations 2002 <sup>[24]</sup>, updated from 1994. Its purpose is to protect people and the environment from the effects of chemicals by requiring suppliers to provide information about their hazards and to package them safely. Together these regulations implement European directives which form the main legal framework for controlling the supply, handling and use of hazardous substances.

In the U.K. workers, industry, local government and independent experts are involved in the decision-making processes and are members of advisory bodies. These parties are represented in the Health and Safety Commission (HSC). The operational arm of the HSC is the Health and Safety Executive which includes policy-making and the various health and safety inspectorates.

## 1.2 Dermal Absorption

### 1.2.1 The Structure of Skin

The skin is a complex membrane that performs many physiological functions such as metabolism, synthesis, temperature regulation, and excretion. Its upper layer, the stratum corneum, is considered to be the main barrier to the percutaneous penetration of exogenous materials. This barrier is also important in the maintenance of water within the body as well as in the absorption of pharmaceutical and other agents.

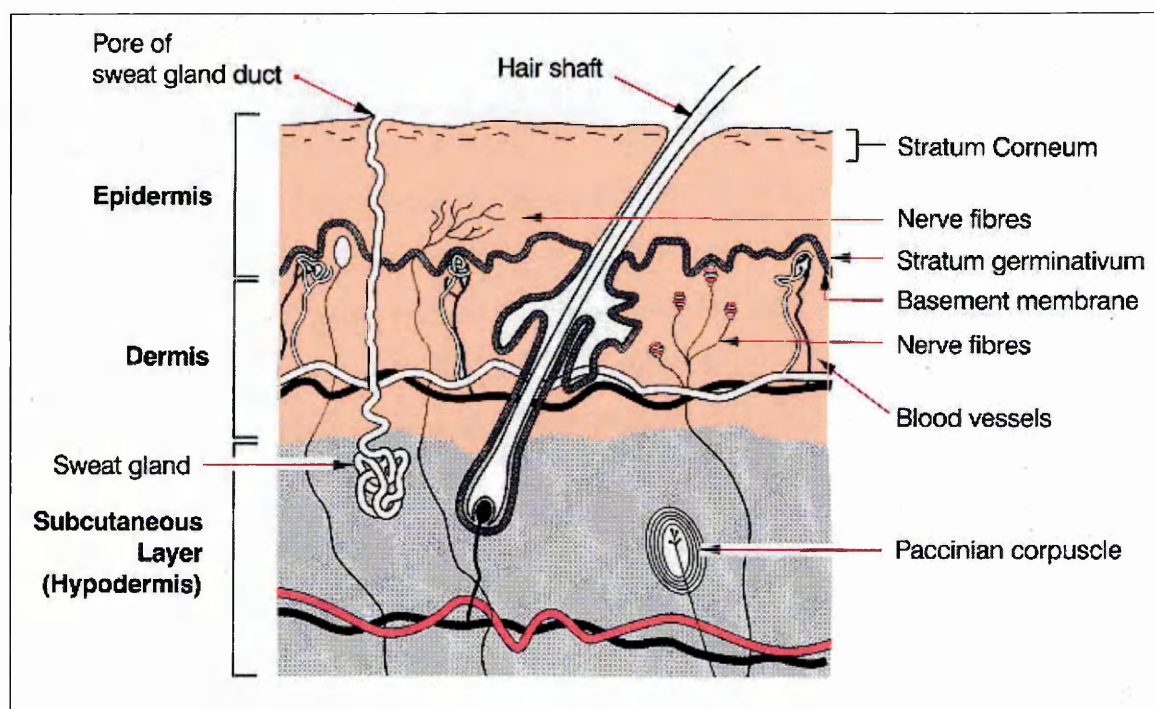


Figure 1.1 The structure of skin as shown through a horizontal cross section <sup>[25]</sup>

In the simplest description the skin consists of 2 layers; the epidermis and the dermis (figure 1.1). The epidermis is located on the outside of the skin in permanent contact with the environment. It is chemically robust yet is renewed completely once each month to maintain its optimum protective properties. The epidermis (figure 1.2) is 100-150 $\mu$ m thick and is subdivided into five strata:

Stratum corneum which consists of dead and dying cells

Stratum lucidum that consists of approximately five layers of clear dead skin cells

Stratum Granulosum named because it contains keratinocytes which accumulate dense basophilic keratohyaline granules. The granules contain lipids that help to form a waterproof barrier preventing rapid fluid loss from the body.

Stratum Spinosum, the largest of the five strata which contains a layer of keratinocytes 8 to 10 deep. These accumulate many desmosomes on their outer surface giving rise to characteristic 'prickles' observed in this stratum. It also contains Langerhans cells and Melanocytes (the cells responsible for the production of the skin pigment melanin).

Stratum Basale is composed of a single layer of keratinocytes which are columnar in shape. They are attached to the basement membrane via structures called hemidesmosomes. As well as containing Langerhan's

cells and Melanocytes the stratum basale also contains merkel cells which are believed to function as touch stimuli receptors.

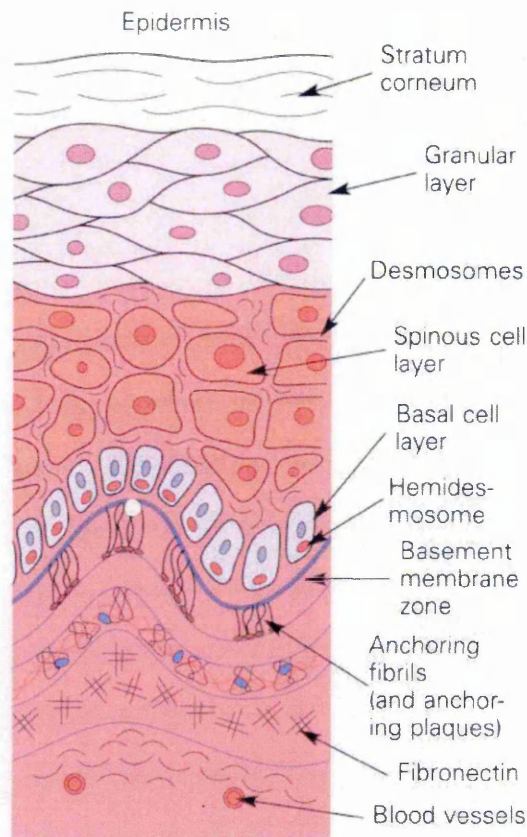


**Figure 1.2** The structure of the Epidermis <sup>[26]</sup>

The epidermis is constantly being replenished. Newly formed cells undergo a maturation process known as keratinisation as they travel from the stratum basale to the surface. Since blood doesn't enter the epithelium, it has to reach the epithelial cells by diffusion. The cells that lie closer to the basement membrane (closer to the underlying dermis which is vascularised) are closer to

the nutrient source. They use the nutrients that are diffusing into the epidermis. The cells in the stratum basale and stratum spinosum use up almost all the nutrients, therefore, once a cell has been pushed up into the stratum granulosum, it stops receiving any nutrients and begins to die. As the newly formed cells are pushed to the surface the older dead cells begin to break apart and are lost from the surface by a process known as desquamation.

The inner skin region is 10-20 times thicker than the epidermis. It is divided into two zones known as the papillary dermis and a reticular layer. The dermis is mechanically stabilised by an interwoven network of collagen fibres and is the chief site of the distribution as well as the major site of biochemical and biological degradation of transported material. It is also the site of immune cells that are involved in defending the body from foreign bodies passing through the epidermis. The dermis shelters the blood and lymph capillaries, nerve endings, glands and hair follicles. Hair and glands are distributed non-uniformly in the skin of the human body. Hair follicles are found all over the human body but at different densities. Hair follicles in humans only cover between 0.1 and 0.5% of the total skin surface <sup>[25]</sup>.

### **1.2.2 Barrier Properties of the Stratum Corneum**

Normal untreated skin is very impermeable to most substances. The stratum corneum is responsible for 80% of this transport resistance. The outermost

stratum corneum layer is relatively dry. It is composed of 10-20 flat and partly overlapping mainly dead corneocytes which are organised into columns and/or columnar clusters coupled together by numerous desmosomes. Lipid matrix material between the corneocytes is structurally arranged to act as intracellular glue sealing the spaces between the cells in the skin. This has been described by Elias <sup>[27]</sup> as a brick and mortar model.

Intracellular lipids in this layer mainly encompass relatively non-polar substances such as free fatty acids, cholesterol and cholesterol esters in addition to more than a dozen different ceramides. Because of the long aliphatic chains of the ceramides and due to the low overall lipid polarity in the skin the inter-corneocyte lipids are tightly packed and appear as lipid multi-lamellae (the mortar of the brick and mortar model). The lipids are covalently bonded to the corneocyte membranes forming a hydrophobic watertight barrier, resulting in a net effect of tightness and impermeability of the intact skin. It is very difficult to bring molecules larger than 300 Da across the intact skin, regardless of their solubility in the skin.

### **1.2.3 Dermal Penetration**

At the skin surface, molecules contact cellular debris, micro-organisms, sebum and other materials. These have a negligible effect on permeation. The penetrant has three potential pathways to the viable tissue (figure 1.3) — through hair

follicles with associated sebaceous glands, via sweat ducts, or across continuous stratum corneum between these appendages. Most compounds penetrate the skin via the intracellular microroute of the stratum corneum with only certain ions and larger polar molecules using routes 1 and 3 as their main pathways. The pores only account for 0.1% of the total skin surface area and so in comparison to transport via the stratum corneum transport via this route can be considered negligible.

The stratum corneum acts as a semi-permeable membrane with absorption occurring as a passive process of diffusion. Absorption through the stratum corneum can follow three routes

- 1) transcellular diffusion through the keratinocytes
- 2) transcellular diffusion through both the keratinocytes and the lipid lamellae (liquid matrix)
- 3) intracellular diffusion via the liquid matrix

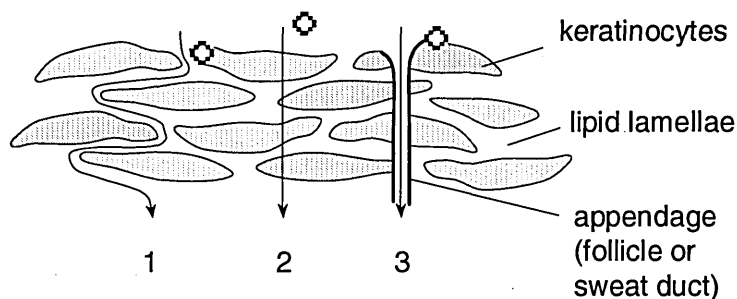


**Figure 1.3** The routes of penetration through the stratum corneum (adapted from Elias 1983) <sup>[27]</sup>

Studies suggest that the main route of permeation is via the intracellular lipid matrices. Studies conducted to investigate permeation through the corneocytes have produced conflicting results. Flynn argued that the density and compactness of the intracellular protein in the keratinocytes of the stratum corneum presents a thermodynamically and kinetically impossible passageway for chemical transport [28]. However Moss et al, using mathematical modelling techniques, propose that this can in fact occur and should not be entirely ignored [29]. Following penetration across the stratum corneum, compounds diffuse across the viable epidermis and dermis and are transported away by the cutaneous microvasculature. The blood supply is very rich, with a flow rate of  $0.05 \text{ ml min}^{-1}$  per  $\text{cm}^3$  of skin, and reaches to within 0.2 mm of the skin surface [30], since it needs to regulate temperature and pressure of the skin, deliver nutrients to the skin, and remove waste products. This generous blood volume usually functions as a 'sink' with respect to the diffusing molecules that reach it during the process of percutaneous absorption

#### **1.2.4 Skin Source and Storage for Dermal Absorption Studies**

The best and most relevant source of skin for dermal absorption studies is human cadaver or surgical excess. However, its availability is sometimes limited and animal skin is therefore frequently used. The most appropriate animal model for human skin is the pig. It is readily available from abattoirs and its histological and biochemical properties have been shown to be similar to human skin [31, 32].

In addition, the permeability of drugs through pig skin has been repeatedly shown to be similar to that through human skin <sup>[33, 34]</sup>. Porcine ear skin is particularly well-suited for permeation studies and gives comparable results to human skin <sup>[35]</sup>.

Many conflicting studies concerning the effects of storage of skin on absorption have been published. For percutaneous absorption studies, the skin is normally stored under frozen conditions and contradictory reports exist in the literature on the effect of storage condition on the *in vitro* percutaneous absorption of drugs. While several reports suggest that the freezing of skin significantly alters the permeability of drugs <sup>[36, 37]</sup> some investigators have shown that the permeability of human cadaver skin is largely unaffected after prolonged freezing at  $-20\text{ }^{\circ}\text{C}$  up to 466 days <sup>[38]</sup>. A recent study concerning the absorption of two drugs (melatonin and nimesulide) showed distinct increases of absorption after storage at  $-22\text{ }^{\circ}\text{C}$  for periods of time in excess of three months <sup>[39]</sup>.

### **1.2.5 Absorption Compounds of Interest**

The majority of percutaneous absorption studies to date have involved drugs of therapeutic benefit and toxic environmental compounds. The risk of toxicity is related to the ability of the toxic compound/s to reach the site of the toxic effect, (unless the skin surface itself is the site of toxicity). Since chemicals may be encountered in a range of solvents, solvent mixtures and chemical mixtures; the

effect of solvents and chemicals in the mixture on the dermal absorption and kinetics of the chemical of interest is relevant. Solvents such as acetone and ethanol have been shown to affect the stratum corneum and increase permeability. Surfactants may change skin barrier permeability by causing skin irritation resulting in altered structural organization of the stratum corneum lipids.

Percutaneous absorption of therapeutic drugs through skin is of huge interest in the pharmaceutical world. Researchers are striving to enhance the viability of transdermal delivery of drugs such as analgesics, insulin, and more recently, peptides and proteins <sup>[40, 41]</sup>. Transdermal delivery of drugs that require low dosages for long periods can be more effective, less costly, and less painful than traditional alternatives such as injection, intravenous infusion, or oral ingestion.

Investigations have also taken place into the absorption of metal species however, due to species specific interactions occurring which are not yet fully understood this technique has not yet proved viable or fully reproducible <sup>[42]</sup>.

### **1.3 Dermal Absorption Measurement Techniques**

#### **1.3.1 Autoradiography**

Microscopic autoradiography was developed during the late 1940s and 1950s and is a photographic technique which enables tissue localization of radio labelled bioactive substances. In this technique, the spatial distribution of a

radiolabelled substance within a biological specimen is detected by exposure of the specimen to radiation-sensitive film. With this method, it is possible to visualize and measure, by means of a software program, the analyte concentrations in the hair follicles, glands and various skin layers without resorting to mechanical horizontal sectioning. The procedure requires a long exposure time of the film, usually between 4 and 7 weeks <sup>[43]</sup>.

Autoradiography has been widely used for *in vivo* investigation of the localization of drugs and environmental toxins in tissue. It may be performed as a whole body technique, which is limited in sensitivity and resolution, or on smaller areas of the body producing high resolution results that require close and permanent contact between tissue and recording medium. *In vitro* analysis can also be conducted using receptor autoradiography, a high resolution technique enabling frozen skin sections to be investigated and low molecular weight compounds to be localised without translocation and loss of the radioactive label <sup>[44]</sup>. Autoradiography has been shown to be a viable technique for the localisation of the pesticide Malathion in dermal exposure studies conducted *in vivo* and *in vitro* <sup>[45]</sup>. Quantitation may be performed by superimposing the autoradiograph onto a histological image of the tissue and the application of imaging software to count the labelled analyte. A more recent beta imaging method devised by Barthe et al enables direct counting of radioactivity from the tissue which is up to 500 times faster than classical film and vastly more sensitive <sup>[46]</sup>

### 1.3.2 Diffusion Cells

In vitro diffusion cell methods measure the diffusion of chemicals into and across skin to a fluid reservoir (which can be static or flow cell design) and can utilise non-viable skin to measure diffusion only, or fresh, metabolically active skin to simultaneously measure diffusion and skin metabolism. Such methods have found particular use as a screen for comparing delivery of chemicals into and through skin from different formulations and can also provide useful models for the assessment of percutaneous absorption in humans

The test substance, which may be radiolabelled, is applied to the surface of a skin sample separating the two chambers of a diffusion cell. The chemical remains on the skin for a specified time under specified conditions, before removal by an appropriate cleansing procedure. The receptor fluid is sampled at time points throughout the experiment and analysed for the test chemical and/or metabolites. When metabolically active systems are used, metabolites of the test chemical may be analysed by appropriate methods. At the end of the experiment the distribution of the test chemical and its metabolites are quantified. Absorption of a test substance during a given time period is measured by analysis of the receptor fluid and the treated skin. The test substance remaining in the skin should also be classed as having been absorbed. Analysis of these other components (material washed off the skin and remaining within the skin layers) allows for further data evaluation, including total test substance disposition and percentage recovery. Analysis of the receptor fluid is usually conducted by high

performance liquid chromatography (HPLC) and often combined with mass spectrometry. This enables sensitive and rapid analysis to be performed for a range of compounds and their respective metabolites.

This method does not show the spatial resolution of the analyte in the skin, but produces quantitative data showing the amount of a compound to pass through the skin into the bloodstream after time (not just within the skin itself). This technique was used by Santhanam et al for quantitative investigation of the dermal absorption of the insecticide Meta-N,N-diethyl toluamide (DEET) <sup>[47]</sup>.

### **1.3.3 Tape Stripping**

This technique involves the application of an analyte to the surface of the skin. After a defined period of exposure the excess analyte is rinsed from the surface and the stratum corneum is removed by the consecutive application of adhesive tape. The quantity of the analyte in each strip can be determined using a suitable analytical technique, commonly liquid chromatography mass spectrometry (LC-MS) or gas chromatography (GC-MS). Another technique is by use of a radiolabelled analyte with a digestion or combustion step followed by scintillation counting. From the derived data it is possible to generate a profile representing analyte concentration versus penetration depth of the skin. *In vivo* and *in vitro* investigations can be conducted. *In vivo* studies are conducted on healthy human

subjects who suffer no long term effects from the removal of the stratum corneum from a small area of skin (usually the forearm) <sup>[48]</sup>.

One fundamental limitation of tape stripping is that the stratum corneum cannot be totally removed by stripping. Generally, about one third of the layer will remain attached, as 'islets', to the epidermal surface <sup>[49]</sup>. A recent X-ray microanalytical study showed that even after the removal of 40 tape strips, significant residues of unstripped material were present within the macroscopic furrows of human skin <sup>[50]</sup>. As a result of this, the corneocytes harvested on one tape strip may be derived from different depths, depending upon the position of the tape in relation to the slope of the furrow. Moreover, any given tape will remove different amounts of stratum corneum at different depths and sites of the skin. Additionally, the amount of stratum corneum removed can be affected by the contact time as well as by inter-individual variability. It is therefore necessary to quantify the mass of stratum corneum removed with each strip by weighing the tape before and after the stripping procedure.

## **1.4 Direct Spectrometric Analysis**

### **1.4.1 Attenuated Total Reflectance Fourier Transform Infrared Spectroscopy (ATR FTIR)**

The wavelength of light absorbed by a molecule is characteristic of any chemical bonds it contains. By interpreting the infrared absorption spectrum, the chemical

bonds in a molecule can be determined. This can enable the identification of an unknown compound or be used to indicate the presence of a known compound in a sample. Quantification can be achieved as the strength of the absorption is proportional to the concentration of the compound at the specific location. For analysis to take place it is essential that the compound to be monitored has a unique infra red absorbance profile distinct from those inherently found within the dermal tissue.

Over the last decade, ATR-FTIR skin analysers have become commercially available for the detection of drugs applied to the skin <sup>[51]</sup>. In these devices, an infrared beam is emitted through an infrared-transparent crystal (internal reflection element; IRE) which is in contact with the skin sample. The crystal configuration results in the multiple internal reflection of the beam until it exits from the opposite face, back towards the spectrophotometer. During passage through the crystal, the radiation penetrates slightly beyond the reflecting surface of the crystal, into the skin. As a result, the radiated stratum corneum absorbs infrared energy at frequencies corresponding to its normal absorption spectrum. Multiple reflections amplify the signal. Since the beam only interacts with the most superficial layer of the skin which is in immediate contact with the IRE, ATR-FTIR studies are ideally performed in conjunction with tape-stripping. This allows the generation of a series of ATR spectra, each representing absorption at successive depths within the stratum corneum.

Singh and Singh demonstrated the use of ATR-FTIR for analysing the percutaneous absorption of certain jet fuel chemicals including naphthalene and tridecane <sup>[52]</sup>. ATR-FTIR can also be used to examine the physical properties of the skin during the absorption process and changes which occur in lipid chemistry when penetration enhancing chemicals are used.

#### 1.4.2 Remittance Spectroscopy

The process of remittance spectroscopy utilises the detection of backscattered light from the interior of the stratum corneum. The presence of a light absorbing analyte in the skin reduces the light which is backscattered and hence it is possible to quantify analytes within the skin. This technique has been utilised to determine skin pigmentation effects and analyse indigenous compounds in skin. Investigations have also been conducted into the *in vivo* quantification of drugs in skin using remittance spectroscopy <sup>[53]</sup>.

Sennhenn *et al* studied absorption into the forearms of human volunteers with an emulsion containing the drug Uvinol T150 versus a placebo emulsion. A UV-vis spectrometer was used to generate a monochromatic beam in the UV spectral range. This beam was directed perpendicular to the subject's skin surface. The remitted energy from a defined area was analysed by a photomultiplier angled at 45° from the forearm surface. The experiment was repeated at different UV wavelengths to cover the entire wavelength range 220-380nm. A plot of

percentage remittance versus wavelength indicated a decreased remittance in the range 300-340nm when T150 was present in the emulsion. The compound was determined to be concentrated in the outermost parts of the stratum corneum as the measured depth was dependant on the beam wavelength. Quantitation was determined from the remittance decrease. They concluded the technique to be sensitive, highly reproducible and ideally suited to detect and quantify small quantities of UV absorbing penetrants<sup>[53]</sup>.

### 1.4.3 Fluorescence Spectroscopy

This technique is similar to remittance spectroscopy, however, only a specific wavelength is detected by use of a second monochromator prior to detection. Direct fluorescence spectroscopy concerns the detection of remitted light from a self fluorescent analyte. Indirect fluorescence spectroscopy measures the decrease in skin fluorescence caused by a light absorbing penetrant. Fluorescent labelling of the skin is required and one compound utilised for this is dansyl chloride as demonstrated by Jansen *et al*<sup>[54]</sup>. A study conducted by Weiner *et al* of a self fluorescent marker (carboxyfluorescein) in the sebaceous glands of Syrian hamster ear skin yielded reproducible, quantifiable results<sup>[55]</sup>.

#### **1.4.4 Photothermal Spectroscopy**

Photothermal spectroscopy is a technique where a modulated monochromatic UV beam is projected upon the skin and the increase in temperature (caused by light absorbance) is measured. An increase in surface temperature is observed if a UV-absorbing drug is present within the tissue. This in turn leads to pressure oscillations at the skin surface which are detected by the use of a highly sensitive microphone. Measurement depth is controlled by changing the modulation frequency, a lower frequency results in increased measurement depth. Reproducibility suffers at lower frequencies due to the skins natural elasticity limiting the effective depth profile range to the stratum corneum only. This method has been demonstrated by Kolmel *et al* for the quantification of sunscreen agents into the stratum corneum <sup>[56]</sup>.

### **1.5 Mass Spectrometry**

#### **1.5.1 Introduction to Mass Spectrometry**

Mass spectrometry is an instrumental approach that allows for the mass measurement of molecules. A mass spectrometer consists of 5 parts: a vacuum system, a sample introduction device, an ionization source, a mass analyzer and an ion detector. The mass spectrometer determines the molecular weight of chemical compounds by ionizing, separating and measuring molecular ions (and

their fragments) according to their mass to charge ratio ( $m/z$  value). The ions are generated in the ionization source by inducing the loss or gain of a charge (electron ejection, protonation or deprotonation). Once the ions are formed (as an ion plume in the gaseous phase) they can be electrostatically directed into a mass analyzer, separated according to mass, and finally detected.

Data is observed in the form of a mass spectrum which provides molecular weight and structural information. In modern instruments the spectrum is displayed on a computer connected to the instrument and more complex data analysis can be conducted using specialist software.

### **1.5.2 History of Mass Spectrometry**

The founder of mass spectrometry was Joseph John Thomson working at the Cavendish Laboratories, Cambridge University <sup>[57]</sup>. While researching the electron he discovered that ions move through parabolic trajectories proportional to their "mass-to-charge" ratios. Thomson received the 1906 Nobel Prize in Physics "in recognition of the great merits of his theoretical and experimental investigations on the conduction of electricity by gasses." Over the next few years a number of key names took up the early development of mass spectrometry, including Dempster <sup>[58]</sup>, Herzog, Bainbridge and Nier. By the end of

the 1930's mass spectrometry had become an established technique for the separation of atomic ions by mass.

Vast improvements in instrumentation occurred from the 1940's to the 1970's. Francis Aston <sup>[59]</sup> and Arthur J Dempster developed much-improved higher accuracy mass spectrometers. Alfred Nier coupled these developments with more advanced vacuum technology to greatly decrease the size of mass spectrometers <sup>[60]</sup>. One important development in mass spectrometry occurred in 1946 with the proposal of the time of flight mass spectrometer by William E Stephens <sup>[61]</sup>. The TOF mass analyzer separates ions by measuring velocities of ions traveling in a straight path towards a detector. The 1950's saw the development of the quadrupole mass analyzer by Wolfgang Paul <sup>[62]</sup>. This analyzer separates ions with an oscillating electrical field further increasing the utility of mass spectrometers. Paul also developed the quadrupole ion trap in 1983 which specifically traps and measures ions. He was awarded the Nobel Prize for physics in 1989 for his work in the field.

New ionization techniques developed over the last 25 years (fast particle desorption, electrospray ionization and matrix-assisted laser desorption/ionization) have opened up the world of biological chemistry to mass spectrometry. Just about every compound class can be analyzed by some sort of mass spectrometry including species with masses extending well into the megadalton range.

### 1.5.3 Time of Flight Mass Spectrometry (TOF-MS)

Time of flight (TOF) mass analyzers (although first introduced in the mid 1940's) were successfully demonstrated as a reliable method for mass spectrometry in 1955 [63].

All TOF mass spectrometers consist of a minimum of components; a pulsed ion source, a field-free drift space, and a detecting device. The theory behind TOF-MS is based on the principle that ions of different mass to charge ratios ( $m/z$  values) have the same energy, but different velocities after being accelerated from an initial ion source. As the ions travel at different velocities the time taken for each to traverse the field free drift tube is different. Low mass and multiply charged ions will reach the detector faster than high mass or singly charged ions [64].

The theory can be expressed by an equation as shown in equation 1.1

$$zeV = \frac{1}{2}mv^2 \qquad \text{Equation 1.1}$$

In this equation:

- z = number of charges
- e = electron charge
- V = accelerating potential from ion source
- m = mass of the ion
- v = velocity of ion

The velocity of the particle can be determined in a time-of-flight tube since the length of the path ( $d$ ) of the flight of the ion is known and the time of the flight of the ion ( $t$ ) can be measured

$$v = \frac{d}{t} \quad \text{Equation 1.2}$$

Equations 1.1 and 1.2 can be combined to produce equation 1.3

$$zeV = \frac{1}{2} m \left( \frac{d}{t} \right)^2 \quad \text{Equation 1.3}$$

The time of flight of an ion ( $t$ ) can be determined by rearranging equation 1.3 (shown in equations 1.4 and 1.5)

$$t^2 = \frac{d^2}{2eV} \frac{m}{z} \quad \text{Equation 1.4}$$

$$t = \frac{d}{\sqrt{2eV}} \sqrt{\frac{m}{z}} \quad \text{Equation 1.5}$$

To make practical use of this principle a definite starting pulse is needed to initiate the flight of the ions. The width of the starting pulse is in the range of 10ns, in order to yield sufficient mass resolution. After the starting pulse is fired, a

relative long waiting period follows in the range of 100 $\mu$ s, during which all expected ions reach the detector. After pulsed excitation the ion plume is confined to a dense packet. Although ions of different mass spread out from each other as they travel in the drift region, ions of the same mass-per-charge ratio remain together. The space charge, generated between ions in the ion packet may result in decreased mass resolution and sensitivity. A high acceleration voltage (4–40 kV) is used to combat this. However, the mass resolution will be limited by the short flight times of the ions <sup>[65]</sup>.

A reflectron can be used to improve mass resolution. The reflectron, located at the end of the flight tube, is used to compensate for the difference in flight times of the same  $m/z$  ions of slightly different kinetic energies by means of an ion reflector. This results in focusing the ion packets in space and time at the detector. Ions of higher energy will travel further into an electrostatic repeller field (ion mirror) and will be retained longer and arrive at the detector at the same time as ions of lower initial energy which penetrate the field less.

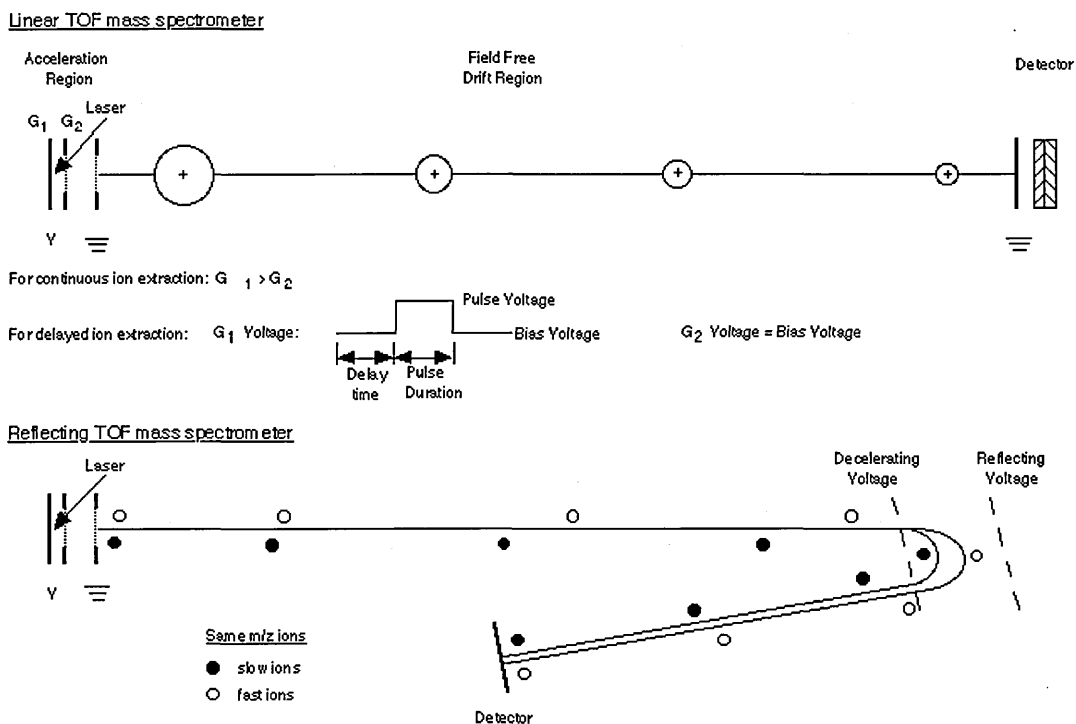


Figure 1. Basic components of a linear (upper) and reflecting (lower) TOF mass spectrometer.

**Figure 1.4** Comparison of a linear and reflecting ToF instrument <sup>[66]</sup>

Linear TOF instruments suffer from lower resolution as fragment ions generated in the field free drift region (metastable ions) cannot be distinguished from the original ion due to their velocity remaining the same. The metastable ions have a lower energy than the original parent ion and hence penetrate the reflectron less. They can be distinguished when linear and reflectron-acquired spectra are compared due to their time difference in reaching the detector.

One main factor leading to the loss of resolution is the range of slightly differing flight times of identical  $m/z$  ions arising from their different initial velocities formed during laser ionisation in MALDI. The actual final velocity that is attained for ions

as they are accelerated out of the ion source and into the field free region includes this initial velocity component and hence can vary for the same mass to charge ratio. No compensation is made with continuous ion extraction linear TOF-MS for ions with the same  $m/z$  but different initial ion velocities. Improvements in mass resolution can be achieved by utilizing a time delayed pulsed ion extraction <sup>[67]</sup>. Delayed extraction (DE) is achieved by observing a calculated time delay following the firing of the laser at the sample. This delay occurs before the extraction potential is applied, enabling ions of a particular kinetic energy to be brought into better focus as they are accelerated into the TOF region.

Because of their relatively low cost, simple design and high mass-to-charge range, ToF mass spectrometers are often the analyzers of choice for high sensitivity, high  $m/z$  range analysis work, especially for species of biological interest.

#### **1.5.4 Quadrupole Time of Flight**

The quadrupole time of flight tandem mass spectrometer (QToF) combines the quadrupole and the time of flight mass analyzers. A simple description of the instrument is a triple quadrupole with the last quadrupole section replaced by a ToF mass analyzer. The instrument often benefits from the addition of a further

r.f Quadrupole to provide collisional damping. An illustration of a typical QToF instrument is shown in figure 1.5.

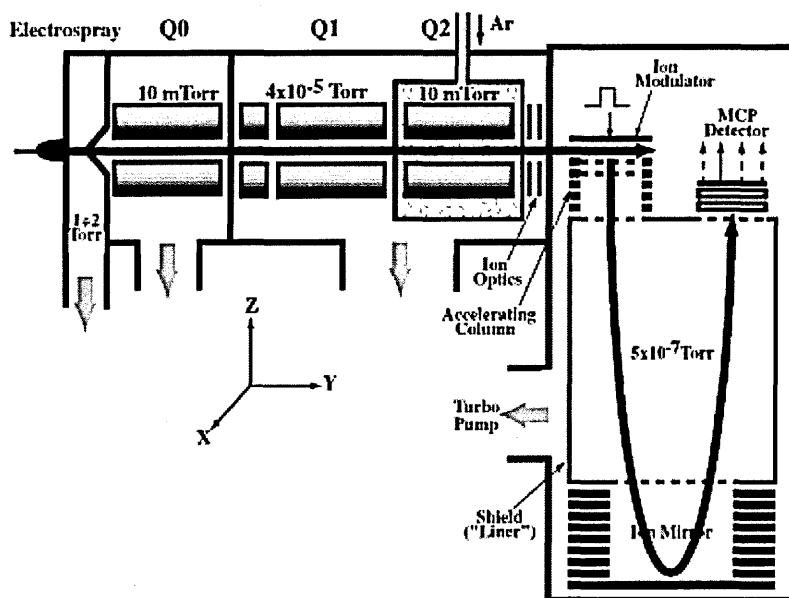


**Figure 1.5** Schematic diagram of a standard quadrupole time of flight mass spectrometer (quadrupole number is indicated as Q0, Q1 and Q2) <sup>[68]</sup>

ToF-MS data is acquired by operating the Q1 mass filter in r.f mode only, thus acting solely as a transmission element. The ToF analyzer actively records the spectra, resulting in spectra displaying the high resolution and mass accuracy typically associated with this analyzer. MS/MS data are acquired by operating Q1 in the mass filter mode to transmit only the selected precursor ion (allowing a large enough mass window for the inclusion of isotopes if required). Collision induced dissociation occurs in Q2 with the resulting product ions being collisionally cooled and focused before being reaccelerated and focused into the

ion modulator of the ToF analyzer. A pulsed electric field is applied at a frequency of several kilohertz (kHz) across the modulator gap pushing ions in a direction orthogonal to their trajectory into the accelerating column. It is here that they acquire their final energy of several kilo-electronvolts (keV) per charge.

The advantage of using the QToF is the combination of the high sensitivity of quadrupole instruments and the vastly superior mass resolution of time of flight mass analyzer in one instrument as demonstrated in the analysis of phosphopeptides by Steen et al <sup>[69]</sup>.

#### **1.5.5 Matrix Assisted Laser Desorption Ionisation (MALDI)**

Laser desorption ionisation (LDI) as a technique for the analysis of organic compounds was first demonstrated in the 1960's. Irradiation of organic samples (of low mass) with a high intensity laser produces ions which are mass analyzed (usually by time of flight mass spectrometry).

The primary requirement for successful LDI is that the efficiency of the energy transfer from the laser beam to the analyte. The probability of obtaining a useful mass spectrum depends on the specific properties of the analyte such as its volatility and photoabsorption. In molecules with a large mass >5000Da the ions produced are almost always fragmentation products of the original molecule, thus the analyte is not desorbed as the intact molecule in any significant amount

resulting in a spectrum of low-mass fragment ions only. Matrix Assisted Laser Desorption Ionisation (MALDI) was first utilised in 1988 by Hillenkamp and Karas [70]. It was revolutionary as it enabled the analysis of compounds up to 350000 Daltons in size which was approximately a 30 fold increase in comparison with the standard laser desorption ionization techniques. It enabled large proteins to be analysed at sub fmol sensitivity levels. At the same time, developments by Koichi Tanaka (using an inorganic suspension matrix) demonstrated the application of MALDI-MS to a whole range of biological macromolecules [71].

In MALDI a solid matrix is used, which absorbs electromagnetic radiation at the wavelength of the laser. The sample is mixed with an excess of matrix solution (optimally in the 1:1000-1:10000 analyte to matrix range) and allowed to co-crystallize on a target plate. The resultant analyte molecules are singularized and fully surrounded by matrix molecules. When the laser is fired at the target the matrix absorbs the laser energy which vaporizes it (it desorbs from the surface) and this carries some of the sample with it (figure 1.6). At the time that the laser is pulsed a voltage is applied to the target plate to accelerate the ionized sample towards a time-of-flight mass analyzer.

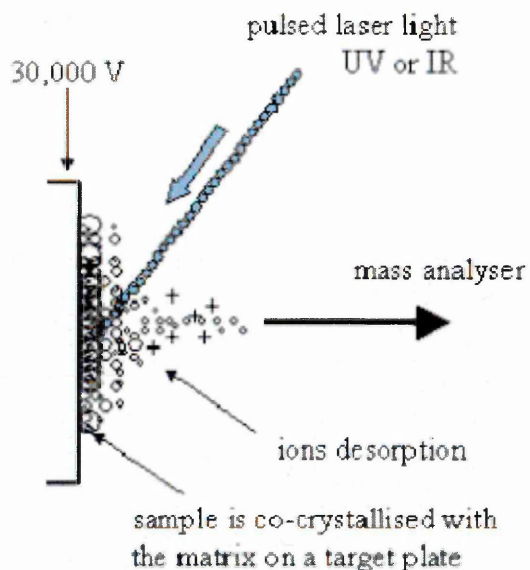


**Figure 1.6** Diagram showing the formation of ions by MALDI

The most common lasers used in MALDI are from the UV wavelength range. Of these Nd-YAG (355nm) and Nitrogen (337nm) are the most frequently used. Laser spot sizes are commercially available in the region of 50µm diameter. The laser diameter is the defining factor of image resolution in most analysis.

### 1.5.5.1 Ion Formation

The method by which ionization occurs is not completely understood however the widely accepted view is that, following their desorption as neutrals, the sample molecules are ionized by acid-base proton transfer reactions with the protonated matrix ions in a dense phase just above the surface of the matrix. The protonated

matrix molecules are generated by a series of photochemical reactions. In the majority of cases it is believed that the matrix provides a source of gas phase protons for ionisation in the positive ion mode. However, in some cases, cationisation with a salt ( $\text{Na}^+$  or  $\text{K}^+$ ) is the observed pathway of ionisation <sup>[72]</sup>. Arguments against this mechanism are supported by the lack of a viable explanation for matrix suppression effects commonly observed during MALDI-MS analysis. Matrix suppression occurs when the analyte is preferentially ionised over the matrix resulting in few or no matrix ions being observed <sup>[73]</sup>. In the photochemical ionisation (PI) theory all analyte ions must be produced from collision processes between neutral analyte molecules and protonated or deprotonated matrix molecules. Hence it is difficult to explain matrix suppression in this model due to short proton transfer times (less than  $1\mu\text{s}$ ) and the significantly lower quantity of analyte molecules being present in relation to matrix molecules <sup>[74]</sup>.

A cluster ionization theory for MALDI ion formation has described in several papers published by Karas and co-workers <sup>[75, 76]</sup>. This is based around the assumption that large protonated analyte clusters are pre-existing in the organic acid matrix. It is hypothesised that laser irradiation causes the clusters to be desorbed and thus analyte ions are produced in the gas phase by desolvation of neutral matrix molecules. However these proposals are all still unproven theories and a full validated explanation for MALDI ion formation is awaited.

### 1.5.5.2 Matrix

The choice of a suitable matrix is essential in the MALDI process. In order to successfully fulfil its role a matrix must possess certain properties:

- 1) Solubility in the same solvent as the analyte to be investigated
- 2) It must display a high molar absorptivity at the same wavelength as the laser
- 3) Be able to produce ionisation of the analyte
- 4) It must be stable under the vacuum conditions of the instrument.
- 5) Be unreactive towards the analyte.

Properties which are not desired in a matrix:

- 1) Excessive fragmentation of the analyte
- 2) Formation of analyte adducts
- 3) Produce ions with  $m/z$  values coinciding with those of the analyte ions.

Different matrices are suitable for the analysis of certain compounds for example  $\alpha$ -Cyano-4-hydroxy cinnamic acid ( $\alpha$ -CHCA) is used for compounds of low molecular weight and peptide fragments/smaller proteins whereas 2,5-Dihydroxybenzoic acid (DHB) is more suited to larger proteins (e.g. bovine serum albumin). Particle suspension matrices can be used to analyse compounds containing ions which would be masked or suppressed by matrix related peaks. Many different particle suspension matrices have been utilised, these include

titanium oxide, graphite and silicon <sup>[77]</sup>. Their mode of action is believed to be due to thermal absorption of the laser causing ionisation of the analyte <sup>[78]</sup>.

### 1.5.6 Secondary Ion Mass Spectrometry (SIMS)

Secondary ion mass spectrometry is a surface analytical technique, which was designed in the 1960s by Castaing and Slodzian. The basic principle of the technique is based on the mass spectral analysis of secondary ions extracted from the top few nanometers of the surface of a solid sample under the impact of an energetic beam of primary ions. The ejected species may include atoms, clusters of atoms and molecular fragments. Only a small fraction of these species are ions. The ionisation efficiency is strongly influenced by electron exchange processes between the ejected species and the surface. A variety of primary ion sources may be used. The most popular source is a liquid metal ion (LMI) source <sup>[79]</sup>, which produces an ion beam of Ga<sup>+</sup> or In<sup>+</sup> at spot sizes of less than 1µm in diameter. Newer ion sources have been designed which employ full molecular ions (SF<sub>6</sub><sup>+</sup> and C<sub>6</sub>Br<sub>6</sub><sup>+</sup>) as the primary ion source; this has the advantage that the cumulative effects of chemical primary ion damage to the sample do not significantly diminish secondary ion emission <sup>[80]</sup>. Traditionally it is the positive ejected ions which are analysed. However, negative ion methods can be used and a primary oxygen beam (O<sup>2+</sup>) is usually used for this purpose.

Rastering the ion beam across the surface and collecting the data at each raster spot enables an overall image to be produced (each spot becoming a pixel in the image). One of the main problems with this type of analysis is the damage which is caused to the tissue surface during the rastering process. This results in the static SIMS limit ( $10^{13}$  primary ion  $\text{cm}^{-2}$ ) where the entire tissue surface has been completely damaged and recognisable secondary ion emission ceases.

## **1.6 Biological Imaging Mass Spectrometry**

Imaging mass spectrometry (IMS) is a relatively new technique that utilises a range of MS technologies to record spatial information on the distribution of a substance on the surface of a biological sample or 'blot' (of a tissue). In its most common form a sample is moved under a stationary ionising source and a mass spectrum is acquired. Further movement and ionisation in a defined pattern over the sample results in the acquisition of many spectra. The spatial dimensions x and y may be plotted against the abundance of a selected ion or ion range with each spectrum representing a single pixel in the resulting image. Ion intensity is observed in greyscale or as a single colour or colour range. The use of multiple colours can enable several different ions to be observed in the same 2 dimensional image. A range of ionising sources can be used for imaging mass spectrometric analysis and these will be discussed further.

### 1.6.1 Imaging MALDI-MS (MALDI-MSI)

Imaging MALDI –MS is a relatively new technique which can be applied to the analysis of biological tissue samples. The principles of the technique involve the application of a suitable matrix to the tissue or membrane blot of the tissue before a laser is rastered across the sample surface in a snakelike pattern acquiring spectra at pre determined intervals. This can occur in two ways, either by moving the laser across the static target plate or by holding the laser in position and moving the target plate underneath it. Each spectrum is the result many consecutive laser shots at each coordinate, depending on instrumental settings and type of laser used.

Each mass spectrum is represented as a pixel in the resultant MALDI image. The brighter the pixel the higher the intensity of the analyte in that mass spectrum.

Imaging software can produce three dimensional images by plotting the spatial dimensions of x and y versus the absolute ion intensity of the analyte. The ion intensity is representative of the analyte concentration; however, it is not an accurate method of quantitation.

## 1.6.1.1 Instrumentation

### 1.6.1.1.1 Lasers

A wide range of lasers have been demonstrated for use for MALDI imaging analysis. Nitrogen lasers operating at a wavelength of 337nm have been the most frequently used although commercial available lasers include solid state Nd:YAG (at 355nm) and most recently infra red. Nd:YAG lasers are attractive due to the increased lifespan, reproducibility and vastly increased repetition rate demonstrated during the high throughput image acquisition process. Nd:YAG lasers have shown significantly poorer results over surfaces coated with a thin layer of matrix in comparison to nitrogen lasers<sup>[81]</sup>. The beam profile is believed to provide the advantages of the N<sub>2</sub> lasers for imaging purposes. A recent paper produced by Bruker<sup>[82]</sup> demonstrates a method of modulation of the Nd:YAG laser beam (the distribution of the laser intensity over the target surface). This modulation enables the Nd:YAG laser to 'mimic' the beam profile of the N<sub>2</sub> laser. A comparison conducted between the structured Nd:YAG and N<sub>2</sub> lasers over thin layer matrix applications (such as utilised for imaging samples) showed similar analytical properties thus indicating its suitability for imaging MALDI purposes. Another method of increasing the sensitivity of imaging experiments with a Nd:YAG laser is the dynamic pixel software provided by Applied Biosystems. The focused laser is moved around the defined area (pixel in the resulting image) in a

figure of 8 shape thus facilitating the production of an increased amount of analyte ions.

The use of an infra red (IR) laser allows for excitation of the vibrational modes of the matrix as opposed to their electronic states. A distinct advantage of using the IR wavelength range is the ability to use matrices which do not alter the physiological conditions of the sample being investigated. Popular matrices demonstrated for this technique include ice and glycerol allowing for the analysis of biomolecules directly from tissue and cells which may otherwise be adversely affected by an organic acid matrix. Difficulties occur with focusing the laser beam to produce a spot size small enough to enable cellular level microprobe imaging. The coupling of an IR laser with the mass microscope method of image acquisition enables a vastly increased spatial resolution to be achieved. Experiments conducted by Luxumbourg et al <sup>[83]</sup> produced images with a spatial resolution of 4 $\mu$ m, far lower than the theoretically achievable resolution of 28 $\mu$ m by use of the conventional microprobe scanning method.

#### **1.6.1.1.2 Oversampling**

One limitation to the resolution of a MALDI-MS acquired image is the diameter of the laser beam. For cellular level imaging a maximum beam diameter of less than 20 $\mu$ m would be required (approximately the size of a mammalian cell).

Generally the raster increments possible on an instrument are much smaller than the laser size with instruments often capable of 1-5 $\mu\text{m}$  increments. An oversampling technique has been developed and demonstrated by Sweedler and co-workers<sup>[84]</sup>. Using this technique the limiting factor for spatial resolution is the raster increment. However to ensure accurate results complete ablation of the matrix must occur between each subsequent increment. Images of peptide standards on electron microscopy calibration grids with a spatial resolution of 25 $\mu\text{m}$  were obtained using commercial lasers of sizes up to 200 $\mu\text{m}$ .

#### **1.6.1.1.3 MALDI Mass Microscope**

The applications of imaging mass spectrometry are limited by sample preparation methods, spatial resolution and analysis time. A major limiting factor in the spatial resolution achievable by imaging MALDI is the size of the laser spot rastered across the sample surface. Heeren et al have demonstrated the use of a mass spectrometric microscope instrument in which the spatial resolution is independent of the ionizing laser spot size<sup>[85]</sup>. This allows a larger laser focus field to be analyzed without resorting to movement of the sample or laser beam. After a single laser shot the produced ions travel through the time of flight mass spectrometer forming an ion optical image on a position sensitive detector. A series of mass spectrometric images are created separated by their respective  $m/z$  value showing spatial information from within the focus field of the laser spot.

The limiting factors of spatial resolution in this mode are the quality of the ion optics and the detector resolution as opposed to the laser spot size. Images generated in this way have been demonstrated with a lateral resolution of 4 $\mu\text{m}$  far smaller than a typical optimised MALDI ion probe (approx 25 $\mu\text{m}$ )<sup>[86]</sup>.

Other advantages from decoupling the spatial resolution from the size of the laser spot include a vast reduction in analysis time (by several orders of magnitude) and the potential to use a increased variety of ionization methods such as a larger ionizing beam for example infra red MALDI for high resolution imaging analysis<sup>[82]</sup>. A limitation of this instrument is however that the ability to select masses of interest to image is very poor ( $\pm 2$  Da) and hence improvements would be necessary for it to be applicable for the imaging of complex biological samples.

### **1.6.1.2 Sample Preparation**

#### **1.6.1.2.1 Matrix Application Methods**

Retention of spatial resolution is of paramount importance in the production of a high quality MS image. However, with application of the matrix there is potential for analyte spreading to occur. Various manual methods of matrix application have been investigated. The two most commonly used techniques are electrospray deposition<sup>[87]</sup> and airspray<sup>[88]</sup>. Automated matrix application has

been commercially developed i.e. devices that deposit small matrix droplets across the sample surface. Automated matrix deposition by has enabled the deposition of matrix droplets smaller than the laser spot size onto tissue samples [89]. Thus making the size of the matrix droplet the new limiting factor for the image resolution. Even smaller droplets can be deposited on the sample surface by commercially available instruments utilizing acoustic deposition [90].

#### **1.6.1.2.2 Membrane Blotting**

MALDI was first used as a method for imaging the surface of biological samples by Caprioli et al [87]. Two methods of sample preparation were initially investigated:

- 1) Direct analysis of a fresh tissue section coated with matrix
- 2) Blotting of the tissue onto a target coated with C18 beads. The matrix was then deposited on the blotted areas of the target.

In the investigation successful localization was observed for hormone peptides in a rat pituitary tissue section. Metabolites were observed as well as molecular ions. The conclusion of the investigation was that blots from the C18 beads provided superior images. However in the time elapsed since (and with advances

in instrumentation and methodology) direct tissue analysis has been more widely utilized for biological molecular imaging.

A range of blotting media has been investigated as a support medium for MALDI imaging analysis. Chaurand et al conducted further research into carbon-based membranes. Their study conducted in 1999<sup>[91]</sup> used carbon filled polyethylene membranes which were considered suitable due to their electrical conductivity and the fact they adhered proteins enabling clean up of the protein blot (by washing with water) but without loss of spatial information. Other membranes investigated include nylon<sup>[92]</sup>, nitrocellulose<sup>[93]</sup>, polyethylene<sup>[94]</sup>, and most recently cellulose<sup>[88]</sup>.

The combination of suitable matrix and blotting membrane is essential to produce the highest possible quality of image. The crystals formed on the surface of the membrane or direct tissue must be smaller than the image resolution to avoid becoming a limiting factor.

The majority of investigations conducted with indirect blotting imaging MALDI have concentrated on the analysis of proteins in tissue. Some studies have been conducted into the detection of low molecular weight compounds in biological tissue. Bunch et al<sup>[88]</sup> used imaging MALDI MS for the detection and localization of ketokonazole from cellulose membrane blots taken from porcine ear skin surface and vertical cross sections.

### 1.6.1.2.3 MALDI – MS Analysis of Direct Tissue

Direct tissue MALDI-MS imaging allows for the simultaneous mapping of many endogenous molecular components or exogenous analytes from a thin section of a tissue sample. Direct analysis of tissues eliminates the risk of analyte spreading or loss of spatial resolution due to actions occurring during a membrane blotting procedure. A diagrammatic outline showing a standard sample preparation technique for direct tissue analysis is illustrated in figure 6.

A frozen sample is sectioned, usually by cryostat and transferred to a MALDI target plate. The sample may be mounted on backing before the transfer, such as an aluminium backing plate, charged paper film <sup>[96]</sup> or directly onto double-sided standard polymer tape <sup>[97]</sup>. The matrix coating may be applied before or after transfer onto the target plate and a range of matrices and matrix deposition methods have been utilized in various investigations.

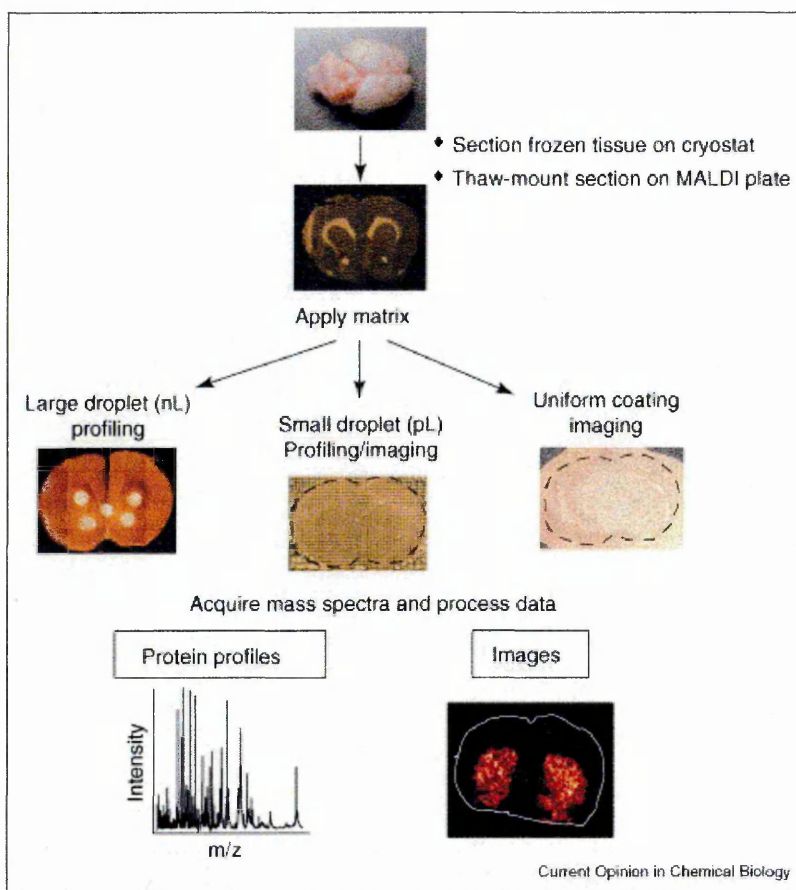


**Figure 1.7** Overview of direct tissue imaging MALDI-MS <sup>[95]</sup>

The matrix application is a critical step in sample preparation and research is ongoing in this field. The correct choice of matrix and application technique is dependant upon the analyte or tissue being investigated, with most published studies opting for airspray deposition <sup>[96]</sup> <sup>[98]</sup>. Recent advances in automated spotting devices will add a new dimension to matrix deposition directly on tissue and the publication of more independent results by these methods is eagerly awaited.

The application of a thin metal layer over the matrix usually by a process of sputter coating has been shown to produce significantly higher analyte and matrix ion yields particularly for low mass analytes <sup>[99]</sup>. Gold and other metals including aluminium and silver have been investigated (unpublished data, Sheffield Hallam University).

### **1.6.1.3 Applications of MALDI-MSI**

#### **1.6.1.3.1 Peptide and Protein Analysis**

Many different tissues have been investigated using MALDI-MSI. Mouse and rat brain sections have been imaged for the presence of protein changes occurring as a result of normal cognitive function <sup>[100, 101]</sup>. Neurological disorders including Parkinson's <sup>[102]</sup> and Alzheimer's <sup>[97]</sup> have been profiled by imaging protein patterns occurring during progression of the disease. Imaging profiling of human brain tumour xenografts has been investigated in a study conducted by Stoeckli et al in 2001 <sup>[103]</sup>. The mass microscope has been used for the investigation of peptides in rat, mouse and human pituitary sections. The increased resolution offered by the mass microscope providing high quality images with a pixel size of 500nm and a resolving power of 4 $\mu$ m <sup>[104]</sup>.

Imaging MALDI-MS is frequently used for the analysis of proteins and biomarkers within tumour regions, tumour margins and within healthy tissue. The analysis is conducted directly on tumour biopsy tissue and without the need for homogenation or separation techniques. Tumours and tissue studied in this way include human brain tumours <sup>[105]</sup> <sup>[106]</sup> allowing for the tumour grade to be determined with a 95% degree of accuracy when combined with statistical algorithms. Other tissues examined include human breast tissue <sup>[107]</sup> and human lung tissue <sup>[106]</sup>.

A recent paper published by Crecelius et al in 2005 is the first to investigate three-dimensional images acquired by MALDI <sup>[108]</sup>. A single mouse brain was sectioned into 264 20µm thick sections 10 of which (in 500µm steps through the tissue) were chosen for imaging MS analysis. A 3D volume was created for all 264 sections by a computer program into which the 10 imaged sections were placed. This allows for full 3D localization of myelin within the brain.

However, spatial information in the 3<sup>rd</sup> dimension is low and many sections would need to be imaged and inserted to provide a high resolution 3 dimensional image.

#### **1.6.1.3.2 Analysis of Pharmaceutical Compounds**

MALDI MS has been utilized to investigate pharmaceutical compound in direct tissue sections. Troendle et al <sup>[109]</sup> profiled the pharmaceutical compound

paclitaxel in human ovarian tumor tissue sections. Imaging MALDI-MS is a highly effective tool for the analysis of small molecules and pharmaceuticals within tissue. It has the particular advantage of allowing a range of drugs and metabolites to be investigated during one experiment in comparison to a specifically labeled technique such as autoradiography. Whole body imaging (such as conducted on rats and mice) enables the localization of metabolites in different organs from an orally administered drug <sup>[110]</sup>. Direct comparison with whole body autoradiography is feasible, with the whole compound and selective metabolites being identifiable in organ tissues. Imaging MALDI-MS offered the advantage of specificity and speed but sensitivity was lower and this differed over the organs due to tissue specific ion signal suppression.

### **1.6.2 Desorption Electrospray Ionization (DESI) Mass Spectrometric Imaging**

Desorption Electrospray Ionization Mass Spectrometry (DESI-MS) is a combination of two ionization methods desorption ionization (DI) and electrospray (ESI). In this process the surface of the sample being analyzed is bombarded with charged droplets of solvent generated via electrospray. Impact of the solvent droplets on the surface causes the ejection of charged particles from the sample which can be measured by typical mass spectrometric methods. The analysis is conducted at atmospheric pressure and without need for a matrix

or other sample interference prior to analysis, therefore enabling true in situ measurement.

Initial results from mass spectrometric imaging experiments utilising DESI as the ion source were published in 2004 by Takats et al <sup>[111]</sup>, imaging alkaloid distribution in plant tissue. These were the first images acquired under ambient conditions and at atmospheric pressure. The results were soon followed by the profiling of thin sections of human liver for a range of phospholipids in metastatic adenocarcinoma tissues <sup>[112]</sup> distinguishing between tumour and non tumour regions. The presented images were acquired as linear profiles as opposed to 2-dimensional maps. A recent publication by Cooks and co-workers <sup>[113]</sup> utilised an automated DESI platform to acquire 2D images of corneal sections of rat brain tissue showing the distinct localisation of individual phospholipids throughout the brain. The sample is placed on the target and is moved under the fixed spray nozzle around the area of interest. Limiting factors for the spatial resolution of DESI imaging include the electrospray capillary diameter and the distance from the spray tip to the sample surface. However significant spatial information is lost from the initial impacting spot diameter and only resolutions as low as 300µm have been demonstrated on biological tissue thus far.

### **1.6.3 Laser Ablation Inductively Coupled Plasma (LA-ICP) Imaging Mass Spectrometry**

Laser ablation inductively coupled plasma mass spectrometry (LA-ICP-MS) is a powerful technique for the analysis of inorganic elements at concentrations ranging from major to trace levels. A pulsed laser beam is used to ablate a small quantity of material from the surface of the sample which is transported into the plasma of the ICP-MS instrument by a stream of Argon carrier gas. The sample to be analyzed is placed in a sample chamber with a quartz glass lid transparent to UV light. A stream of carrier gas enters the sample chamber through a small opening in the floor, travels through the interior of the chamber in a cyclonic pattern and exits at the top, in the process picking up fine sample particles produced by the ablation process and transporting them into the Argon plasma of the ICP-MS instrument. The sample chamber is mounted on a stage that allows the sample to be moved relative to the laser beam. Once passed into the argon plasma source the ablated particles are rapidly ionized and then measured by mass spectrometric techniques, usually by time of flight or quadrupole instrumentation.

LA-ICP-MS is frequently utilised as a powerful microlocal element analytical technique for the fast and direct determination of metal concentrations in biological tissue and protein research <sup>[114]</sup> allowing qualitative localization of both free and protein bound metals.

LA-ICP-MS is a suitable technique for imaging due to a spatial resolution of 50µm or less being achievable as well as being a sensitive and precise method (with the use of an appropriate internal standard). Imaging experiments have been performed by Becker et al <sup>[115]</sup> for the localisation of elements such as P, S, Cu, Zn, Th and U in thin cross sections of rat brain and also human brain hippocampus <sup>[116]</sup>. The published results showed a deficiency of Cu and Zn both in and around tumour regions of the rat brain.

#### **1.6.4 Imaging SIMS and NanoSIMS**

The use of SIMS for imaging purposes enables high quality images to be produced at a resolution unparalleled by alternative mass spectrometric methods. This comes at the expense of a lower mass range than can be achieved by either MALDI or DESI ionization methods. SIMS imaging has been demonstrated at submicron resolution and has been applied to elemental imaging of single cells <sup>[117]</sup>. Many biological tissues have been imaged by ToF-SIMS including human kidney <sup>[118]</sup> nervous tissue <sup>[119]</sup> and aorta <sup>[120]</sup> for both pharmaceutical <sup>[121]</sup> and endogenous compounds <sup>[117, 119]</sup>. The low mass range of SIMS has meant that the compounds studied could only have a low molecular mass or be larger mass molecules which produce characteristic fragment ions enabling identification.

Techniques have been developed to enable a greater ion yield to be obtained from larger mass molecules including coating the sample with an organic acid matrix (in similar techniques as used in MALDI-MS) known as matrix enhanced SIMS (ME-SIMS) <sup>[122]</sup>. This technique can produce spectra comparable to those observed in MALDI for molecules of a mass of up to 2KDa <sup>[123]</sup>. Molecular ions from samples as large as lysozyme have been observed with the addition of the matrix <sup>[123]</sup>. A further method of increasing sensitivity for larger analytes is by the application of a thin coating of metal to the sample surface. Gold, silver and platinum have been demonstrated to increase the yield of large ions such as lipids and fatty acids <sup>[124]</sup> for imaging purposes. Heeren et al reported the most favourable results using coatings less than 5nm thick <sup>[123]</sup>. A complication of this technique is that the ions produced are often observed as metal adducts or clusters. This may make peak assignment more difficult but once the correct peak is identified valuable images may be produced. One impressive example is the distribution of cholesterol within rat kidney sections <sup>[124]</sup> by imaging of the silver cationized molecular ions.

The accepted theory is that the metallic coating results in the production of nano-islands on the sample surface onto which the analytes migrate. Sensitivity is further enhanced by catalytic properties displayed by the nano-islands <sup>[125]</sup>.

High resolution imaging of such high mass compounds would not be possible without the coatings due to the lack of sensitivity exhibited. Ion optics

incorporating gold or bismuth cluster guns <sup>[126, 127]</sup> have been demonstrated to provide a narrow focused beam aptly suited for high resolution microprobe imaging.

SIMS can be combined with tandem mass spectrometry for improved identification of fragment ions. However, images comprised solely of MS/MS data from one fragment will be poor due to the substantial loss in ion current during the MS/MS process <sup>[128]</sup>.

### **1.6.5 Statistical Interpretation of MS-Imaging Data Sets**

New data processing software supplied commercially enables manipulation and new ways of presenting MS images. The application of principal component analysis (PCA) to images enables variance and co-variance of analyte ions in the image to be investigated, which would previously have been impossible due to the amount of data contained in a high resolution image. These new advances in the field point to a bright future for imaging analysis of a range of compounds using this technique.

## **1.7 Conclusion**

The need for the legislation and control of hazardous chemicals is clearly important. The Health and Safety Executive play a crucial role in the monitoring

of occupational exposure to hazardous compounds. Dermal exposure is considered an important route of exposure to many hazardous compounds in the workplace. Advances in current methods for occupational exposure monitoring are constantly being sought by the HSE particularly in the field of dermal penetration studies.

A wide variety of techniques are available for the analysis of compounds in skin although the only one to offer localization of analytes is autoradiography and the lengthy time of analysis is a crucial factor for the proposed monitoring of dermal exposure.

A range of techniques and sample preparation methods have been discussed for the mass spectrometric imaging of biological tissue. Imaging SIMS enables the production of high resolution images (to submicron levels) but at the expense of only operating over a low mass range. Laser ablation ICP imaging mass spectrometry is particularly suited to the analysis of inorganic elements in tissue. It has been demonstrated as a quantifiable technique. DESI-MS imaging is a recently developed technique and has been demonstrated for the analysis of phospholipids in rat brain sections at atmospheric pressure. It enables true *in situ* measurement of analytes as no matrix application or other sample interference in

necessary prior to analysis. However, only low spatial resolutions (300 $\mu$ m) have been demonstrated thus far.

Imaging MALDI-MS in microprobe mode has been shown to be applicable to a wide range of biological imaging applications including dermal penetration studies from membrane blots. With the recent advances in instrumentation and methodology it is proposed as a rapid and sensitive method well suited for the analysis and localization of hazardous compounds both on the skin surface and penetrating into the skin.

The mass microscope enables the rapid production of images at high spatial resolutions by decoupling spatial resolution from the laser spot size. However, current instrumental limitations result in a low mass resolution making this technique unsuitable for the analysis of complex biological tissues.

## 1.8 References

- [1] Boleij, J.S.M., Buringh, E., Heederik, D., Kromhout, H., Occupational Hygiene. In Occupational hygiene of chemical and biological agents. 1<sup>st</sup> edition. 1994 Elsevier
- [2] Trimbali, J.A., types of exposure and response. In: Introduction to toxicology 3<sup>rd</sup> edition. 2002, Taylor and Francis
- [3] Trimbrell, J.A., Factors affecting toxic responses. In: Principles of Biochemical Toxicology 3<sup>rd</sup> Edition. 2000, Taylor Francis
- [4] Nebert, D.W., Inter individual susceptibility to environmental toxicants – A current assessment. Toxicol. Appl. Pharm. 2005, 207 p34-42
- [5] Weyel, D.A., Rodney, B.S., Alarie, Y., Sensory irritation, pulmonary irritation and acute lethality of a polymeric isocyanate and sensory irritation of 2,6-toluene diisocyanate. Toxicol. Appl. Pharm. 1982, 64 p423-430
- [6] Chang – Yeung, M., Lam, S., Occupational asthma. Am. Rev. Respir. Dis. 1986, 133 p686-703
- [7] Bernstein, I.L., Bernstein, D.I., Chang – Yeung, M., Malo, J.L., Defenition and classification of asthma. In: Asthma in the workplace. 1999, New York: Marcel Dekker
- [8] Vandenplas, O., Malo, J.L., Definitions and types of work – related asthma: a nosological approach. Eur. Respir. J. 2003, 21 p706-712

- [9] Surber, C., Wilhelm, K.P., Maibach, H.I., Hall, L.L., Guy, R.H., Partition of chemicals into human stratum corneum: Implications for risk assessment following dermal exposure. *Fundamen. Appl. Toxicol.* 1990, 15 p99-107
- [10] Kezic, S., Mahieu, K., Monster, A.C., De Wolff, F.A., Dermal absorption of vapourous and liquid 2-methoxyethanol and 2-ethoxyethanol in volunteers. *Occor. Environ. Med.* 1997, 53 p38-43
- [11] Rycroft, R.J.G., Occupational Dermatoses. In: textbook of dermatology 6<sup>th</sup> edition. 1998, Blackwell
- [12] Kutting, B., Drexler, H., Effectiveness of skin protection creams as a preventive measure in occupational dermatitis: a critical update according to criteria of evidence-based medicine. *Int. Arch. Occup. Environ. Health.* 2003, 76 p253-259
- [13] Zhai, H., Maibach, H.I., effect of barrier creams : Human skin in vivo. *Contact Dermat.* 1996, 35 p92-96
- [14] Cohen, D.E., Contact dermatitis: a quarter century perspective. *J. Am. Acad. Dermaol.* 2004, 51 p60-63
- [15] Health and safety statistics highlights 2002-2003, 2003, HSE Books MISC623
- [16] Wilkinson, J.D., Willis, C.M., Contact dermatitis: irritant. In: Textbook of dematology 6<sup>th</sup> Edition. 1998, Blackwell
- [17] Jacob, S.E., Steele, T., Contact dermatitis and workforce economics. *Semin. Cutan. Med. Surg.* 2006, 25 p105-109

[18] Doutre, M.S., Occupational contact urticaria and protein contact dermatitis. Eur. J. Dermatol. 2005, 15 p419-424

[19] Adams, R.M., Occupational skin disease 3<sup>rd</sup> edition. 1999, WB Saunders Philadelphia

[20] NIOSH (National Institute for Occupational Safety and Health). Allergic and irritant dermatitis. Additional Information. Accessed online <http://www2a.cdc.gov/nora/NaddinfoAllergy.html> - 12-December 2006

[21] Health and safety act at work, 1974, 2000 edition. Her Majesty's Stationary Office UK

[22] The control of substances hazardous to health regulations 2002. The stationary office Ltd UK

[23] The notification of new substances regulations 1993. The stationary office ltd UK

[24] Chemicals (hazard information and packaging for supply) 2002. The stationary office ltd UK

[25] Yu J.T., The Epidermis  
<http://sprojects.mmi.mcgill.ca/dermatology/epidermis.htm> 2003. Last accessed 22/10/2005 at SHU.

[26] Gawkrödger, D.J., Dermatology: An Illustrated Colour Text, 2nd ed., Churchill Livingstone, New York, 1997, p2.

[27] Elias P.M., Epidermal Lipids, Barrier Function and Desquamation. J. Invest. Dermatol. 1983, 80, p44-49

- [28] Flynn, G. L. (1990). Physicochemical determinants of skin absorption. In Principles of Route-to-Route Extrapolation for Risk Assessment (T. R. Gerrity and C. J. Henry, Eds.), pp. 93–127. Elsevier Science Publishing, New York.
- [29] Moss G.P., Dearden J.C., Patel H., Cronin M.D., Quantitative Structure Permeability Relationships for Percutaneous Absorption. Toxicology in Vitro. 2001, 8, p1-119
- [30] Ceve G., Blume B., Schatlien A., Gebauer D., Paul A., The Skin: A Pathway for Treatment with Patches and Lipid-Based Agent Carriers. Adv. Drug Delivery Reviews. 1996, 18, p349-378
- [31] Gray, G.M. and Yardley, H.J., Lipid compositions of cells isolated from pig, human, and rat epidermis. J. Lipid Res. 1975, 16 p434–440
- [32] Meyer, W., Schwarz, R and Neurand, K., The skin of domestic mammals as a model for the human skin, with special reference to the domestic pig. Curr. Probl. Dermatol. 1978, 7 p39–52
- [33] Dick, I.P and Scott, R.C., Pig ear skin as an in-vitro model for human skin permeability. J. Pharm. Pharmacol. 1992, 44 p640–645.
- [34] Sato, K., Sugibayashi, K and Y. Morimoto, Species differences in percutaneous absorption of nicorandil. J. Pharm. Sci. 1991, 80 p104–107
- [35] Chambin, O., Bevenan, B and Teillaud, E., Pig skin as an animal model for in-vitro percutaneous absorptions studies. Prediction Percutan Penetrat. 1993, 38 p111–116.

- [36] Wester, R.C., Christoffel, J.C., Hartway, T., Poblete, T., Maibach, H.I and Forsell, J., Human cadaver skin viability for in vitro percutaneous absorption: storage and detrimental effects of heat-separation and freezing. *Pharm. Res.* 1998, 15 p82–84
- [37] Casting, G.B and Bowman, L.A., Electrical analysis of fresh, excised human skin: a comparison with frozen skin. *Pharm. Res.* 1990, 7 p1141–1146
- [38] Harrison, S.M., Barry, B.W and Dugard, P.H., Effect of freezing on skin permeability. *J. Pharm. Pharmacol.* 1984, 36 p261–262
- [39] Babu, R.J., Kanikkannan, N., Kikwai, L., Ortega, C., Andega, S., Ball, K., Yim, S and Singh, M., The influence of various methods of cold storage of skin on the permeation of melatonin and nimesulide. *J. Control. Rel.* 2003, 86 p49-57
- [40] Amsden, B.G., Goosen, M.F.A., Transdermal delivery of peptide and protein drugs: an overview, *AIChE Journal.* 1995, 41 p1972-1997
- [41] Kalia, Y. N and Guy, R. H. Modeling transdermal drug release. *Advanced Drug Delivery Reviews.* 2001, 48 p159-172
- [42] Hosteynek, J.J., Factors determining percutaneous metal absorption. *Food and Chemical Toxicology.* 2003, 41 p327-345
- [43] Fabin, B and Touitou, E., Localization of lipophilic molecules penetrating rat skin in vivo by quantitative autoradiography. *Int. J. Pharm.* 1991, 74 p59–65
- [44] Stumpf, W.E., Vitamin D sites and mechanisms of action: A histochemical perspective. Reflections on the utility of autoradiography and cytopharmacology for drug targeting, *Histochem. Cell Biol.* 1995, 104 p417–427

[45] Dary, C.C., Blancato, J.N., Saleh, M.A., Chemomorphic analysis of malathion in skin layers of the rat: implications for the use of dermatopharmacokinetic tape stripping in exposure assessment to pesticides, *Regul. Toxicol. Pharmacol.* 2001, 34 p234-248

[46] Barthe, N., Coulon, P., Hennion, C., Ducassou, D., Basse-Cathalinat, B and Charpak, G., Optimization of a new scintillation gas detector used to localize electrons emitted by <sup>99m</sup>Tc, *Journal of Nuclear Medicine.* 1999, 40 p868-875

[47] Santhanam, A., Miller, M.A., and Kasting, G.B., Absorption and evaporation of *N,N*-diethyl-*m*-toluamide from human skin in vitro, *Toxicol. Applied Pharmacol*

[48] Rougier, A., Lotte, C and Maibach, H.I., In vivo percutaneous penetration of some organic compounds related to anatomic site in humans: predictive assessment by the stripping method. *J. Pharm. Sci.* 1987, 76 p451–454

[49] R.G. van der Molen, Spies, F., van't Noordende, J.M., Boelsma, E., Mommaas, A.M and Koerten, H.K., Tape stripping of human stratum corneum yields cell layers that originate from various depths because of furrows in the skin. *Arch. Dermatol. Res.* 1997, 289 p514–518

[50] Marttin, E., Neelissen-Subnel, M.T.A., De Haan, F.H.N and Bodde, H.E., A critical comparison of methods to quantify stratum corneum removed by tape stripping. *Skin Pharmacol.* 1996, 9 p 69–77.

[51] Klimich, H.M and Chandra, G., Use of Fourier transform infrared spectroscopy with alternate total reflectance for in vivo quantification of polydimethylsiloxanes on human skin. *J. Soc. Cosmet. Chem.* 1986, 37 p73–87

[52] Singh, S., Singh, J., Percutaneous absorption, biophysical, and macroscopic barrier properties of porcine skin exposed to major components of JP-8 jet fuel, *Environmental Toxicology and Pharmacology*. 2003 , 14 p77-85

[53] Sennhenn, B., Giese, K., Plamann, K., Harendt N and Kolmel, K., In vivo evaluation of the penetration of topically applied drugs into human skin by spectroscopic methods. *Skin Pharmacol*. 1993, 6 p152–160.

[54] Jansen, L.M., Hojyo-Tomodo, M.T and Kligman, A.M., Improved fluorescence staining for estimating turnover of the human stratum corneum. *Br. J. Dermatol*. 1974, 90 p9–12.

[55] Lieb, L.M., Ramachandran, C., Egbaria, K and Weiner, N., Topical delivery enhancement with multilamellar liposomes into pilosebaceous units: 1. In vitro evaluation using fluorescent techniques with the hamster ear model. *J. Invest. Dermatol*. 1992, 99 p108–113

[56] Kolmel, K., Sennhen, B and Giese, K., Evaluation of drug penetration into the skin by photoacoustic measurement. *J. Soc. Cosmet*. 1986, 37 p375–385

[57] Thomson J.J., On the Masses of the Ions in Gases at Low Pressures, *Philosophical Magazine*, 1899, 48 p547-567

[58] Dempster A.J., A new method of positive ray analysis, *Physics Review*, 1918, 11, p316-324

[59] Aston F.W., The Mass Spectra of Chemical Elements, *Philosophical Magazine*, 1920 39 p611-635

[60] Nier, A. O. *Nat. Bur. Stand. Circ. (U.S.)* 1953, 522, p29-36

- [61] Stephens W., Physics Review, 1946, 69 p.691
- [62] Paul W., Steinwedel H., A new Mass Spectrometer Without Magnetic Field, Z. Naturforsch., 1953, 8A, p448-450
- [63] Wiley W.C., McLaren, I.H., Time of Flight Mass Spectrometer with Improved Resolution, Rev.Sci.Instrum., 1955, 26 p1150-1157
- [64] Guilhaus, M., Principles and Instrumentation in Time of Flight Mass Spectrometry. Physical and Instrumental Concepts, Journal of Mass Spectrometry, 1995, 30, p1519-1532
- [65] Mamyurin B.A., Time-of-flight mass spectrometry (concepts, achievements, and prospects), International Journal of Mass Spectrometry, 2001, 206, p251-266
- [66] Ingendoh, A., Karas, M., Hillenkamp, F. and Giessmann, U., Factors affecting the mass resolution in matrix-assisted laser desorption-ionization mass spectrometry. Int. J. Mass Spectrom. Ion Process. 1994, 131 p 345
- [67] Vestal, M.L., Juhasz, P., and Martin, S.A., Delayed Extraction Matrix Assisted Laser Desorption Time of Flight Mass Spectrometry, Rapid Comms in Mass Spectrometry, 1995, 9, p1044-1050
- [68] Chernushevich, I.V., Loboda, A.V., Thomson, B.A., An introduction to quadrupole time of flight mass spectrometry. J.Mass Spectrom, 2001, 36 p849-865
- [69] Steen, H., Kuster, B., Mann, M., Quadrupole time of flight versus triple quadrupole mass spectrometry for the determination of phosphopeptides by precursor ion scanning. J.Mass Spectrom. 2001, 36 p782-790

[70] Karas M., Hillenkamp F., Laser Desorption Ionisation of Proteins with Molecular Masses exceeding 10,000 Daltons, *Anal.Chem*, 1988, 60 p2299-2301

[71] Tanaka K., Waki H., Ido Y., Akita S., Yoshida, Y., Yoshida T., Protein and Polymer Analyses up to  $m/z$  100,000 by Laser Ionisation Time of Flight Mass Spectrometry, *Rapid Comm. Mass Spectrom.* 1988, 2, p151-153

[72] Harvey D. J., Matrix Assisted Laser Desorption Ionisation Mass Spectrometry of Oligosaccharides and Glycoconjugates. *J. Chromatogr*, 1996, 720, p429-426

[73] Knochenmuss, R., Dubois, F., Dale, M.J., Zenobi, R., Matrix suppression effect and ionization mechanisms in matrix assisted laser desorption ionization. *Rapid Comm. Mass Spectrom.* 1996, 10 p871-877

[74] Chang, W.C., Huang, L.C.L., Wang, Y.S., Peng, W.P., Chang, H.C., Hsu, N.Y., Yang, W.B., Chen, C.H., Matrix assisted laser desorption ionization mechanism revisited. 2007, 582 p1-9

[75] Karas, M., Gluckmann, M., Schafer, J., Ionization in matrix assisted laser desorption ionization: singly charged molecular ions are the lucky survivors. *J.Mass Spectrom.* 2000, 35 p1-12

[76] Karas, M., Kruger, R., Ion formation in MALDI: the cluster ionization mechanism. *Chem.Rev.* 2003, 103 p427-439

[77] Crecelius, A., Clench, M.R., Richards, D., Parr, V., Thin layer chromatography-matrix assisted laser desorption ionization time-of-flight mass spectrometry using particle suspension matrices. *J. Chromat.* 2002, 958 p249-260

[78] Ren, S.F., Guo, Y.I., Oxidized carbon nanotubes as matrix for matrix-assisted laser desorption/ionization time-of-flight mass spectrometric analysis of biomolecules. *Rapid Comm. Mass Spectrom.* 2004 19 p255-260

[79] Barofsky, B.F., Giessmann, U., Swanson, L.W., Bell, A.E., Molecular sims with a liquid metal field ion point source. I. *J. Mass Spectrom. Ion Phys.* 1983, 46 p495-497

[80] Appelhans, A.D., Delmore, J.E., Comparisons of polyatomic and atopic primary beams for secondary ion mass spectrometry of organics. *Anal. Chem.* 1989, 61 p1087-1099

[81] Nordmann, C., Suckau, D., Kowlaski, P., Gvozdyak, O., Performance differences between YAG and nitrogen lasers for various MALDI applications. In proceedings of the 53<sup>rd</sup> ASMS conference on mass spectrometry and applied topics, presented San Antonio 2005

[82] Holle, A., Haase, A., Kayser, M., Hohndorf, J., Optimising UV laser focus profiles for improved MALDI performance. *J. Mass Spectrom.* 2006, 41 p705-716

[83] Luxembourg, S.L., McDonnell, L.A., Mize, T.H., Heeren, R.M.A., Infrared mass spectrometric imaging below the diffraction limit. *J. Proteom. Res.* 2004, 4 p672-675

[84] Jurchen, J., Rubakin, S.S., Sweedler, J.V., MALDI-MS imaging of features smaller than the size of the laser beam. *J. Am. Soc. Mass Spectrom.* 2005, 16 p1654-1659

[85] Luxembourg, S.L., Mize, T.H., McDonnell, L.A., Heeren, M.R.A., High spatial resolution mass spectrometric imaging of peptide and protein distributions on a surface. *Anal. Chem.* 2004, 76 p5339-44

[86] Luxembourg, S.L., Vaezaddeh, A.R., Amstalden, E.R., Zimmermann-Ivol, C.G., Hochstrasse, D.F., Heeren, R.M.A., The molecular scanner in microscope mode. *Rapid Comm. Mass Spectrom.* 2006, 20 p3435-3442

[87] Caprioli, R.M., Farmer, T.B., and Gile, J. Molecular Imaging of Biological Samples : Localisation of Peptides and Proteins Using MALDI-TOF-MS, *Anal. Chem.*, 1997, 69, p4751-4760

[88] Bunch, J., Clench M. R., Richards D.S., Determination of Pharmaceutical Compounds in Skin by Imaging Matrix Assisted Laser Desorption Ionisation Mass Spectrometry, *Rapid Comm. Mass Spec.*, 2004, 18, p3051-3060

[89] Garrett, T.J., Yost, R.A., Analysis of intact tissue by intermediate pressure MALDI on a linear ion trap mass spectrometer. *Anal. Chem.* 2006, 78 p2465-2469

[90] Aerni, A.R., Cornett, D.S., Caprioli, R.M., Automated acoustic matrix deposition for MALDI sample preparation. *Anal. Chem.* 2006, 78 p827-834

[91] Chaurand, P., Direct Profiling of proteins in Biological Tissue Sections by MALDI Mass Spectrometry, *Anal. Chem.* 1999, 71, p5263-5270

[92] Zaluzec E.J., Gage D.A., Allison J., Watson J.T., Direct Matrix Assisted Laser Desorption ionisation Mass Spectromeric Analysis of Proteins Immobilised on Nylon Based Membranes. *J. Am. Soc. Mass Spec.* 1994, 5, p230-237

- [93] Preston L.M., Murray K.K., Russell D.H., Reproducibility and Quantification of MALDI-MS: Effects of Nitrocellulose on Peptide Ion Yields. *Biol. Mass. Spec.* 1993, 22, p544-550
- [94] Blackage J.A., Alexander A.J., Polyethylene Membrane as a Sample Support for Direct Matrix Assisted Laser Desorption Ionisation Mass Spectrometric Analysis of High Mass Proteins. *Anal. Chem.* 1995, 67, p843
- [95] Reyzer, M.L., Caprioli, R.M., MALDI-MS based imaging of small molecules and proteins in tissues. *Curr. Op. Chem. Bio.* 2007, 11 p1-7
- [96] Khatib-Shahidi, S., Andersson, M., Herman, J.L., Gillespie, T.A., Caprioli, R.M., Direct molecular analysis of whole body tissue sections by imaging MALDI mass spectrometry. *Anal. Chem.* 2006, 78 p6448-6456
- [97] Stoeckli, M., Staab, D., Staufenbiel, M., Wiederhold, K.H., Signor, L., Molecular imaging of amyloid  $\beta$  peptides in mouse brain sections using mass spectrometry. *Anal. Biochem.* 2002, 311 p33-39
- [98] Rohner, T.C., Staab, D., Stoeckli, M., MALDI mass spectrometry imaging of biological tissue sections. *Mech. Ageing Dev.* 2005, 126 p177-185
- [99] McCombie, G., Knochenmuss, J., Enhanced MALDI ionization efficiency at the metal matrix interface: Practical and mechanistic consequences of sample thickness and preparation method. *Am. Soc. Mass Spectrom.* 2006, 17 p737-746
- [100] Laurent, C., Levinson, D.F., Schwartz, S.A., Harrington, P.B., Markey, S.P., Caprioli, R.M., Levitt, P., Direct profiling of the cerebellum by matrix assisted laser desorption/ionization time-of-flight mass spectrometry: a methodological study in postnatal and adult mouse. *J. Neurosci. Res.* 2005, 81 p613-621

[101] Ceuppens, R., Dumont, D., Brussel, L.V., Van de Plas, B., Daniels, R., Noben, J.P., Verhaert, P., Van der Gucht, E., Robben, J., Clerens, S., Arckens, L., Direct profiling of myelinated and demyelinated regions in mouse brain by imaging mass spectrometry. *Int. J. Mass Spectrom.* 2007, 260 p185-194

[102] Pierson, J., Norris, J.L., Aerni, H.R., Svenningsson, P., Caprioli, R.M., Andren, P.E., Molecular profiling of experimental Parkinson's disease: direct analysis of peptides and proteins on brain tissue sections by MALDI mass spectrometry. *J. Proteom. Res.* 2004, 3 p289-295

[103] Stoeckli, M., Chaurand, P., Hallahan, P.E., Caprioli, R.M., Imaging mass spectrometry: A new technology for the analysis of protein expression in mammalian tissues. *Nat. Med.* 2001, 7 p493-496

[104] Altelaar, A.F.M., Taban, I.M., McDonnell, L.A., Verhaert, P.D., de Lange, R.P.J., Adan, R.A.H., Mooi, W.J., Heeren, R.M.A., Piersma, S.R., High-resolution MALDI imaging mass spectrometry allows localization of peptide distributions at cellular length scales in pituitary tissue sections. *Int. J. Mass Spectrom.* 2007, 260 p203-211

[105] Schwartz, S.A., Weil, R.J., Thomson, R.C., Shyr, Y., Moore, J.H., Toms, S.A., Johnson, M.D., Caprioli, R.M., Proteomic based prognosis of brain tumour patients using direct-tissue matrix assisted laser desorption ionization mass spectrometry. *Cancer Res.* 2005, 65 p7674-7681

[106] Yanagisawa, K., Shyr, Y., Xu, B.J., Massion, P.P., Larsen, P.H., White, B.C., Roberts, J.R., Edgerton, M., Gonzalez, A., Nadaf, S., Proteomic patterns of tumour subsets in non-small-cell lung cancer. *Lancet.* 2003, 362 p433-439

[107] Cornett, D.S., Mobley, J.A., Dias, E.C., Andersson, M., Artega, C.L., Sanders, M.E., Caprioli, R.M., A novel histology directed strategy for MALDI MS

tissue profiling that improves throughput and cellular specificity in human breast cancer. *Molecular Cellular Proteom.* 2006, 5 p1975-1983

[108] Crecelius, A.C., Cornett, D.S., Caprioli, R.M., Williams, B., Dawant, B.M., Bodenheimer, B., Three-dimensional visualization of protein expression in mouse brain structures using imaging mass spectrometry. *J. Am. Soc. Mass Spectrom.* 2005, 16 p1093-1099

[109] Troendle, F., Reddick, C.D., Yost, R.A. Detection of Pharmaceutical Compounds in Tissue by Matrix Assisted Laser Desorption Ionisation and Laser Desorption Chemical Ionisation Tandem Mass Spectrometry with a Quadrupole Ion Trap. *J. Am. Soc. Mass. Spec.* 1999, 10, p1315-1321

[110] Stoeckli, M., Staab, D., Schweitzer, A., Compound and metabolite distribution measured by MALDI mass spectrometric imaging in whole-body tissue sections. *Int. J. Mass Spectrom.* 2007, 260 p195-202

[111] Takats, Z., Wiseman, J.M., Gologan, B., Cooks, R.G., mass spectrometry sampling under ambient conditions with desorption electrospray ionization. *Science.* 2004, 306 p471-473

[112] Wiseman, J.M., Puolitaival, S.M., Takats, Z., Cooks, R.G., Caprioli, R.M., Mass Spectrometric Profiling of Intact Biological Tissue by Using Desorption Electrospray Ionization. *Angew. Chemie.* 2005, 44 p7094-7097

[113] Ifa, D.R., Wiseman, J.M., Song, Q., Cooks, R.G., Development of capabilities for imaging mass spectrometry under ambient conditions with desorption electrospray ionization (DESI). *Int. J. Mass Spectrom.* 2007, 259 p8-15

[114] Becker, S.J., Zoriy, M., Pickhardt, C., Przybylski, M., Becker, J.S., Investigation of Cu, Zn and Fe-containing human brain proteins using isotope enriched tracers by LA-ICP-MS and MALDI-FTICR-MS. *Int. J. Mass spectrom.* 2005, 242 p135-144

[115] Becker, J.S., Zoriy, M.V., Pickhardt, C., Denhandt, K., Zilles, K., Copper, zinc, phosphorus and sulfur distribution in thin section of rat brain tissues measured by laser ablation inductively coupled plasma mass spectrometry: possibility for small-size tumor analysis. *Anal. At. Spectrom.* 2005, 20 p912

[116] Becker, J.S., Zoriy, M.V., Pickhardt, C., Palomero-Gallagher, N., Zilles, K., Imaging of Copper, Zinc, and Other Elements in Thin Section of Human Brain Samples (Hippocampus) by Laser Ablation Inductively Coupled Plasma Mass Spectrometry. *Anal. Chem.* 2005, 77 p3208-3216

[117] Chandra, S., Lorey, D.R., SIMS ion microscopy imaging of boronophenylalanine (BPA) and  $^{13}\text{C}^{15}\text{N}$ -labelled phenylalanine in human glioblastoma cells: relevance of subcellular scale observations to BPA-mediated boron neutron capture therapy of cancer. *Int.J. Mass Spectrom.* 2007, 260 p90-101

[118] Touboul, D., Roy, S., Germain, D.P., Chaminade, P., Brunelle, A., Laprevote, O., MALDI-ToF and Cluster-ToF SIMS imaging of Fabry disease biomarkers. *Int. J. Mass Spectrom.* 2007, 260 p158-165

[119] Sjovall, P., Lausmaa, J., Johansson, B., Mass spectrometric imaging of lipids in brain tissue. *Anal. Chem.* 2004, 76 p4271-4278

[120] Malmberg, P., Borner, K., Chen, Y., Friberg, P., Haggendorf, B., Mansson, J.E., Nygren, H., Localization of lipids in the aortic wall with imaging TOF-SIMS. *Biochim. Biophys. Acta.* 2007, doi10.1016/j.bbailip.2006.12.003

[121] Chandra, S., Smith, D.R., Morrison, G.H., Dynamic secondary ion mass spectrometry of boron from boron neutron capture therapy drugs in co-cultures: single cell imaging of two different cell types within the same ion microscopy field of imaging. *Anal. Chem.* 2001, 73 p3947-3953

[122] Wu, K.J, Odom, R.W., Matrix enhanced secondary ion mass spectrometry: a method for molecular analysis of solid surfaces. *Anal. Chem.* 1996, 68 p873-882

[123] McDonnell, L.A., Heeren, R.M.A., de Lange, R.P.J., Fletcher, I.W., Higher sensitivity secondary ion mass spectrometry of biological molecules for high resolution, chemically specific imaging. *J. Am. Soc. Mass Spectrom.* 2006, 17 p1195-1202

[124] Nygren, H., Malmberg, P., Kriegeskotte, C., Arlinghaus, H.F., Bioimaging TOF-SIMS: localization of cholesterol in rat kidney sections. *FEBS. Lett.* 2004, 566 p291-293

[125] Delcourte, A., Bour, J., Aubriet, F., Muller, J.F., Bertrand, P., Sample metallization for performance improvement in desorption ionization of kilodalton molecules: quantitative evaluation, imaging secondary ion MS and laser ablation. *Anal. Chem.* 2003, 75 p6875-6885

[126] Benguebera, M., Brunelle, A., Della-Negra, S., Depauw, J., Joret, H., Le Beyec, Y., Blain, M.G., Schweikert, E.A., Assayag, G.B., Sudraud, P., Impact of slow gols clusters on various solids: nonlinear effects in secondary ion emission. *Nucl. Instrum. Methods Phys. Res.* 1991, 62 p8-22

[127] Touboul, D., Kollmer, F., Niehuis, E., Brunelle, A., Laprevote, O., Improvement of biological secondary ion mass spectrometry imaging with bismuth cluster ion source. *J. Am. Soc. Mass Spectrom.* 2005, 16 p1608-1618

[128] Todd, P.J., Schaaff, T.G., Chaurand, P., Caprioli, R.M., Organic ion imaging of biological tissue with secondary ion mass spectrometry and matrix assisted laser desorption/ionization, *J. Mass. Spectrom.* 2001, 36 p355-369

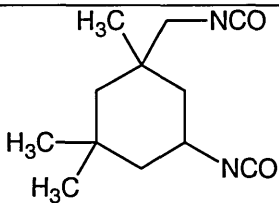
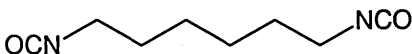
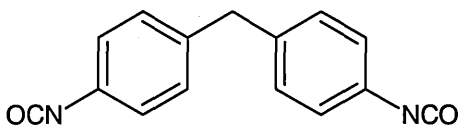
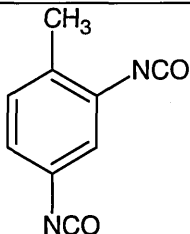
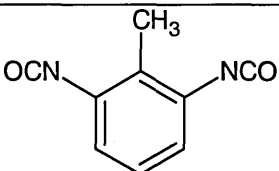
## **2.0 Applications of MALDI-MS to the Study of Diisocyanate Stability and Introduction of a Novel Ethanol-Derivatization Method for Extraction from Workplace Surfaces**

## 2.1 Introduction

### 2.1.1 Introduction to Isocyanates

Isocyanates are a group of highly reactive compounds containing the functional group NCO. Diisocyanates (molecules containing two functional isocyanate groups) are the most important for industrial use. Isocyanates can be either aliphatic or aromatic. A list of diisocyanates commonly used in industry is shown in table 2.1. 1,6-hexamethylene diisocyanate (HDI) 4,4-methylene biphenyl diisocyanate (MDI) 2,4- and 2,6-toluene diisocyanate (2,4-and 2,6-TDI) account for greater than 90% of commercially used diisocyanates in the UK <sup>[1]</sup>

Isocyanates have a variety of uses in industry, the most common being in the manufacture of polyurethane foams and paints <sup>[2]</sup>. The most recent major survey on isocyanate use and control in the UK was conducted by the HSE in 2005 <sup>[3]</sup>. A wide variety of industrial uses were investigated including motor vehicle repair (MVR), foam manufacturers, vehicle manufacturers, coatings and adhesives, industrial painters, printers and laminators and insulation contractors.

Isocyanate Name	Molecular Weight	Structural Formula
Isophorone diisocyanate (IPDI)	222.3	
1,6-Hexamethylene diisocyanate (HDI)	168.2	
4,4-Methylenebiphenyl diisocyanate (MDI)	250.3	
2,4-Toluene diisocyanate (2,4-TDI)	174.2	
2,6-Toluene diisocyanate (2,6-TDI)	174.2	

**Table 2.1** Structural information for common industrial diisocyanate monomers

For the majority of industries and tasks investigated in this study the amount of recorded airborne NCO was small (below  $1\mu\text{g NCO}/\text{m}^3$  in 75% of cases). The largest single group of reported isocyanate users was small firms (less than 5

employees) car body repairers and the highest measurements of NCO were collected during the spray painting process in the truck and car manufacturing industry.

Maximum isocyanate exposure limits (as specified by COSHH regulations) are  $20\mu\text{g}/\text{m}^{-3}$  over an 8 hour period. A short term exposure limit, 15 minute reference period, of  $70\mu\text{g}/\text{m}^{-3}$  is specified <sup>[4]</sup>. This limit is expressed as weight of total NCO groups not of a specific monomer or other NCO containing unit.

### **2.1.2 Hexamethylene Diisocyanate and Pre-Polymers**

HDI is an aliphatic isocyanate that is used almost exclusively in the manufacture of paints and surface coatings due to the presence of the aliphatic radical which provides light and weather stability to the painted product. The majority of 2-component spray paints contain HDI in biuret or isocyanurate ring form as shown in figure 2.1. The pre-polymers have higher molecular weights and are thus less volatile than their parent monomer. They still contain reactive isocyanate groups which may be inhaled when generated in aerosol form during the spraying process <sup>[5, 6]</sup>. At the time of manufacture, biuret prepolymer contains approximately 0.7% of the HDI monomer. However, the monomeric HDI content may increase to as much as 1.6% due to *in situ* breakdown of the biuret <sup>[7]</sup>. The HDI polyurethane component of the coating may undergo thermal degradation to

the HDI monomer and reactive pre polymer forms, thus increasing the amount of reactive monomer present [8].

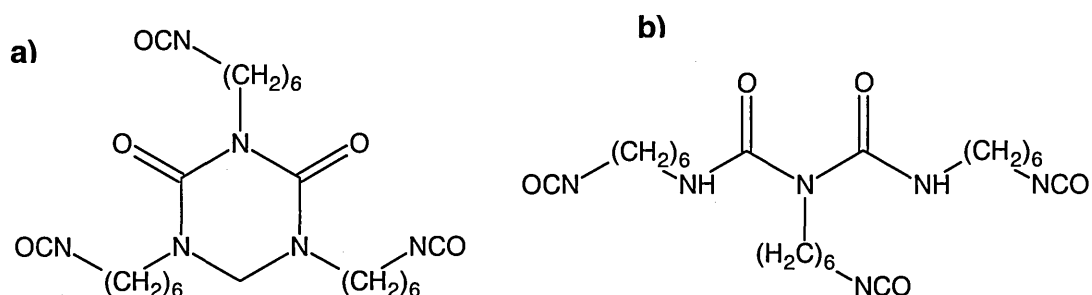


**Figure 2.1** Pre-polymer forms of HDI: **a)** isocyanurate ring and **b)** HDI biuret

### 2.1.3 Reactivity of Isocyanates

Isocyanates will react with one or more alcohol groups to form a urethane (figure 2.2). Polyurethanes (as used in spray paints) are manufactured using poly-functional NCOs (such as HDI biuret or isocyanurate) and poly-functional alcohols (polyols).

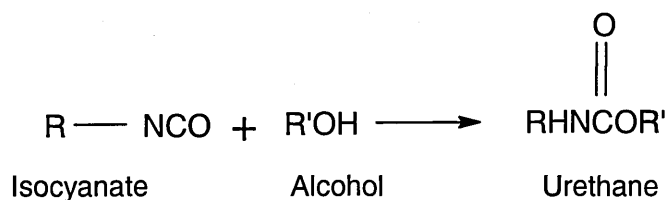


**Figure 2.2** The formation of a urethane from the reaction of an isocyanate with an alcohol

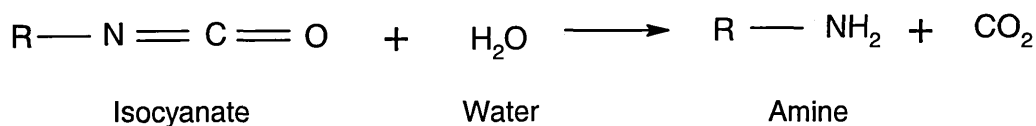


**Figure 2.3** The hydrolysis of an isocyanate to an amine with the release of carbon dioxide

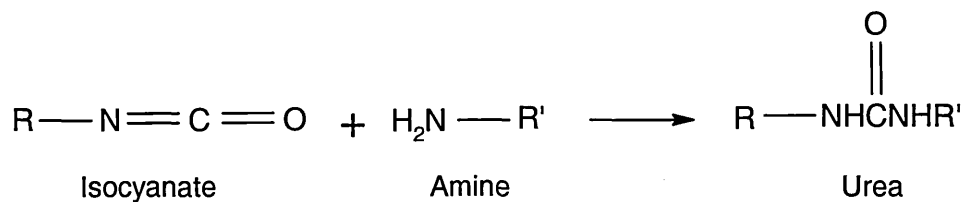


**Figure 2.4** The formation of a urea from the reaction of an isocyanate with an amine

Isocyanates are highly reactive with water and will readily hydrolyse to their corresponding amine as shown in figure 2.3. These amines can react with further intact isocyanate groups to form a urea (figure 2.4). In the case of diisocyanates (difunctional isocyanates), large polyurea polymer chains can be constructed by

hydrolysis of one NCO group and subsequent reactions between the resulting NH<sub>2</sub> and further diisocyanate molecules

Due to the highly reactive nature of the isocyanates, sample analysis can be compromised. Derivatizing the isocyanate with a suitable derivatizing agent is the preferred method of stabilizing isocyanates for storage and analysis

#### **2.1.4 Potential for Isocyanate Exposure**

Occupational exposure to airborne isocyanates is of great concern. Pulmonary exposure may result from inhalation of vaporized monomeric isocyanates (such as TDI) or by larger / less volatile isocyanates in aerosol form (i.e HDI pre-polymers) <sup>[6]</sup>.

There is significant opportunity for dermal exposure to occur even with use of full personal protective equipment (PPE) <sup>[9]</sup>. Any penetration, by a hazardous compound, of coveralls or protective gloves leads to prolonged exposure. Most research on protective gloves has concentrated on permeation and durability particularly for solvents and solvent-based products. However, investigations have shown that chemical agent penetration inside protective gloves is common, if not inevitable, for dusts, water-based and solvent-based products alike <sup>[10]</sup> and that resultant hand exposure inside gloves is prolonged and occluded <sup>[11]</sup>.

### 2.1.5 Occupational Health

With the dramatically increased use of polyurethane paints, plastics, foams and coatings, diisocyanates have emerged as the most commonly identified cause of occupationally induced asthma in the developed world <sup>[12]</sup>. It is estimated that approximately 5-20% of workers exposed to diisocyanates develop asthma with the possibility of sensitisation increasing with prolonged exposure time and increased frequency <sup>[13]</sup>. The majority of investigations have concentrated on occupational exposure to airborne isocyanates

Studies conducted previously have concluded that monomeric, pre-polymeric and polyisocyanate species are all capable of causing asthma in exposed workers <sup>[14, 15]</sup>. Despite the substantial research on isocyanates, the pathogenic mechanisms, host-susceptibility factors and dose response relationship remain unclear <sup>[16]</sup>.

The primary route of exposure and sensitisation is believed to be via inhalation of airborne isocyanates via the respiratory tract. Studies conducted using animal models have suggested however, that dermal exposure to isocyanates may also be an important route of respiratory sensitisation. An investigation conducted by Karol in 1981 concluded that dermal exposure of guinea pigs to the isocyanate TDI resulted in pulmonary sensitisation <sup>[17]</sup>. Although the data for human dermal exposure is more limited it is likely that skin exposure can induce isocyanate

sensitization <sup>[18, 19]</sup>. Skin exposure may be especially important with less volatile diisocyanates such as polyisocyanates and MDI, where skin contact may be the main route of exposure. Exposure to isocyanates can also result in contact dermatitis, skin irritation and less commonly hypersensitivity pneumonitis <sup>[22]</sup>.

The high reactivity of the NCO functional group is believed to be key to the sensitization response. Isocyanates can bind to carrier proteins, via reaction of the NCO group with nucleophiles such as the SH, NH<sub>2</sub>, NH and OH groups present in these proteins. Several peptides and proteins found in airway epithelial cells, serum and skin have been observed to bind to diisocyanates. These include albumin <sup>[20]</sup> and keratin <sup>[21]</sup>. The covalent binding of the isocyanate group to these carrier proteins is a vital link leading to sensitization.

## **2.1.6 Monitoring Isocyanate Exposure**

### **2.1.6.1 Airborne Isocyanate**

In the UK, airborne isocyanate exposure is measured by a personal sampler attached directly to a worker <sup>[23]</sup>. The sampler consists of a pump (to maintain and regulate airflow), a filter cartridge and/or an impinger containing a derivatising liquid for trapping and stabilizing the isocyanate.

A measured volume of air is drawn through a glass fibre filter impregnated with the derivatising agent 1-(2-methoxyphenyl) piperazine (1-2MP) and/or an impinger filled with 1-2MP solution. Any organic isocyanate groups present react with the 1-2MP to form non volatile urea derivatives. The filters are desorbed into acetonitrile and the solution may be concentrated prior to analysis. Analysis is conducted by high performance liquid chromatography (HPLC) using ultraviolet and electrochemical detection methods. Quantification is by comparison with the relevant isocyanate monomer standard. Total concentration of isocyanate in air is calculated from the sum of all detected isocyanate derived peaks. Using this method the estimated limit of quantitation is  $\sim 0.1 \mu\text{g NCOm}^{-3}$ .

The use of both the impinger and the impregnated filter enables airborne isocyanates in the vapour phase and airborne aerosol isocyanate particles to be detected. The methodology from which the Health and Safety Executive Method for the Determination of Hazardous Substances (MDHS) was constructed was evaluated by Brown et al in 1984<sup>[24]</sup> and has been demonstrated to be suitable for analysis of both aromatic and aliphatic isocyanates<sup>[25]</sup>. The method has been evaluated for pre-polymer formulations of HDI (Desmodur N3390), TDI (Desmodur L) and MDI (Desmodur VL)<sup>[26]</sup>.

Other derivatising agents have been investigated for stabilizing isocyanates for analysis including 9-(methylaminomethyl)anthracene<sup>[27]</sup>, N-4-nitrobenzyl-n-propylamine<sup>[28]</sup> and 1-(2-pyridyl)piperazine<sup>[29]</sup>. Their mode of action is by the

formation of a stable urea compound by the reaction between the amine derivatising agent and the free NCO groups.

#### **2.1.6.2 Surface and PPE Sampling**

There is no current HSE approved protocol for the extraction and analysis of isocyanates from exposed workplace surfaces. The HSE promote the use of an alcohol wipe method for the extraction of aromatic amines from surfaces in the workplace <sup>[30]</sup>. This method involves wiping a defined area of the surface with a wipe moistened with 1ml of methanol. This is followed by extraction into a further 10ml of methanol. Aliquots are removed and analyzed by high performance liquid chromatography (HPLC).

The US Occupational Safety and Health Administrator (OSHA) propose the use of a wipe sampling method using commercially prepared pads that change colour upon contact with isocyanates <sup>[31]</sup>. These types of indicators are particularly suitable as a screening tool when assessing the extent of surface contamination because they are inexpensive and the results are immediate. If an indicator wipe yields a positive result, a wipe sample can then be taken and sent to a laboratory for confirmation. The colorimetric wipes utilized are SWYPE™ (CLI Colormetric Laboratories) <sup>[32]</sup> and a pink coloration is observed upon contact with isocyanates (which becomes progressively darker with increasing isocyanate concentration).

SWYPES™ are available for both aromatic and aliphatic isocyanates. However, they cannot distinguish between different isocyanates in each respective group and are only indicative of total free NCO present. The sensitivity of the wipes is reported by the manufacturer as being as low as 3-5 µg for aromatic isocyanates.

Once the presence of isocyanates are confirmed by the SWYPE™, OSHA promotes the use of an acetonitrile saturated glass fibre filter wipe (untreated) over a 100cm<sup>2</sup> area of surface exposed to isocyanates. The filter wipe is then placed into a 1ml vial of acetonitrile containing 10 mg of the derivatising agent 1-(2-pyridyl)piperazine. The derivatising agent acts to stabilize and enhance sensitivity of the isocyanate during analysis. HPLC analysis is conducted for the quantitation of TDI [33] or MDI [34].

Chemicals have been observed to penetrate through gloves and personal protective equipment (PPE). The OSHA method for analyzing the penetration of isocyanates through gloves and other PPE is by use of PERMEA-TEC™ sensors (CIL laboratories) [32]. These adhesive colorimetric sensors are placed directly under the workers' PPE before paint spraying commences. At the end of a workers shift period the pads are removed from the worker and any colour change is noted. The pads are available for either aromatic or aliphatic isocyanates with sensitivity as low as 5µg for aromatic isocyanates. The pads cannot differentiate between isocyanates present (except aromatic or aliphatic

forms) and are non quantitative (however, increasing colour depth does relate to increased free NCO content).

### **2.1.7 Aims**

The highly reactive nature of diisocyanates has been discussed. The aim of the investigation was to assess the reactivity of diisocyanates and devise a method for stabilising them prior to analysis. This derivatisation method would then be incorporated into a surface sampling technique which would be applied to occupational exposure monitoring.

## **2.2 Methods**

### **2.2.1 Materials**

Trifluoroacetic acid (TFA), and HPLC grade acetone, acetonitrile, and ethanol were purchased from Fisher (Leicester, U.K). 2,4-Toluene diisocyanate (95% with 4% 2,6 isomer), 1,6-hexamethylene diisocyanate,  $\alpha$ -Cyano-4-Hydroxy Cinnamic Acid ( $\alpha$ -CHCA), titanium oxide and graphite (fine powder) were purchased from Sigma-Aldrich.

### **2.2.2 MALDI-MS Analysis of TDI Using Suspension Matrices**

A 50/50 mixture of titanium oxide / graphite suspension matrix was prepared in acetonitrile at 25 mg/ml. 2 $\mu$ l of the matrix was pipetted on to the target plate and left to dry prior to spotting of TDI (1mg/ml in acetone) onto the dry suspension matrix.

### **2.2.3 Analysis of Ethanol-Derivatised HDI (HDI Urethane)**

Neat HDI was added to ethanol at a concentration of 1 mg/ml. The sample was stored at room temperature for a period of 10 minutes. Aliquots containing a 50 / 50 mixture of HDI in ethanol and  $\alpha$ -CHCA (25mg/ml in ethanol containing 0.1% TFA) were prepared and 1 $\mu$ l of the mixture was spotted onto the target for MALDI-MS analysis.

### **2.2.4 HDI Stability in Acetone**

HDI was added to acetone at concentrations of 1, 0.1, 0.01 and 0.001 mg/ml. 4 repetitions were performed. Samples were analysed at the following time points 0, 1, 2, 3, 5, 7, and 14 days. At each time point aliquots containing a mixture of 5 $\mu$ l of each HDI sample and 5 $\mu$ l of  $\alpha$ -CHCA (25mg/ml in acetone containing

0.1%TFA) were prepared. 1 $\mu$ l of the mixture was spotted onto the target for MALDI-MS analysis.

### **2.2.5 Stability of Ethanol-Derivatized HDI**

HDI was added to ethanol at concentrations of 1, 0.1, 0.01 and 0.001 mg/ml, and 4 repetitions were performed. Samples were analysed at the following time points: 0, 1, 2, 3, 5, 7 and 14 days. At each time point aliquots of a mixture of 5 $\mu$ l of each HDI/ethanol sample and 5 $\mu$ l of  $\alpha$ -CHCA (25mg/ml in ethanol containing 0.1%TFA) were prepared. 1 $\mu$ l of the mixture was spotted onto the target for MALDI-MS analysis.

### **2.2.6 Ethanol Swab Method and Extraction Efficiency**

Standards were prepared by adding HDI to ethanol at 0, 0.2, 0.4, 0.6, 0.8 and 1mg/ml concentrations. 5 x 5 cm square areas were marked on a latex glove and 5 $\mu$ l of neat HDI was pipetted and spread over this area. The sample was left at 18°C for a period of 15 minutes. A sterilized standard hygiene swab (Technical Service Consultants, Lancashire U.K) was fully submerged in ethanol for 5 seconds. The swab was removed and allowed to air-dry for 30 seconds. The swab was then wiped over the marked surface in a snakelike pattern for 30 seconds ensuring the whole area had been covered. The swab was immediately placed into a vial containing 5ml of ethanol and sealed. Four repetitions were

conducted using separate gloves. The method was repeated with swabs being taken from a marked 5 x 5 cm aluminium plate in place of the glove (n=4)

### **2.2.7 Mass Spectrometric Analysis**

All analyses were performed using an Applied Biosystems/MDS Sciex API "Q-Star" Pulsar I hybrid quadrupole time of flight instrument, fitted with an orthogonal MALDI ion source and "O-MALDI Server 4.0" ion imaging software. The Nd:YAG laser used has an elliptical laser spot size of 150  $\mu\text{m}$  x 100  $\mu\text{m}$ . The laser was used at an energy setting of 30% (3.2  $\mu\text{J}$ ) and a repetition rate of 1 kHz. The laser was rastered over the sample spot for 2 minutes following a pre-designed automated spiral search pattern

## **2.3 Results**

### **2.3.1 Analysis of TDI Using Suspension Matrices**

Due to the high reactivity of TDI, suspension matrices were used to prevent any possible reactions occurring between an organic acid matrix (and / or solvent) and the isocyanate.

Spectra were acquired showing the presence of the TDI molecular ion at  $m/z$  174 (figure 2.5). However, a peak was observed at  $m/z$  148 at a much greater intensity than the molecular ion.

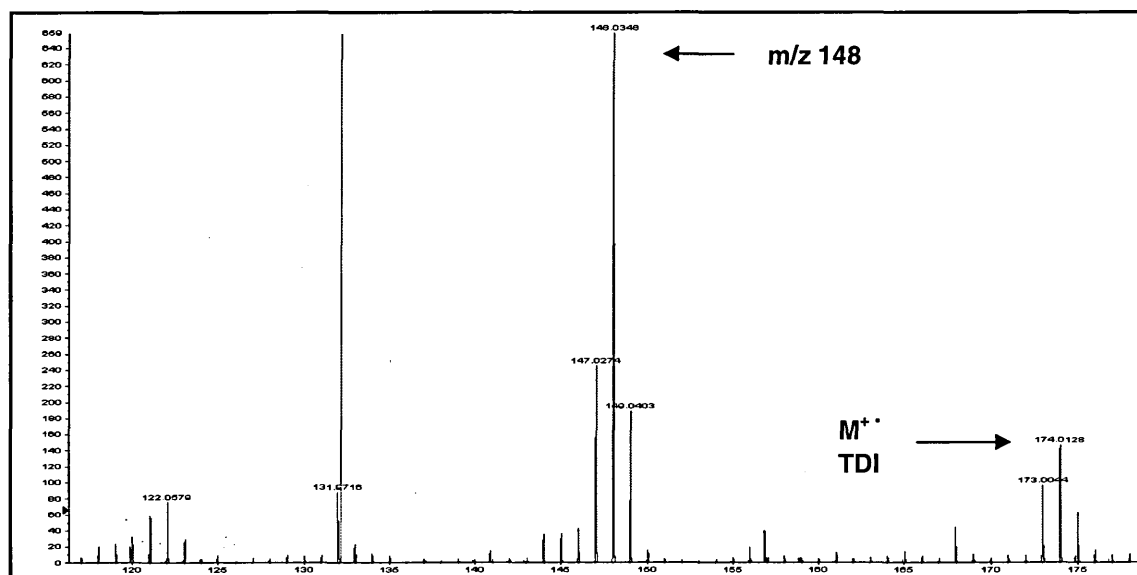
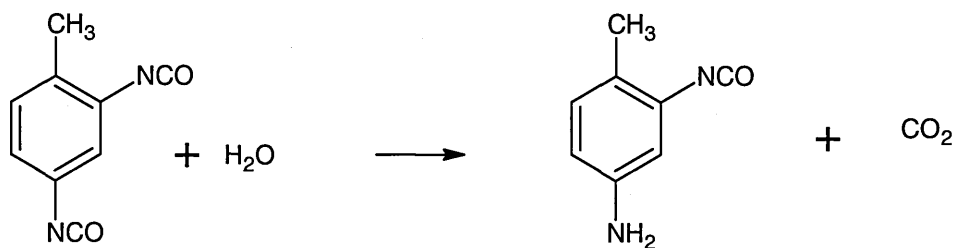


Figure 2.5 MALDI-MS Spectrum showing the presence of  $M^+$  TDI and a subsequent peak at  $m/z$  148

### 2.3.2 Tandem MS of Peak at $m/z$ 148

As the peak at  $m/z$  148 was present in all the TDI spectra produced it was proposed that this was a reaction product, presumably produced during sample preparation. The unknown compound was observed at an  $m/z$  value of 26 lower than TDI. Based on this mass difference the compound shown in figure 2.6 was proposed:



**Figure 2.6** The formation of a TDI derived monoamine by hydrolysis of one NCO group. Carbon dioxide gas is released

It was postulated that during the sample preparation process and exposure to the laboratory atmosphere, one of the isocyanate groups of TDI is hydrolysed to an amine. Isocyanates are known to hydrolyse readily to amines in the presence of water. Tandem mass spectrometry was performed on both the TDI molecular ion and the proposed TDI-derived monoamine to confirm the structure.

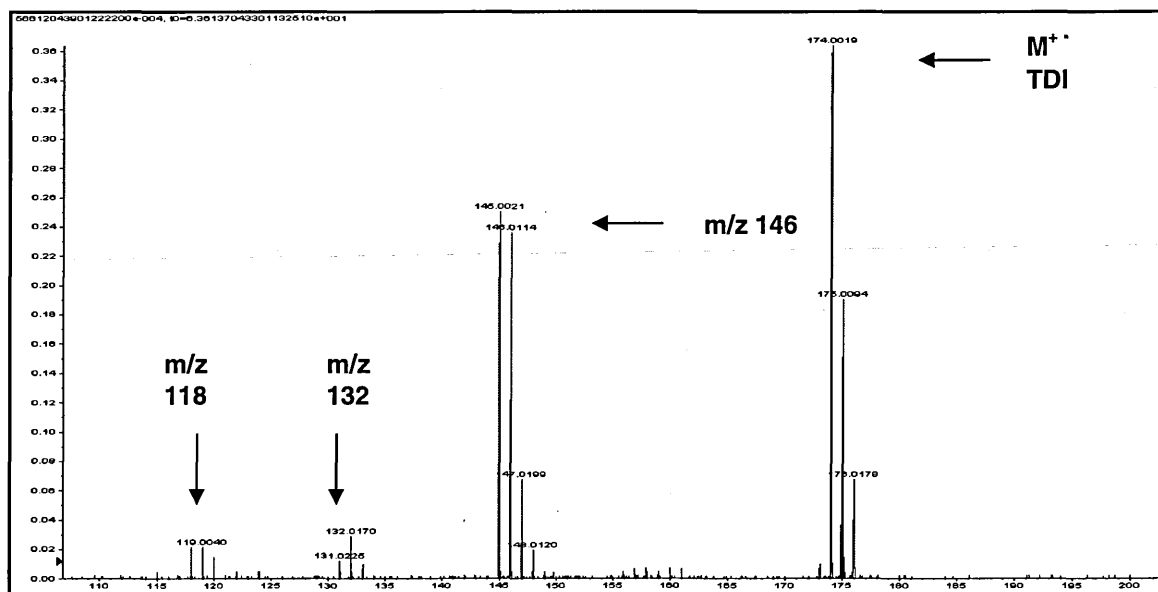


**Figure 2.7** MALDI-MS/MS product ion spectrum for the dissociation of TDI at m/z 174. A smaller peak for the protonated molecule of TDI is observed at m/z 175.

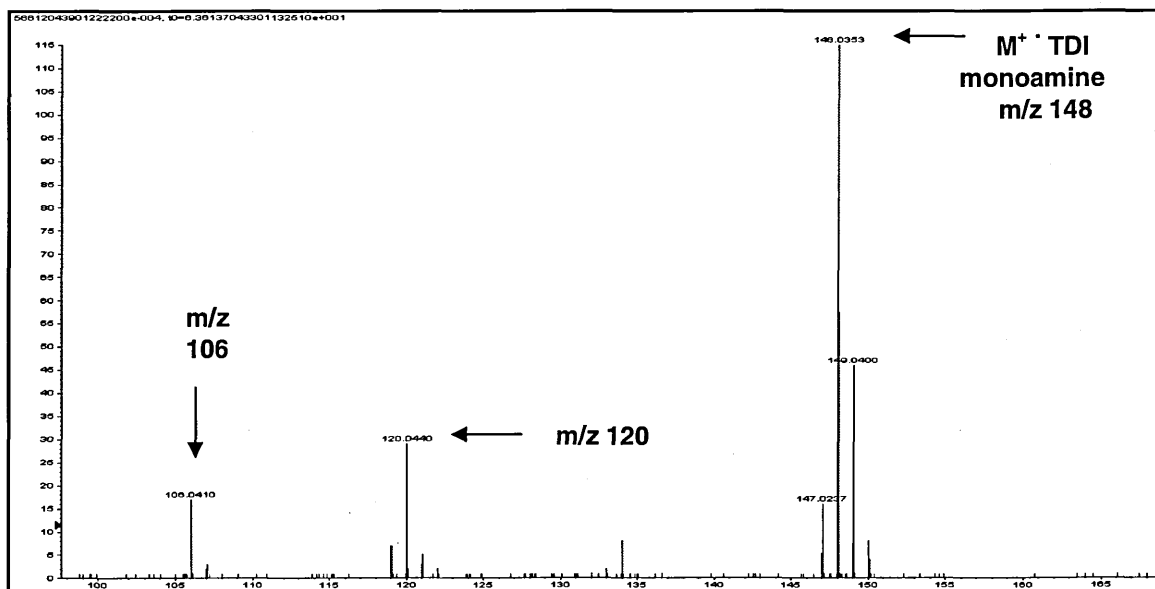


**Figure 2.8** MALDI-MS/MS product ion spectrum for the dissociation of the TDI derived monoamine at m/z 148

The product ions observed from the tandem MS spectra (figures 2.8 and 2.9) are summarized in table 2.2.

TDI	TDI-Monoamine	Mass loss	Proposed loss
174	148	N/A Molecular ion	N/A Molecular ion
146	120	28	CO
132	106	42	NCO
118	n/a	56 (2x28)	2x CO

**Table 2.2** Product ions resulting from the dissociation of TDI (m/z 174) and the TDI-derived monomer (m/z 148)

As observed from the data displayed in the table both compounds follow a similar fragmentation pattern with initial loss of CO and NCO from one isocyanate group occurring. The spectrum for intact TDI also shows a product ion at  $m/z$  118 which corresponds to loss of 2 CO groups. As the monoamine only contains 1 NCO group the loss of a further CO is not possible and thus this product ion peak is not present in the tandem MS of the  $m/z$  148 monoamine precursor ion.

### **2.3.3 Reactivity of HDI with Ethanol**

A relatively stable urethane is formed by the reaction of an alcohol with an isocyanate. The spectrum showing the products of the reaction between ethanol and HDI is shown in figure 2.9 and summarised in table 2.3. Unreacted intact HDI monomer is only observed in the spectrum at low levels indicating a high amount of the HDI monomer had either reacted with the ethanol or undergone partial hydrolysis to monoamine and polymer species within the 10 minutes of exposure. The protonated molecule of the urethane (ethanol derivatised HDI) is present at  $m/z$  261 (mass 260 Da). However, other reactions had occurred during the experiment resulting in the production of a range of HDI species both derivatised and underderivatised by reactions with ethanol and these are also shown in table 3.

The HDI-derived monoamine is clearly observed at  $m/z$  143 where 1 NCO group has hydrolysed to the amine but the remaining NCO has not reacted with ethanol. A derivatised monoamine is also observed where the intact NCO group remaining on the monoamine has been derivatised by an ethanol. Derivatised dimer species were observed as well as underivatised. Trimer species were present in underivatised form only. This may be due to the rate of reaction decreasing as the polymers increase in size (because of steric hindrance). From this spectrum it can be determined that HDI is derivatised as a urethane by reaction with ethanol. However, not all HDI species are derivatised during the 10 minute reaction time. The fact that only a relatively low amount of intact HDI is present (in comparison to other HDI species) indicates that the initial hydrolysis to the monoamine occurs rapidly upon exposure to the laboratory atmosphere although the presence of only very low levels of hexamethylene diamine (formed by full hydrolysis of both NCO groups of HDI) indicates that the HDI monoamine is an important intermediary in the formation of HDA after this short time period.

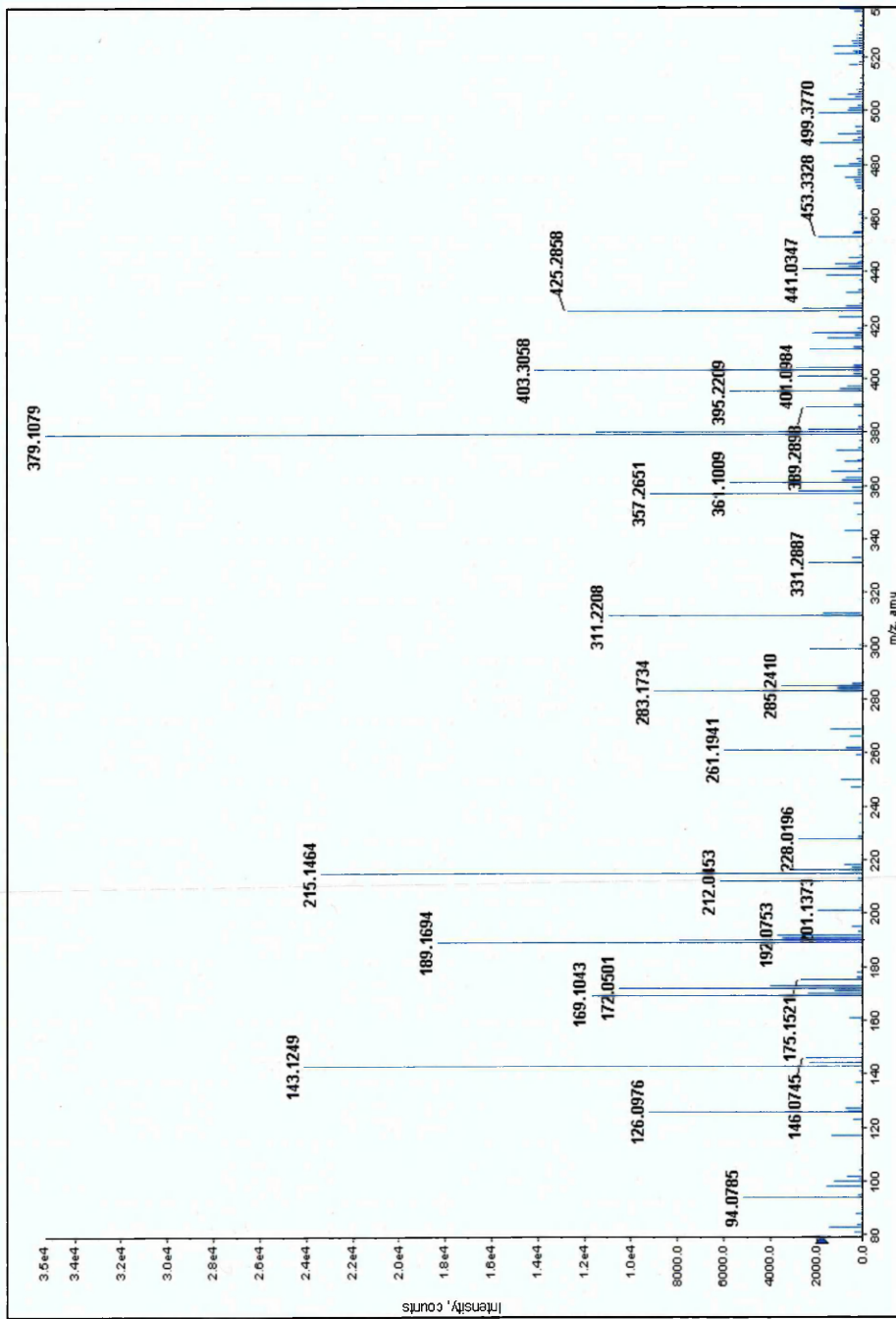


**Fig 2.9** MALDI-MS Spectrum showing derivatised and underivatised HDI species following addition of the HDI monomer to ethanol (10 minute exposure time)

Compound Structure $R = (CH_2)_6$	m/z value	Name
$H_2N-R-NH_2 \left[ \right]^+ H^+$	119	Hexamethylene Diamine
$H_2N-R-NCO \left[ \right]^+ H^+$	143	Underivatised Monoamine
$H_2N-R-NH-CO-OCH_2CH_3 \left[ \right]^+ H^+$	189	Derivatised Monoamine
$OCN-R-NCO \left[ \right]^+ H^+$	169	Underivatised HDI monomer
$H_3CH_2CO-OC-HN-R-NH-CO-OCH_2CH_3 \left[ \right]^+ H^+$	261	Derivatised HDI monomer
$OCN-R-NH-CO-HN-R-NCO \left[ \right]^+ H^+$	311	Underivatised HDI dimer
$H_3CH_2CO-OC-HN-R-NH-CO-HN-R-NH-CO-OCH_2CH_3 \left[ \right]^+ H^+$	403	Derivatised HDI dimer
$OCN-R-NH-CO-HN-R-NH-CO-HN-R-NCO \left[ \right]^+ H^+$	453	Underivatised HDI trimer

**Table 2.3** Summary of ethanol derivatised and underivatised HDI species as observed from the spectra shown in figure 2.9

### 2.3.4 Stability of HDI in Acetone

The ion intensity of the peaks of interest at m/z 143 (HDI monoamine), m/z 311 (HDI dimer) and m/z 453 (HDI trimer) were normalised against the matrix  $[M+H]^+$  peak at m/z 190. Normalization enabled highly reproducible results to be achieved.

The HDI monomer was not observed even at the initial time point. Hydrolysis to the monoamine appears to occur rapidly upon exposure to moisture in the lab atmosphere during the sample preparation procedure. The predominant species observed from the spectra was the HDI-derived monoamine although little or no hexamethylene diamine (HDA) was observed even after 14 days storage in acetone. Thus indicating that full hydrolysis of the HDI had not occurred during the period of the experiment (14 days).

HDI monoamine, HDI dimer and HDI trimer species were observed even at the initial (~0 hour) time point and so formation of these species occurs rapidly upon spiking into acetone, mixing with the matrix and spotting onto the target plate. At the highest concentration of 1mg/ml (figure 2.10) an increase in monoamine occurs between time points 0 and 1 day. This is followed by a gradual decrease in the amount of monoamine observed over the remaining time period indicating possible degradation of the monoamine over time or further reactions occurring between the monoamine and other isocyanate species present.

A large increase in both dimer and trimer formation was observed after 3 days of storage in acetone. The amount decreased fairly rapidly between day 3 and 5 and then remained relatively stable. The reduction in the amount of dimer and trimer observed after day 3 is possibly due to further polymerisation occurring of the HDI dimer and trimer species.

A similar pattern is observed for the lower HDI concentration at 0.1mg/ml (figure 2.11). Once more the HDI monamine is the predominant species observed and a slight increase in formation is observed up to 1 day storage. A decrease is again observed between day 1 and day 5. A slight increase is observed at day 7 and a further decrease occurs between day 7 and day 14. Trimer formation was not observed until 2 days storage time and a large relative increase in dimer and trimer formation was recorded after 3 days storage. As was observed for the greater concentration samples, dimer and trimer quantities decreased after 5 days storage possibly due to further polymerisation reactions.

The lowest concentration of HDI in acetone to produce detectable species other than the HDI monoamine was 0.01mg/ml (figure 2.12). At this concentration HDI monoamine was again the main species observed and the concentration increased between day 0 and day 1. Once again the general trend was for HDI monoamine concentration to gradually decrease over the remaining time period investigated. Trimer formation was not observed to occur even after 14 days storage. HDI dimers were observed after 3 days and concentrations remained relatively stable up to the 14 day time point.

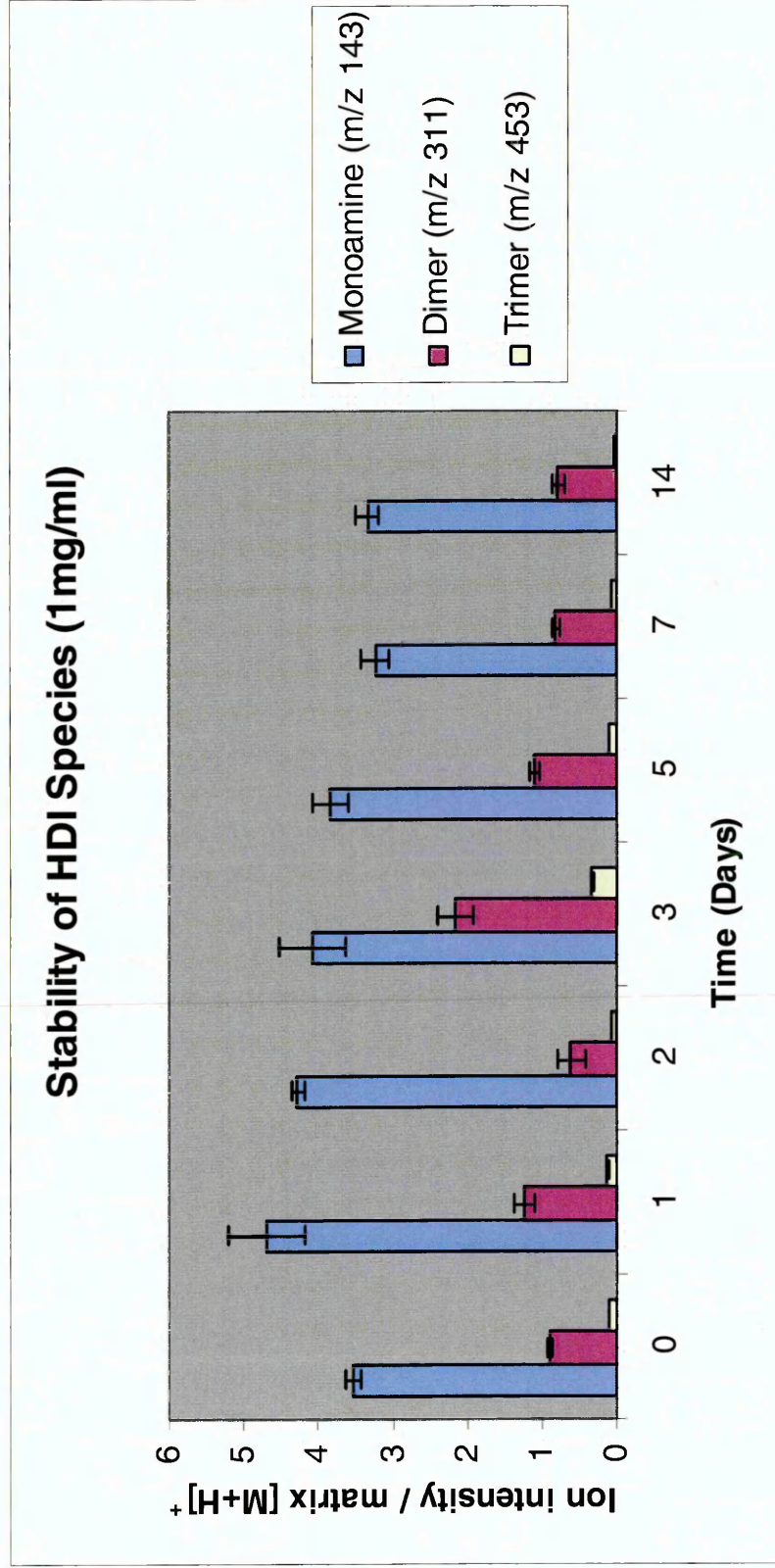


**Figure 2.10** Graph showing the stability of the HDI monoamine, dimer and trimer in acetone over a 14 day sampling period. HDI was added to acetone at 1 mg/ml. Ion intensities of the protonated molecule of each HDI species were normalised against the intensity of  $\alpha$ -CHCA  $[M+H]^+$  at m/z 190 (n=4)

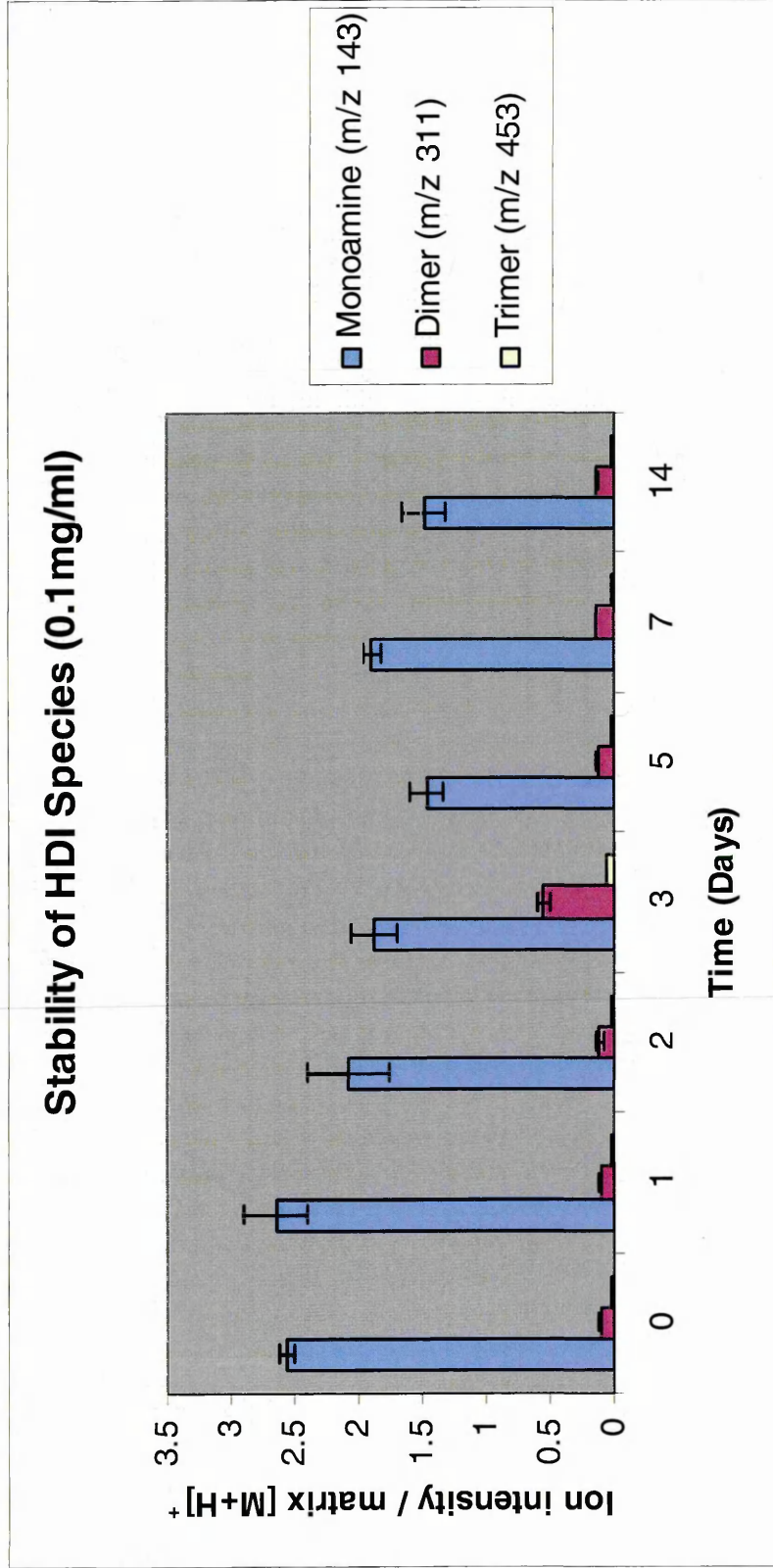


**Figure 2.11** Graph showing the stability of the HDI monoamine, dimer and trimer in acetone over a 14 day sampling period. HDI was added to acetone at 0.1 mg/ml. Ion intensities of the protonated molecule of each HDI species were normalised against the intensity of  $\alpha$ -CHCA  $[M+H]^+$  at m/z 190 (n=4)

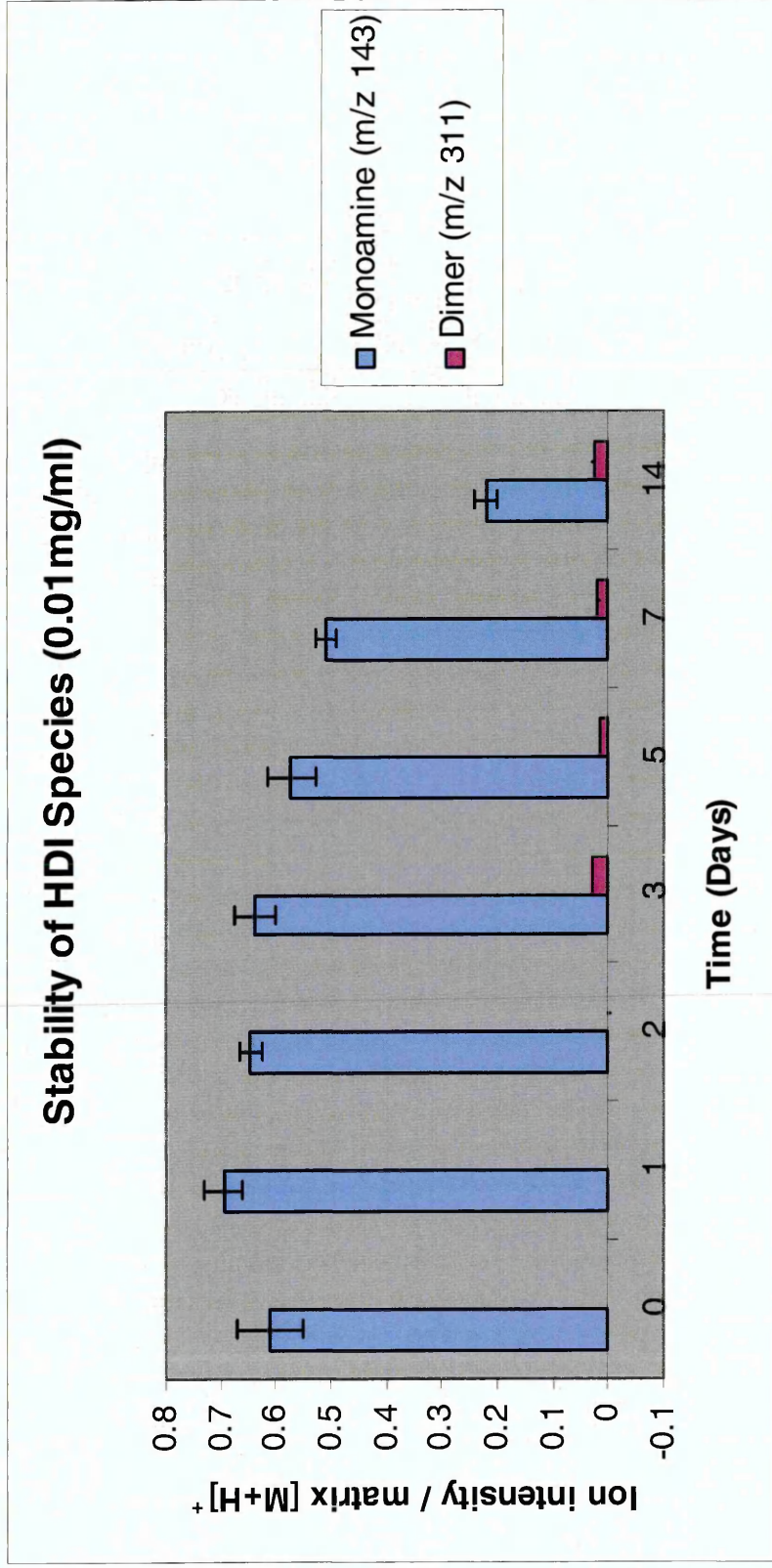


**Figure 2.12** Graph showing the stability of the HDI monoamine, dimer and trimer in acetone over a 14 day sampling period. HDI was added to acetone at 0.01 mg/ml. Ion intensities of the protonated molecule of each HDI species were normalised against the intensity of  $\alpha$ -CHCA  $[M+H]^+$  at m/z 190 (n=4)

### 2.3.5 Stability of Ethanol-Derivatised HDI

The ethanol-derivatised HDI monomer at  $m/z$  261 was observed even at the initial time point (~0 hours) for all concentrations. The amount of ethanol-derivatised HDI monomer (HDI urethane) appeared to increase gradually over the 14 day period and no degradation was observed over this time (figure 2.13).

Both derivatised and underderivatised HDI monoamine species were observed over all concentration ranges investigated. Following 1mg/ml spiking of ethanol with HDI the predominant HDI species at the 0 hour time point is the derivatised monoamine at  $m/z$  189 (figure 2.14). However, there are also large amounts of the underderivatised monoamine and the ethanol derivatised HDI monomer present. A rapid decrease in the amount of both derivatised and underderivatised HDI monoamine is observed between day 0 and day 1, possibly due to further reactions occurring between these species or degradation. Following this rapid decrease, the levels of both remain relatively stable over the remaining time period. Levels of derivatised HDI monomer gradually increase up to the 14 day limit.

At the 0.1mg/ml concentration of HDI, derivatised monoamine is again the predominant species at the initial time point (figure 2.15). The underderivatised monoamine is observed at approximately one third of the intensity of the

derivatised monoamine. Derivatised HDI monomer was observed but at much lower levels than the derivatised and underderivatised monoamine. As for the 1mg/ml concentration of HDI, levels of HDI monomer both derivatised and underderivatised dropped rapidly between day 0 and day 1. However, no loss of derivatised HDI monomer was observed over the entire 14 days, indicating the high stability of this species. Underderivatised HDI monomer was not observed at all. This was probably due to the length of time taken to prepare the samples exceeding the time taken for all of the monomer present to react, either with the ethanol or to hydrolyse and / or polymerise.

At the lowest concentration of 0.01mg/ml HDI in ethanol the same pattern was observed (figure 2.16). The derivatised monoamine was the most predominant species at the initial time point. Once more there was a rapid reduction in derivatised and underderivatised HDI monoamine observed between 0 and 1 day. The ethanol-derivatised HDI monomer is therefore shown to be stable at this concentration and no degradation occurs over the entire time period investigated.

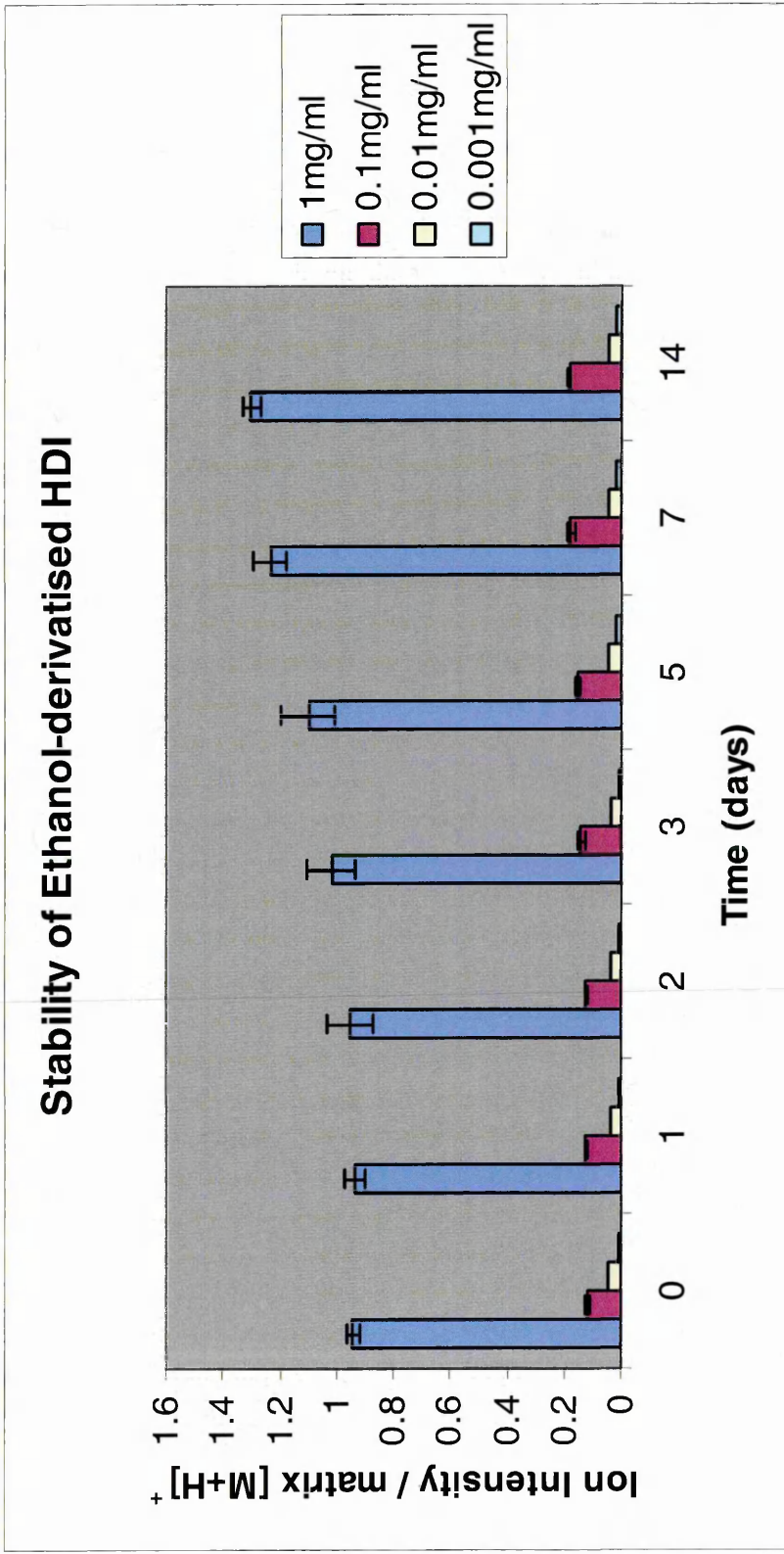


**Figure 2.13** Graph showing the stability of the Ethanol-derivatised HDI monomer (urethane) over a 14 day sampling period. Ion intensities of the protonated molecule of ethanol-derivatised HDI ( $m/z$  261) was normalised against the intensity of  $\alpha$ -CHCA  $[M+H]^+$  at  $m/z$  190 ( $n=4$ )

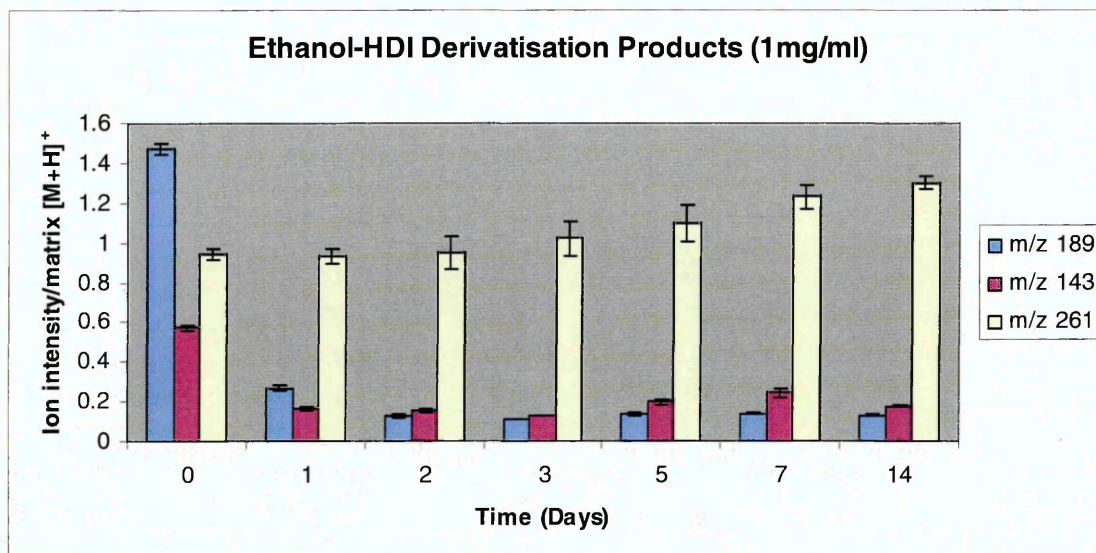


**Figure 2.14** Graph showing the stability of the ethanol-derivatised HDI monomer (m/z 261), monoamine (m/z 189) and underderivatised monoamine (m/z 143) over a 14 day sampling period. HDI was added to ethanol at 1mg/ml. Ion intensities of the protonated molecule of each HDI species was normalised against the intensity of  $\alpha$ -CHCA [M+H]<sup>+</sup> at m/z 190 (n=4)

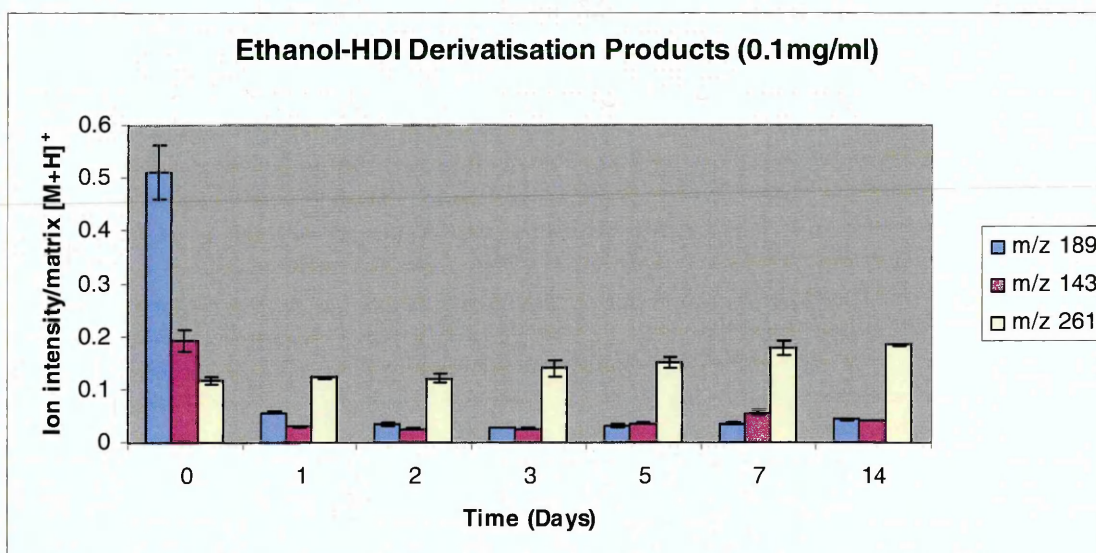


**Figure 2.15** Graph showing the stability of the ethanol-derivatised HDI monomer (m/z 261), monoamine (m/z 189) and underderivatised monoamine (m/z 143) over a 14 day sampling period. HDI was added to ethanol at 0.1mg/ml. Ion intensities of the protonated molecule of each HDI species was normalised against the intensity of  $\alpha$ -CHCA [M+H]<sup>+</sup> at m/z 190 (n=4)

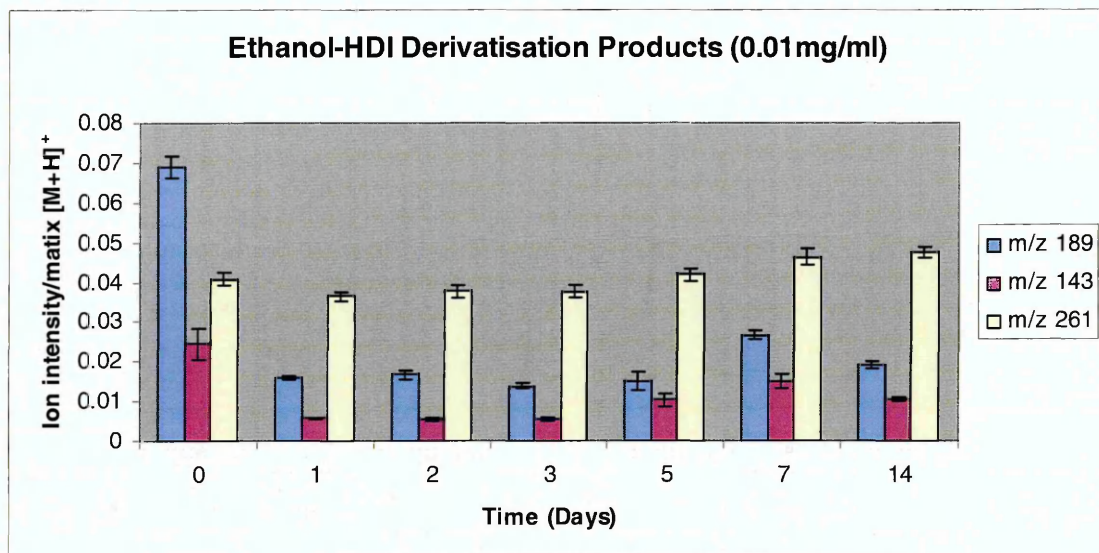


**Figure 2.16** Graph showing the stability of the Ethanol-derivatised HDI monomer (m/z 261), monoamine (m/z 189) and underivatised monoamine (m/z 143) over a 14 day sampling period. HDI was added to ethanol at 0.01mg/ml. Ion intensities of the protonated molecule of each HDI species was normalised against the intensity of  $\alpha$ -CHCA [M+H]<sup>+</sup> at m/z 190 (n=4)

### 2.3.6 Ethanol Swab Method and Extraction Efficiency

A calibration curve was constructed for the ethanol-derivatised HDI monomer standards. A linear increase appears to occur between 0 and 0.6mg/ml of HDI in ethanol as shown in figure 2.17. Above this concentration saturation appeared to occur as indicated by a flattening of the curve. When the 0-0.6 mg/ml HDI range is plotted a clear linear regression is observed and a high R<sup>2</sup> value of 0.991 is recorded, thus, indicating the method's suitability for quantitative analysis over this limited concentration range. The limit of detection (using the statistical method recommended by Miller and Miller<sup>[35]</sup>) was calculated as 8.6  $\mu$ g/ml.

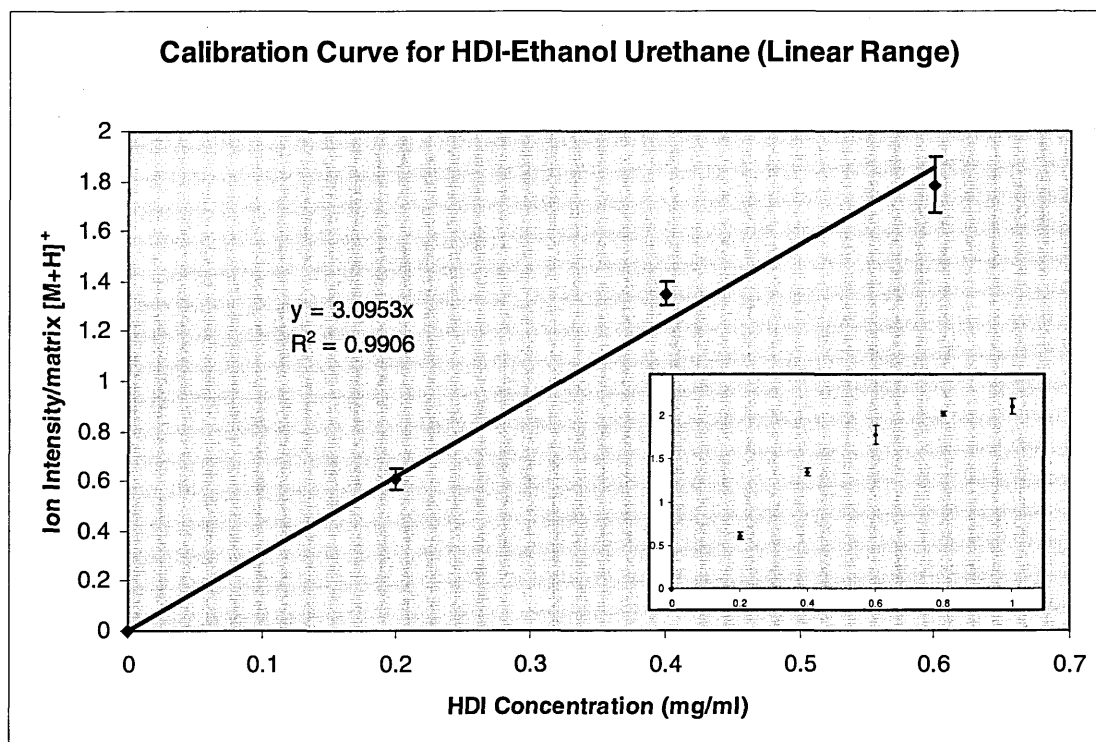


**Figure 2.17** Calibration curve for the Ethanol-derivatised HDI monomer. Ion intensities of the protonated molecule of ethanol-derivatised HDI were normalised against the intensity of  $\alpha$ -CHCA [M+H]<sup>+</sup> at  $m/z$  190 ( $n=4$ ). Insert showing full calibration curve (0-1mg/ml ethanol derivatised HDI)

Using the calibration chart shown in figure 2.17 an average extraction efficiency value of 30.3% ( $SD \pm 0.017$ ) was determined from the aluminium plate. While relatively low, this could be increased by performing successive swabs over the same area of the aluminium plate. The use of a swab with a larger surface area may also enable a higher extraction yield to be obtained. The method was highly reproducible as indicated by the low standard deviation.

A lower extraction efficiency of 12.9% ( $SD \pm 0.018$ ) was obtained from the swabs taken from the latex glove surface. The low extraction efficiency is probably due to absorption of HDI into the glove and hence increased difficulty in extracting it from the surface. Again further swabs over the same area may increase the yield. However, reproducible quantifiable results were clearly obtained even with this low extraction efficiency.

## 2.4 Conclusion

An intermediate product in the hydrolysis of diisocyanates to diamines was observed in the spectra of both an aromatic diisocyanate (TDI) and an aliphatic diisocyanate (HDI). The structure of the intermediate product was determined to be a monoamine by MS/MS analysis, i.e. one of the NCO groups present on the diisocyanate molecule had been hydrolyzed to  $NH_2$ . In preliminary experiments intact HDI monomer was observed at low levels after ethanol derivatisation but it was not observed in the stability testing experiments. This was probably due to the length of time taken to prepare all of the repeats being greater than 15 minutes. Larger amounts of intact TDI monomer were observed as this appears to hydrolyze slower.

The stability of underivatised HDI species was monitored over a 14 day time period. No intact HDI monomer was observed and the predominant HDI species

observed was the monamine at  $m/z$  143. Dimer and trimer formation was observed to occur *in situ* with the highest concentration of these occurring after 3 days storage. Decreases in the amount of dimer and trimer occurred after this time period possibly due to additional polymerization occurring. Similar trends occurred over all concentrations investigated. However, dimer and trimer formation took longer to occur and these species were observed at far lower intensities when lower concentrations of HDI were investigated.

An alcohol derivatisation method was proposed for stabilizing samples of free HDI monomer present in a workplace for subsequent transportation and MS analysis. This was evaluated for HDI. The predominant HDI species observed was the ethanol derivatised HDI monomer and degradation of this compound did not occur over the 14 day experiment period. Slight increases occurred after prolonged exposure of HDI to ethanol indicating that the reaction was still occurring at the end time point.

An ethanol swabbing method was proposed to enable on site derivatisation of the HDI monomer for subsequent MS analysis. By normalizing the intensity of the ethanol derivatised HDI monomer against the  $[M+H]^+$  of the  $\alpha$ -CHCA matrix, a calibration curve was produced which appeared to be linear over the range 0 - 0.6mg.ml HDI. From this calibration curve extraction efficiencies were calculated and the swab method was demonstrated to be reproducible. Extraction efficiencies were relatively low, 30.3% and 12.9% from the aluminium plate and

latex glove respectively. Subsequent swabbing of the same surface would enable higher yields to be obtained.

Ethanol swabbing is a relatively non-hazardous approach to *in-vivo* sampling and with appropriate ethical approval, swabs may be taken directly from workers skin as a non-invasive method to determine dermal isocyanate exposure. MALDI-MS is a useful method for the analysis of such samples as a wide mass range may be investigated enabling the detection and characterization of the different HDI species caused by reactions of HDI in the workplace. This may enable large polymer species to be investigated as well as the alcohol derivatised monomer species.

## 2.5 References

- [1] McAlinden, J.J., "Isocyanate exposure in the United Kingdom", Isocyanates: Sampling, analysis and health effects, ASTM STP 1408, Lesage, J., Graff, I.D., Danchik, R.S., Eds., American Society for Testing and Materials, West Coshohocken, P.A. 2002
- [2] Tarlo S.M., Banks D., Liss G., Brofer I., Outcome Determinants for Isocyanate Induced Occupational Asthma Among Compensation Claimants. *Occup. Environ. Med.* 1997, 54, p. 756-761
- [3] Coldwell, M., White, J., Measurement of airborne isocyanate during sanding and bake cycle. HSL report OMS/2005/10 2005
- [4] Health and Safety Executive. General COSHH ACOP (Control of Substance Hazardous to Health). Control of substances hazardous to health regulations 1994: Approved codes of practice L5 2<sup>nd</sup> Edition 1997 HSE Books
- [5] Hardy, H., Devine, J., Use of organic isocyanates in industry. Some industrial hygiene aspects. *Ann. Occup. Hyg.* 1979 22 p421-427
- [6] Silk, S., Hardy, H., Control limits for diisocyanates. *Ann. Occup. Hyg.* 1983 27 p333-339
- [7] Hulse, P.M., An evaluation of HDI in polyurethane spray paint aerosols. NTIS# AD-AL51 606 1984

- [8] Boutin, M., Lesage, J., Ostiguy, C., Pauluhn, J., Bertrand, M.J., Identification of the isocyanates generated during the thermal degradation of a polyurethane car paint. *J. Anal. Appl. Pyrolysis*. 2004 71 p791-802
- [9] Fenske, R.A., Dermal exposure assessment techniques. *Ann. Occup. Hyg.* 1993 37 p687-706
- [10] Garrod, A.N.I., PHILLIPS, A.M., Pemberton, B., Potential exposure of hands inside protective gloves: A summary of data from non-agricultural pesticide surveys. *Ann. Occup. Hyg.* 2001 45 p55-60
- [11] Health and Safety Executive. Dermal exposure to non-agricultural pesticides exposure assessment document. EH74/3 1999 HSE Books
- [12] Chan-Yeung M., Marlo J.L., Occupational Asthma. *New Eng. J. Med.* 1995, 333 p.107-111
- [13] Tornling G., Alexandersson R., Hedenstierna G., Plato N., Decreased Lung Function and Exposure to Diisocyanates in Car Repair Painters: Observations on re-examination 6 years after Initial Study. *Am. J. Ind. Med.* 1990, 17, p.299-310
- [14] Liss G.M., Bernstein G.I., Moller D.R., Gallagher J.S., Stephenson R.L., Bernstein I.L., Pulmonary and Immunological Evaluation of Foundry Workers Exposed to Methylene Diisocyanate. 1988, 82, p. 55-61
- [15] Vandenplas O., Cartier A., Lesage J., Perault G., Grammar L.C., Marlo J.L., Occupational Asthma Caused by a Prepolymer but not the Monomer of Toluene Diisocyanate. *J. Allergy. Clin. Immunol.* 1992, 89 p.1183-1188

- [16] Diller W.F., Frequency and Trends of Occupational Asthma Due to Toluene Diisocyanate: A Critical Review. *Appl. Occup. Environ. Hyg.* 2002, 17, p.872-877
- [17] Karol M.H., Macina D.T., Cunningham A.C., Cell and Molecular Biology of Chemical Asthma. *Ann. Allergy Asthma Immunol.* 2001, 87, p.28-32
- [18] Kimber I., The Role of Skin in the Development of Chemical Respiratory Hypersensitivity. *Toxicol. Letters*, 1996, 86, p.89-92
- [19] Karol M.H., Hauth B.A., Riley E.J., Magreni C.M., Dermal Contact With Toluene Diisocyanate Produces Respiratory tract Sensitivity in Guinea Pigs. *Toxicol. App. Pharmacol.* 1981, 58, p.221-230
- [20] Wisnewski A.V., Lemus R., Karol M.H., Redlich C.A., Isocyanate Conjugated Human Lung Epithelial Cell Proteins: A Link Between Exposure and Asthma. *J.Allergy Clin. Immunol.* 1999, 104, p.341-347
- [21] Wisnewski A.V., Redlich C.A., Recent Developments in Diisocyanate Asthma. *Curr. Opin. Allery Clin. Immunol.* 2001, 1, p.169-175
- [22] NIOSH (National Institute for Occupational Safety and Health). Preventing Asthma and Death from Diisocyanate Exposure. 1996, DHSS Publication No. 96-111
- [23] Health and Safety Executive. Methods for the determination of hazardous substances: Organic isocyanates in air. MDHS 25/3 1999 HSE Books
- [24] Bagon, D.A., Warwick, C.J., Brown, R.H., Evaluation of total isocyanate in air method using 1-(2-methoxyphenyl)piperazine and HPLC. *Am. Ind. Hyg. Assoc. J.* 1984 45 p39-43

[25] Warwick, C.J., Bagon, D.A., Purnell, C.J., Application of electrochemical detection to the measurement of free monomeric aromatic and aliphatic isocyanates in air by high performance liquid chromatography. *Analyst*. 1981 106 p676-685

[26] White, J., Evaluation of MDHS 25/2 "the determination of isocyanates in a reacting paint mix" HSL internal report. IACS 97/19 1997

[27] Goldberg, P.A., Ellwood, H.L., Walker, R.F., Hardy, H.L., Determination of trace atmospheric isocyanate concentrations by reverse-phase high performance liquid chromatography. *Analyst*. 1979 104 p85-93

[28] Dunlap, K.L., Sandridge, R.L., Keller, J., Determination of isocyanates in working atmosphere by high-performance liquid chromatography. *Anal. Chem.* 1976 48 p497-499

[29] Hardy, H.L., Walker, R.F., Novel reagent for the determination of atmospheric isocyanate monomer concentrations. *Analyst*. 1979 104 p890-891

[30] Health and Safety Executive. Methods for the determination of hazardous substances: Aromatic amines in air and on surfaces. MDHS 75 1993 HSE Books

[31] Occupational Safety and Health Administrator (OSHA). Aromatic isocyanate surface contamination sampling and evaluation techniques. 1997

[32] CLI, Colormetric Laboratories, Inc. 1261A Rand Road, Des Plaines, IL, 60016-3402, Telephone: (847) 803-3737

[33] Occupational Safety and Health Administrator (OSHA). Sampling and analytical methods: Diisocyanates. OSHA method 42. 1989

[34] Occupational Safety and Health Administrator (OSHA). Sampling and analytical methods: Methylene bisphenyl diisocyanate (MDI). OSHA method 47. 1989

[35] Miller, J.C., Miller, J.N., Statistics for Analytical Chemistry. 3<sup>rd</sup> revised edition. 1993, Ellis Horwood

### **3.0 Application of LC-MS to the Determination of the Biotransformation of TDI to TDA by a Human Keratinocyte (HaCaT) Cell Line**

## **3.1 Introduction**

### **3.1.1 Introduction to High Performance Liquid Chromatography Mass Spectrometry (LC-MS)**

High-performance liquid chromatography (HPLC) has been widely established as a separation technique suitable for many analytical applications. In this method components in a mixture are separated due to a variety of chemical and/or physical interactions between the analyte and the chromatography column. The relative affinities of components of a mixture for either a solid stationary phase or a liquid mobile phase will result in different rates of elution through the stationary phase (chromatography column). Compounds which favour the stationary phase will be retained in the column for longer than those with an affinity for the mobile phase.

#### **3.1.1.1 Partition Phases**

The relationship between the analyte and the mobile and stationary phases determines the separation of analytes in a mixture. The two most common types of HPLC are normal and reverse phase.

Normal phase liquid chromatography (NPLC) incorporates a polar stationary phase and a non-polar mobile phase. It is used for the analysis of compounds which are relatively polar in nature. Retention on the column occurs due to the interaction of polar functional groups of the analyte with polar functional groups located on the surface of the stationary phase. Adsorption strengths increase with an increase in analyte polarity and an interaction between a polar analyte and the polar stationary phase will increase the elution time. Steric factors also contribute towards separation as well as hydrogen bonding and dipole-dipole interactions. These factors often enable stereo-isomers to be resolved from one another. The use of water or protic solvents may lead to changes in the hydration state of the chromatographic media and thus lead to irreproducible retention times. This has led to reverse phase HPLC being frequently favoured over NPLC.

In reverse phase (RP) chromatography the retention mechanism is dependent upon the hydrophobicity of the stationary phase and the solute analyte. Hydrogen bonding and dipole-dipole interactions also contribute to the separation mechanism. The stationary phase is usually strongly non-polar and the mobile phase is moderately polar. Non-polar analytes are retained longer on the column and therefore more polar molecules elute more readily. The retention time may be controlled by the choice of solvent used. The inclusion of a more polar solvent in the mobile phase will increase the retention time whereas addition of a more hydrophobic solvent will lead to a reduction in retention time. pH is an important

consideration in method design as changes in pH levels will affect the hydrophobicity of the analyte. Acidic silanol groups on the stationary phase media facilitate interactions between solute analyte molecules and the stationary phase and are also affected by the pH of the experiment <sup>[1]</sup>. Buffering agents may also be used to control and maintain the pH <sup>[2]</sup>. The addition of an organic acid such as trifluoroacetic acid may also be used to adjust the pH of the mobile phase. Additional benefits when using an organic acid include the neutralization of charges on residual exposed stationary phase silica and neutralization of charges on the analyte due to the acid acting as ion pairing agents. The choice of solvent is dependent on the chromatography partition mode and thus solvent polarity is the key consideration. Examples of common solvents used include (in order of increasing polarity) toluene, acetone, acetonitrile, methanol and water. Reverse phase chromatography has a wider range of applications than normal phase and is the most frequently used form of partition chromatography.

#### **3.1.1.2 Columns**

The column consists of the HPLC stationary phase packed into tubing (usually stainless steel). The stationary phase media and the column diameter are dependent upon the partition phase and properties of the investigated analyte. In normal phase chromatography the stationary phase media usually includes polar functional groups such as aminopropyl and cyanopropyl bound to silica. Reverse

phase stationary media includes hydrophobic moieties, most often consisting of C<sub>18</sub> hydrocarbon chains.

The internal diameter (ID) of an HPLC column is critical in determining the quantity of analyte which may be loaded onto a column and also the resulting sensitivity. Reduction in the ID will result in an overall reduction in the total volume of the column. This is of experimental benefit due to decreased solvent consumption (lower flow rate) and increased sensitivity. However this does result in a marked decrease in the loading capacity of the experiment. Standard bore columns (approximately 4-5mm) are used for traditional quantitative HPLC analysis combined with a UV-vis absorbance detector. Narrow-bore columns have an internal diameter of approximately 1-2mm are most commonly used in experiments where higher sensitivity is required. They are frequently combined with a mass spectrometric detection method (LC-MS).

The particle size of the column packing plays an integral role in the chromatographic separation process. Most HPLC analysis is performed using a stationary phase attached to the outside of small silica beads. A range of bead size is used in standard HPLC columns, most commonly 5µm. A reduction in particle size will lead to increased surface area and hence improved separation. Additionally the peak width in the resulting chromatograph is lowered due to the increased uniformity of the flowpath of the analyte as it navigates smaller particles. Any reduction in particle size needs to be offset by an increase in

pressure to maintain the optimum liner velocity, which increases by the inverse of the particle diameter cubed <sup>[3]</sup>. The pore size of a porous stationary phase is also of importance. Smaller pore sizes will result in an increase surface area however larger analytes may become 'trapped' inside the pores and thus slow the kinetics of the elution process.

### **3.1.1.3 Elution Methods**

The elution of an analyte through the chromatographic system may be via isocratic or gradient elution methods. In the isocratic process the mobile phase is kept constant throughout the separation. Gradient elution involves varying the mobile phase composition during the chromatographic run. In reverse phase chromatography this usually involves the increase of hydrophobic solvent over time during the analysis and thus assists the elution of the more hydrophobic components of a mixture later in the analysis. Separation occurs as a function of the affinity of the analyte for the current mobile phase composition in relation to the stationary phase. Other factors may also be manipulated during gradient elution including flow rate and column temperature.

### **3.1.2 Mass Spectrometry**

The coupling of an LC system with a mass spectrometric detector enables a very high sensitivity to be achieved. The formation of ions occurs in the gaseous phase and this can occur under high vacuum i.e. low pressure or atmospheric pressure conditions. The two most commonly used atmospheric pressure ionisation (API) methods for LC-MS are Electrospray (ESI) and Atmospheric Pressure Chemical Ionization (APCI). Good separation of the components within a mixture is essential for quality mass spectra to be obtained for the individual components of the mixture by LC-MS. One of the main areas of concern is the change in physical state from liquid in the LC system to the gaseous phase for the mass spectrometric detection. In gas chromatography the separation is conducted in the same gaseous phase as the ionisation technique. However, gas chromatography is only applicable to the analysis of volatile species. LC-MS is more suited to compounds such as large polymers and highly polar compounds.

#### **3.1.2.1 Electrospray Ionization (ESI)**

The ESI source consists of a very fine needle and a series of skimmers. A sample solution is sprayed into the source chamber to form droplets. The droplets carry charge when they exit the capillary and as the solvent vaporizes the droplets disappear leaving highly charged analyte molecules.

The mechanism by which gas-phase ions are formed during the electrospray ionization process have been greatly debated <sup>[4]</sup> The two proposed mechanisms are the ion evaporation mechanism (IEM) and the charged residual mechanism (CRM). Both mechanisms begin with the production of highly charged droplets that are resistively and/or conductively heated at atmospheric pressure.

The electric field on the droplet surface increases as the charged droplet evaporates (and thus decreases in size). Eventually the field overcomes the surface tension resulting in droplet fission. In the IEM, gas-phase ions are formed by emission from a droplet surface when the electric field becomes sufficiently high. Iribarne and Thomson propose this occurs at a droplet diameter of <20nm <sup>[5]</sup>. The fission event corresponds to an almost negligible loss in droplet mass, but a significant drop in charge. In the CRM, droplet evaporation and successive fission events continue until charged nanodroplets containing only single analyte molecules are formed, which evaporate to dry analyte ions <sup>[6]</sup>. The dry analyte ion will still retain the same charge from the single nanodroplet prior to solvent evaporation. Following initial ion formation, the spray plume is sampled through a small orifice into a region of low pressure to aid the production of a solvent free collimated ion beam.

### 3.1.3 Metabolism of Diisocyanates

Toluene diisocyanate (TDI) is a monomer used in the production of polyurethane products such as urethane foams, surface coatings and varnishes. It is most commonly used as a technical grade mixture of 2,4-TDI (80%) and 2,6-TDI (20%) in the workplace <sup>[7]</sup>. TDI is well documented as a potent occupational sensitizer and is extremely toxic in cases of both acute and chronic exposure <sup>[8]</sup>. Acute exposure to high levels of TDI in humans has been shown to result in severe eye <sup>[9]</sup> and skin irritation <sup>[10]</sup> as well as cause detrimental effects to the gastrointestinal and respiratory tracts <sup>[11]</sup>.

Methods for the biological monitoring of isocyanates have been presented by measurement of the corresponding amine in hydrolysed plasma and urine as summarised in table 3.1.

Experiments conducted by Persson et al <sup>[19]</sup> incorporating direct monitoring of workers exposed to TDI have shown fluctuations in detected TDA concentrations extracted from urine samples over the course of a working day. Interestingly amine concentration in the workers plasma remained constant. Further investigations into the stability of TDA in these media were conducted and a significant difference in the half life of the two TDA isomers was observed in urine <sup>[20]</sup> (5.8-11 days for 2,4-TDA and 6.4-9.3 days for 2,6-TDA). Both isomers were observed to have a half life of 21 days in plasma.

Diisocyanate	Diamine Metabolite	References
2,4-toluene diisocyanate (2,4-TDI)	2,4-toluene diamine (2,4-TDA)	Timchalk et al 1993 <sup>[12]</sup> Sakai et al 2005 <sup>[13]</sup>
2,6-toluene diisocyanate (2,6-TDI)	2,6-toluene diamine (2,6-TDA)	Sakai et al 2005 <sup>[13]</sup> Sakai et al 2002 <sup>[14]</sup>
4,4-Methylene diphenyl diisocyanate (4,4-MDI)	4,4-methylene dianiline (4,4-MDA)	Skarping et al 1994 <sup>[15]</sup> Dalene et al 1997 <sup>[16]</sup>
1,6-hexamethylene diisocyanate (1,6-HDI)	1,6-hexamethylene diamine (1,6-HDA)	Dalene et al 1990 <sup>[17]</sup> Liu et al 2004 <sup>[18]</sup>

**Table 3.1** Summary of the diamine metabolite analyzed during previous quantitative analysis of diisocyanate exposure

Following oral exposure, TDI is understood to undergo hydrolysis and/or polymerisation in the stomach <sup>[21]</sup>. Once hydrolysed to TDA, acetylation may occur resulting in the product bis(acetylamino) toluene which may be quantitatively analysed in urine. Studies conducted by Kennedy et al <sup>[22]</sup> indicated that, following in vivo inhalation exposure, less than 5% of the isocyanate was detected in the bloodstream in low molecular weight form ( i.e. as an amine or glutathione adduct) with the remainder identified as conjugated macromolecular species. This study did not establish whether the reactions are occurring in the lumen of the airways, directly in the circulatory system, or a combination of both.

The detection of TDA in urine following dermal exposure to TDI was first reported by Rosenberg and Savolainen in 1985 [23]. Rats' tails were percutaneously exposed to TDI and its TDA metabolite was quantitatively analysed in the form of acid-labile conjugates excreted in the urine. The reported concentrations of TDA found in the urine after hydrolytic treatment were linearly related to the estimated dermal toluene diisocyanate dose.

### **3.1.3.1 Application of Mass Spectrometry for Diisocyanate Metabolite Monitoring**

Diamine metabolites of diisocyanates have been extracted from biological fluid matrices and quantitatively analysed by a range of analytical methods (table 3.1). High performance liquid chromatography has been previously used. However, modern environmental analysis favours the use of mass spectrometry based methods such as gas chromatography mass spectrometry [19] and liquid chromatography mass spectrometry [14]. Mass spectrometry allows precise identification of hazardous compounds and reaction processes and this is of particular importance when dealing with the highly reactive isocyanate compounds. The introduction of atmospheric ionisation techniques such as electrospray ionisation (ESI) has enabled selected ion recording (SIR) of analyte species with high sensitivity. Karlsson et al [24] have previously demonstrated the use of LC-MS with ESI to analyse the  $[M+H]^+$  di-*n*-butylamine (DBA) derivatives

of a range of diisocyanates at very high sensitivity in SIR mode. Sakai et al (2002) <sup>[14]</sup> described the first use of LC-MS for the determination of urinary TDA in workers exposed to TDI without derivatisation of the TDA. The method was demonstrated to be both sensitive and accurate enough to detect increased levels of TDA in workers' urine and is proposed as a suitable technique for the biological monitoring of TDI exposure.

#### **3.1.4 Dermal Diisocyanate Exposure and Immune Response**

Exposure to TDI has been shown to result in allergic contact dermatitis <sup>[11]</sup>. The mechanism of the allergic response is complex and involves both immune cells and structural cells such as fibroblasts and endothelium. Contact allergy is an example of a delayed type-4 hypersensitivity reaction and is mediated by allergen specific T cells. Langerhans cells (LC) and keratinocytes are an important source of cutaneous cytokines, some of which are only induced following appropriate chemical stimulation. Following an initial exposure to a contact allergen, epidermal LC at the site of exposure are induced to migrate from the skin and move, via afferent lymphatics, to draining lymph nodes. These cells accumulating in the draining lymph nodes are known as dendritic cells (DC) and function by presenting antigen to responsive T lymphocytes. Interleukin 1 (IL-1) and granulocyte macrophage colony-stimulating factor (GM-CSF) are believed to be responsible for the maturation and development of the dendritic cells <sup>[25]</sup>.

Tumour necrosis factor  $\alpha$  (TNF  $\alpha$ ) is a keratinocyte derived cytokine which plays a vital role in the allergy immune response [26]. TNF- $\alpha$ , the expression of which is upregulated in skin sensitization, has been shown to cause a time and dose dependent accumulation of DC in draining lymph nodes. It has been proposed that this epidermal cytokine provides a stimulus for LC migration from the skin [27]. Treatment of mice, prior to skin sensitization, with a neutralizing anti TNF- $\alpha$  antibody was shown to inhibit the ability of a potent contact allergen (oxazolone) to stimulate the accumulation of DC in draining lymph nodes. This was thus shown to inhibit the occurrence of contact sensitization [28].

An investigation conducted by Ban et al in 1997 concluded that the exposure of guinea pigs to airborne TDI resulted in an increased level of TNF- $\alpha$  in broncho-alveolar lavage fluid and increased amounts of DC in the lung-associated lymph nodes [29].

### **3.1.5 Aim**

The aim of this investigation was to determine whether, following dermal exposure, the metabolism of a diisocyanate to the corresponding diamine may initially occur in the skin before entry into the circulatory system. An LC-MS analysis method was used to detect any increase in free TDA following in vitro exposure of human keratinocyte (HaCaT) cells to TDI in comparison to

references containing only water or cell free media. The media matrix surrounding the cells was removed at a range of time points after exposure.

## **3.2. Method**

### **3.2.1 Materials**

2,4-Toluene diisocyanate (95% with 4% 2,6 isomer), ethylene dianiline, sodium hydroxide and dimethyl sulfoxide were purchased from Sigma-Aldrich (Dorset, UK). 2,4-Toluene diamine was provided by the Health and Safety Laboratory (Buxton, UK). HPLC grade acetonitrile, dichloromethane and glacial acetic acid were obtained from Fisher Chemicals (Leicester, UK). Ammonium acetate (HiPerSolv) was purchased from BDH (Dorset, UK). Dulbecco's modified Eagle's medium (DMEM) was purchased from Invitrogen. Foetal calf serum (FCS) was purchased from Perbio Science (FetalClone II batch AMF16511).

### **3.2.2 Preparation of Cells**

HaCaT cells were provided for use at the Health and Safety Laboratory by Professor N. Fusenig (German Cancer Research Centre, Hiedelberg, Germany). Cells were seeded at a 100,000 cells per well in 1ml of DMEM media containing

10% FCS in 12-well tissue culture plates following standard HSL cell passaging protocols. All cell proliferation and exposure was conducted at the HSL in accordance with the materials transfer agreement (MTS) in place for this specific cell line.

### **3.2.3 Preparation of Standards**

A stock solution of 2,4-TDA in dimethyl sulfoxide was used to prepare three replicates of standards consisting of 0, 1, 5, 10, 25, 50, 75 and 100 $\mu$ mol TDA suspended in 1ml of culture medium (DMEM containing 10% FCS). The same stock solution was used to prepare standards of the same concentrations in 1ml of Milli-Q water. In order to eliminate the need to calculate and correct data for recovery factors these standards were then treated in the following manner. 200 $\mu$ L of concentrated sodium hydroxide was added to each standard. 3mL of dichloromethane was added and each sample was placed in a rotary tumbler for 10 minutes. Samples were centrifuged at 3000rpm for 5 minutes to separate out the organic layer containing the TDA. 2mL of the organic layer was extracted and dried under nitrogen gas. The dried TDA was re-suspended in 200 $\mu$ L of acetonitrile containing 5 $\mu$ mol ethylene dianiline (EDA) as an internal standard.

### **3.2.4 Preparation of Samples**

The samples were prepared at the Health and Safety Laboratory, Sheffield.

The plates containing the cells and controls (containing only blank media or water) were removed from incubation. A stock solution of 1mmol TDI in DMSO was pipetted directly into each to produce a final concentration of 10 $\mu$ mol of TDI in each well. This was repeated for a further set of plated cells and controls using a 10mmol stock of TDI to produce a concentration of 100 $\mu$ mol TDI in each well. All plates were returned to incubation at 37°C. A 1ml aliquot was removed from the corresponding well at the following time points: 0, 0.5, 1, 3, 6 and 24 hours. The aliquots were immediately frozen in liquid nitrogen following removal from the well and maintained at -80°C. All experiments were performed in triplicate.

The samples were defrosted rapidly by suspension in boiling water and the addition of sodium hydroxide and extraction with dichloromethane (DCM) was conducted following the same method as for the standards.

### **3.2.5 Improved TDA Extraction Method: Preparation of Standards**

A stock solution of TDA (10mmol) in dimethyl sulfoxide was used to prepare four replicates of standards consisting of 0, 5, 10, 25, 50, 75 and 100 $\mu$ mol TDA suspended in 1ml of HaCaT culture medium. 50 $\mu$ l of 10mmol NaOH was added

to each standard followed by the addition of 500 $\mu$ l of DCM. Each sample was mixed in a rotary tumbler for 10 minutes. The sample was then centrifuged at 3500rpm to separate out the organic layer. 450ml of the organic layer was removed. A further 500 $\mu$ l of DCM was added followed by tumbling and removal of a further 450 $\mu$ l of organic layer. The DCM rinse was repeated for a third time and the three 450 $\mu$ l extracts were combined and dried under nitrogen gas. The dried TDA was re-suspended in 300 $\mu$ l of acetonitrile containing 5 $\mu$ mol of EDA as an internal standard.

### **3.2.6 Preparation of Samples**

Samples were prepared at the Health and Safety Laboratory, Buxton. 12 well plates containing the cells and controls (containing blank media) were removed from incubation. Stock solutions of 1mmol TDI in DMSO was used to add 10 $\mu$ mol of TDI to the cells. A stock of 10mmol TDI in DMSO was used to add 100 $\mu$ mol TDI to a further set of cells. The TDI was added to 1 ml of media (warmed to 37°C) at twice the desired concentration. This media was pipetted onto the cells (which were already sited in 1ml of media) to give the desired final concentration of TDI. All plates were returned to incubation at 37°C. 1ml aliquots were removed from the corresponding well at the following time points: 0, 1, 3, 6 and 24 hours. The aliquots were immediately frozen in liquid nitrogen following removal from the well. Four replicates of each experiment were performed.

The samples were defrosted rapidly by suspension in boiling water and the addition of sodium hydroxide and extraction with DCM was conducted following the same method as for the standards.

### 3.2.7 LC-MS Analysis

#### i) Mass spectrometry

LC-MS analysis was conducted using an Applied Biosystems / MDS Sciex API 365 LC/MS/MS instrument. Samples were acquired in positive ion mode using a turbo ionspray source with the following settings: Temp: 350°C, Nebulising Gas: 10 l/h<sup>-1</sup>, Curtain Gas: 10 l/h<sup>-1</sup>

Experiments were conducted in selected ion recording (SIR) mode monitoring the protonated molecule [M+H]<sup>+</sup> for TDA at m/z 123 and the [M+H]<sup>+</sup> of EDA at m/z 213 with a dwell time of 0.5 seconds and a 0.20 m/z span.

#### ii) High Performance Liquid Chromatography

All HPLC was performed using a LC Packings UltiMate hplc pump with a LC Packings Famos autosampler. A mobile phase was used consisting of 60% acetonitrile with a 40% 0.1M ammonium acetate buffer (lowered to pH 4.7 by addition of glacial acetic acid) at a flow rate of 50 $\mu$ l/min. A Phenomenex Luna 5 $\mu$ m C18 column of dimensions 1x150mm was used. Under these conditions the TDA eluted rapidly from the column with a retention time of 2.5 minutes. A 40 minute run time incorporating a 10 minute flush with 100% acetonitrile was necessary to ensure no analyte remained on the column between samples. An injection volume of 10 $\mu$ l was used throughout.

### **3.3 Results**

#### **3.3.1 Extraction of TDA from TDI spiked HaCaT Cells**

##### **3.3.1.1 Construction of Calibration Curves**

Calibration curves were constructed by linear regression between peak area and compound concentration for the extraction of TDA from water and DMEM media matrices. Even with the incorporation of an EDA internal standard as recommended by the Health and Safety Laboratory, poor reproducibility and linearity were observed for the extractions of TDA from both spiked water (figure 3.1) and media (figure 3.2).

TDA concentrations from the extractions conducted from water were calculated from the water calibration curve whereas the values for both the cell media controls and the HaCaT cell extractions were calculated from the media calibration curve. However, due to the poor linearity of the curves the accuracy of values derived were questioned, which lead to the method developments as utilised in the second experiment.

### **3.1.1.2 Analysis of TDI Spiked HaCaT Cells**

From the graph showing data from the 10 $\mu$ mol TDI exposed cells (figure 3.3) a rapid initial increase of TDA formation is observed in extracts from the cell media control and the media containing the active cells. Between 0 and 30 minutes a 4-fold increase is observed in the media containing the HaCaT cells. This may be due to hydrolysis of TDI occurring within the cells. A smaller, 25% increase, is observed in the media control samples over the same time period with a greater than 2 fold increase occurring between 30 and 60 minutes. Smaller fluctuations in TDA concentration are observed for both the media control and the active cell samples over the remaining time periods (up to 24 hours), with a particular increase occurring between 3 and 6 hours after exposure. This is followed by a similarly sharp decrease in TDA concentration occurring between 6 and 24 hours.

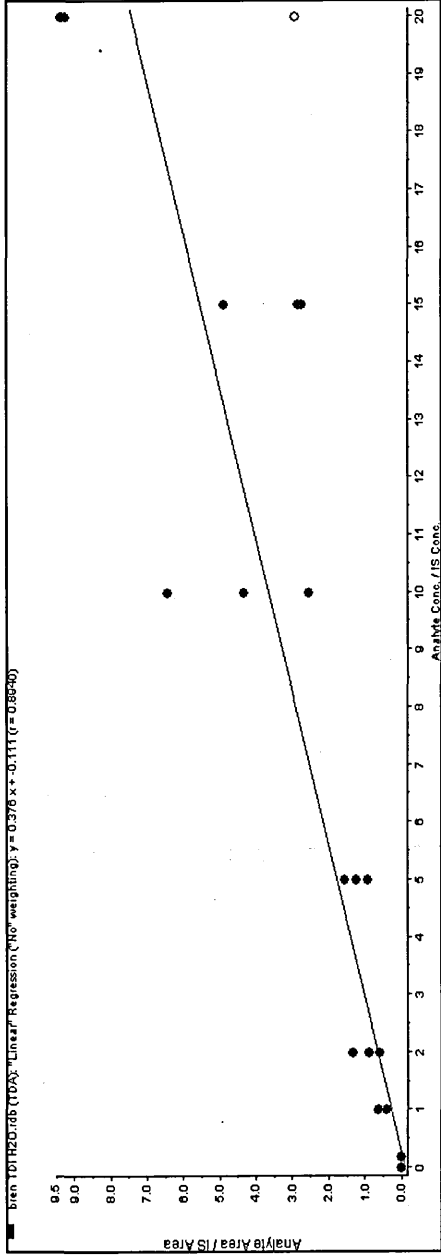


**Figure 3.1** Calibration curve for TDA obtained by LCMS analysis of spiked water extracts. Note concentration is shown as a ratio to the internal standard, in this case 1/5<sup>th</sup> of the true value. Poor linearity ( $R^2 = 0.894$ ) and reproducibility was observed ( $n=3$ )

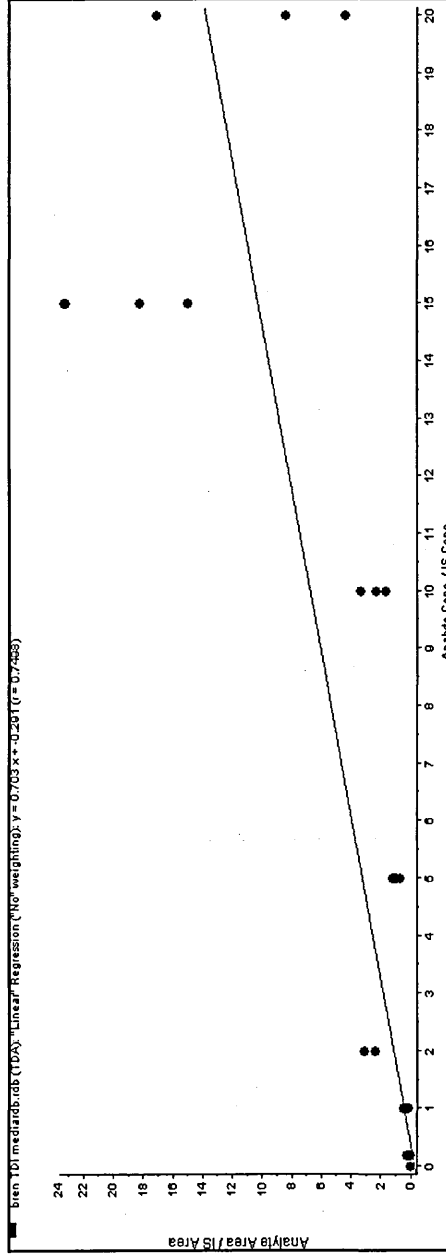


**Figure 3.2** Calibration curve for TDA obtained by LCMS analysis of spiked DMEM media extracts. Note: concentration is shown as a ratio to the internal standard, in this case 1/5<sup>th</sup> of the true value. Poor linearity ( $R^2 = 0.750$ ) and reproducibility was observed ( $n=3$ )

This may be due to further reactions occurring between the TDA and components present in the media although this is unlikely as the same pattern was not observed in the samples spiked with the higher concentration of TDI (figure 3.4). It is proposed that the result may be due to the poor precision of the extraction procedure as discussed for the calibration standards. This appears to be of particular concern for the 10 $\mu$ mol spiked samples.

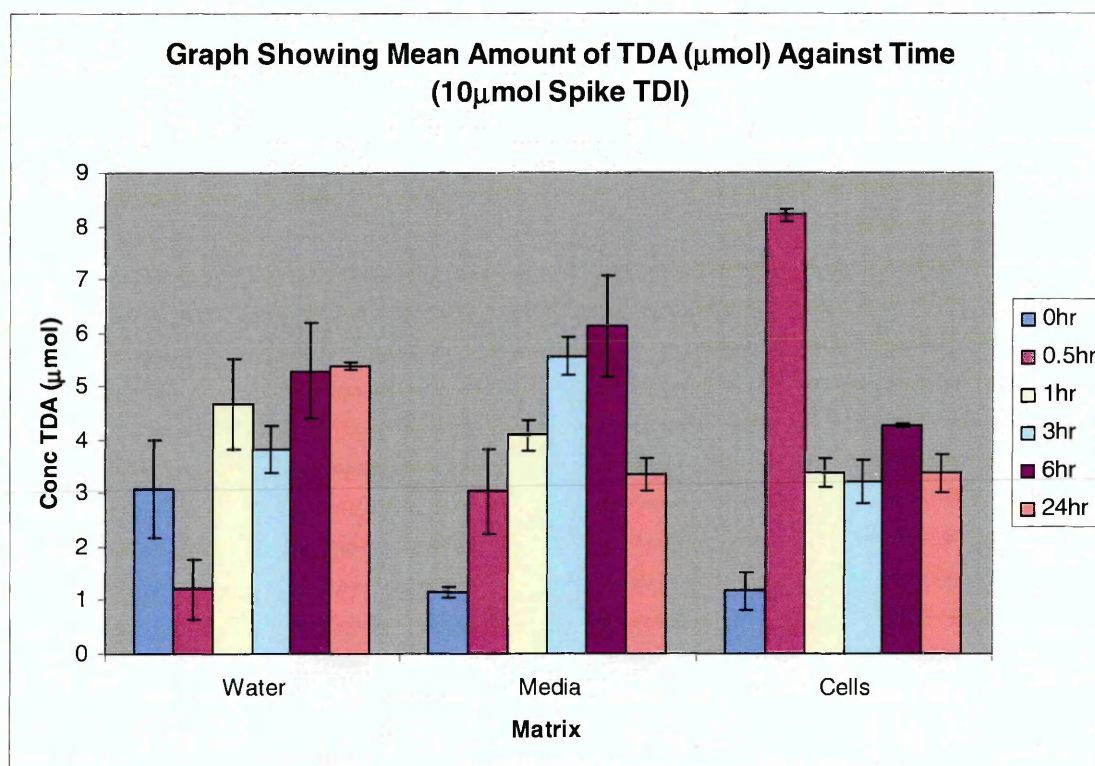


**Figure 3.3** Mean variation of the amount of TDA ( $\mu$ mol) in a culture of HaCaT cells, water and blank culture media with time following addition of 10 $\mu$ mol TDI (n=3)

The addition of a higher concentration of TDI to the media containing cells also resulted in a sharp (3-fold) increase in recorded TDA (figure 3.4) between the 0 and 30 minute time period. Once more, fluctuations occurred for the remaining time periods (1-24 hours) with an overall reduction in detectable TDA observed during this time. Once again it must be reiterated that the fluctuations may be caused by the poor precision of the method.

A 2-fold increase in TDA was observed in the media control samples over the same time period with a smaller increase occurring between 30 and 60 minutes. This was in contrast to the 10 $\mu$ mol spike where the greatest increase occurred during the later time period.

Comparable levels of TDA (between 2 and 6 $\mu$ mol over the 24 hour period) were extracted from the water, media control and active cells following the addition of 10 $\mu$ mol of TDI. The addition of 100 $\mu$ mol of TDI to water resulted in a yield of 22-54 $\mu$ mol of TDA in the extracts over the 24 hour period. Over the same time period the control media and HaCaT cell extracted TDA only ranged between 4.5 – 11.5 $\mu$ mol and 4.8 – 12.8 $\mu$ mol respectively. One theory to explain the low yield is the possibility of reactions or conjunctions occurring between the TDI and components in the media. Isocyanates have been observed to bind to proteins, peptides and amino acids all of which are contained in the media as they are essential components for cell growth, survival and reproduction. Preferential binding to these compounds may explain the low yield of unconjugated TDA.

This theory is further supported by the greater concentration of TDA detected in extractions from the spiked water control which contains no such materials for the TDI to react with.

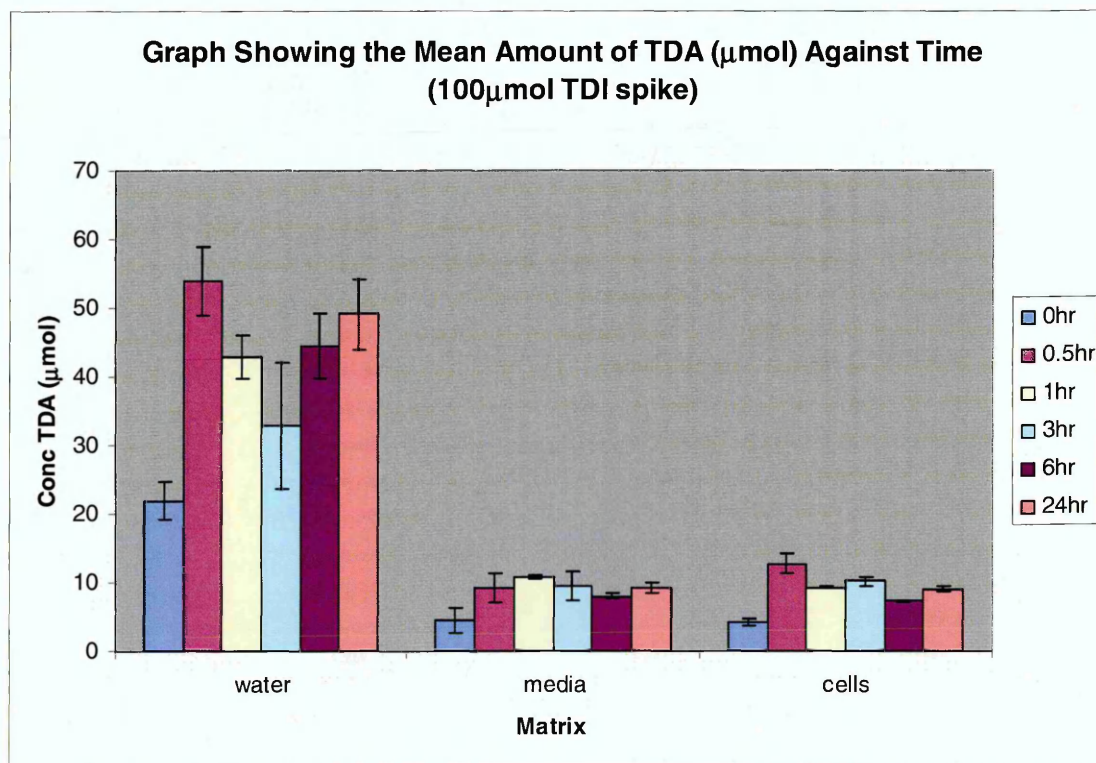


**Figure 3.4** Mean variation of TDA (µmol) in a culture of HaCaT cells, water and blank culture media with time following addition of 100µmol TDI (n=3)

Due to the reproducibility and accuracy issues, particularly with reference to the calibration standards, a triple DCM rinse procedure of the spiked media was developed to enhance the yield and reproducibility of the extraction method. A new delivery vehicle for adding TDI to the cells was proposed. It was thought that

pre-mixing the TDI (in DMSO) with cell media and pipetting this mixture onto the cells would prevent possible cell trauma due to the immediate localised toxic effect of TDI (and/or DMSO) on cells and enhance homogeneous distribution of TDI throughout the media surrounding the cells.

### **3.3.2 Extraction of TDA from TDI Spiked HaCaT Cells Incorporating a Triple Rinse Extraction Procedure**

An optimised repeat of the initial experiment was conducted to reduce the observed extraction errors and the water control was eliminated. A suitable calibration curve was produced (figure 3.5) showing vastly enhanced linearity and increased reproducibility.

For both spiked concentrations reproducibility was increased due to the triple rinse extraction method. Figure 3.6 shows the TDA levels recorded from the 10 $\mu$ mol spiked samples and, as for the previous experiment, an increase in TDA concentration can be seen for both the media control and the HaCaT cells between 0 and 1 hour. A further vast increase in TDA concentration occurs in the media control between 1 and 3 hours following exposure. While the cell extract levels remain relatively constant between 3 and 24 hours, the media control shows a significant drop in TDA over the same time period.

As for the previous experiment, the addition of an increased amount of TDI (100 $\mu$ mol) did not result in a proportional increase in the yield of recorded TDA (figure 3.7). Taking the 6 hour exposure point as an example, the 10-fold increase in TDI concentration only resulted in a mean increase of 4.93 $\mu$ mol of TDA from the HaCaT and 2.76 $\mu$ mol from media control samples (a sample for chromatograph for 10 $\mu$ mol and 100 $\mu$ mol TDI spiked HaCaT cells is shown in figure 3.8).

As isocyanates bind to proteins it may be expected that the TDI would conjugate with peptides and or proteins in the media when the TDI DMSO was pre mixed with warmed media immediately prior to delivery onto the cells. This could possibly result in a further decrease in the levels of TDA recovered after the 100 $\mu$ mol TDI spike. However addition of the TDI DMSO mixture directly on the cells (as conducted in the first experiment) resulted in the same low amount of TDA detected after the 100 $\mu$ mol TDI spike.

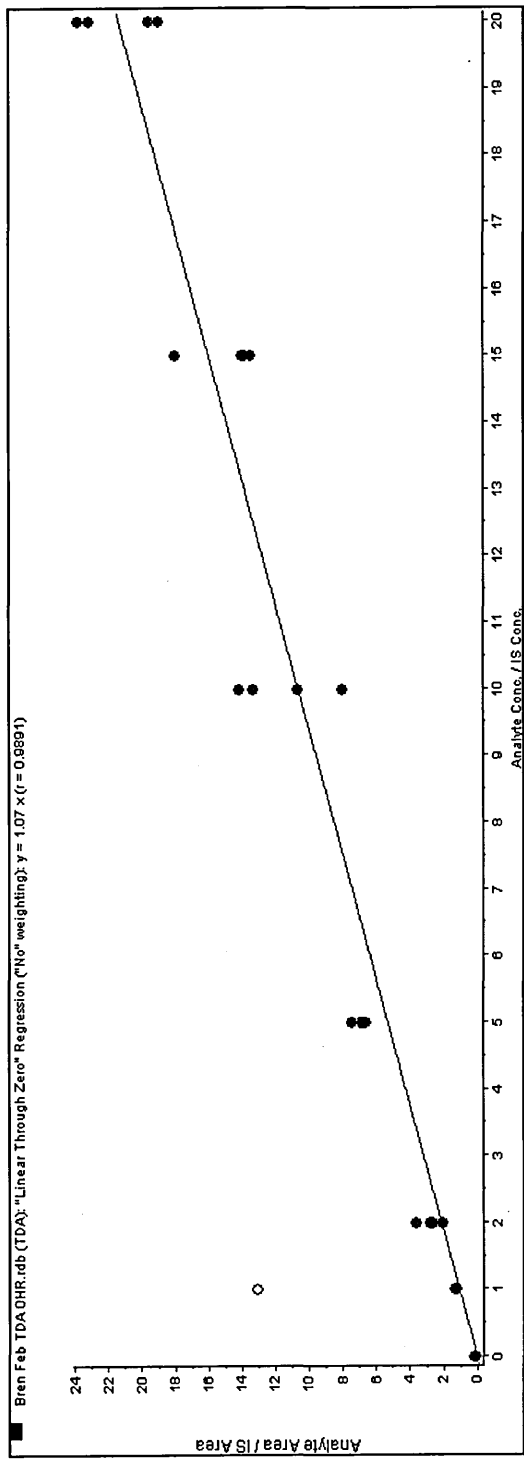


**Figure 3.5** Calibration Data for TDA obtained by LC-MS analysis of spiked media extracts. Note: concentration is shown as a ratio to the internal standard, in this case 1/5<sup>th</sup> of the true value. Satisfactory linearity was observed ( $R^2 = 0.989$ ) ( $n=4$ )

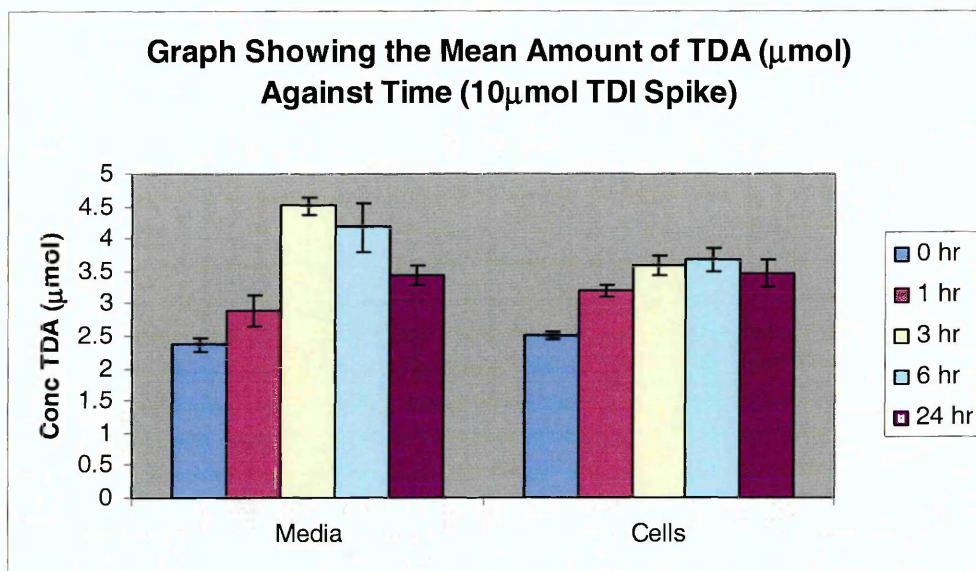


**Figure 3.6** Mean variation of the amount of TDA ( $\mu\text{mol}$ ) in a culture of HaCaT cells and blank media formed over time following addition of 10  $\mu\text{mol}$  TDI (n=4)

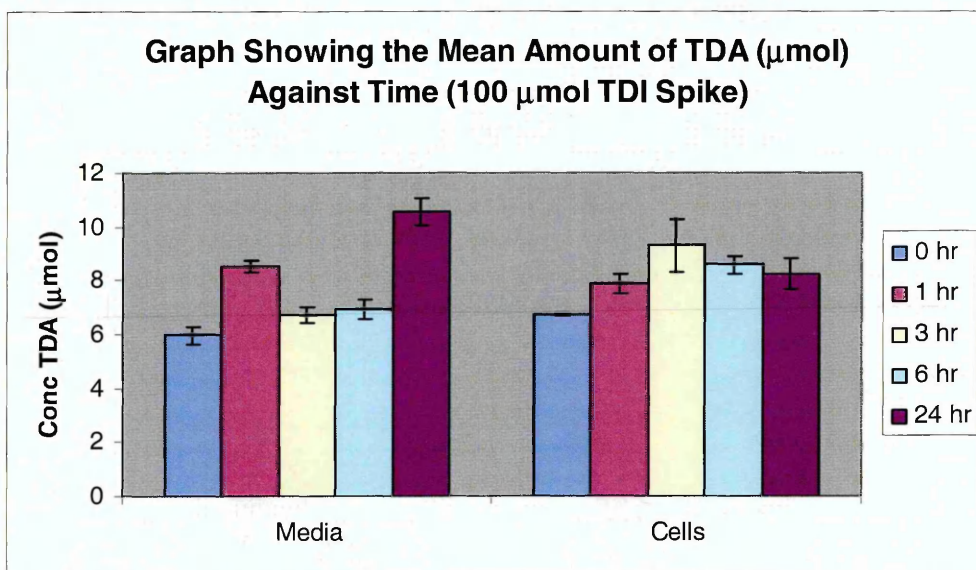
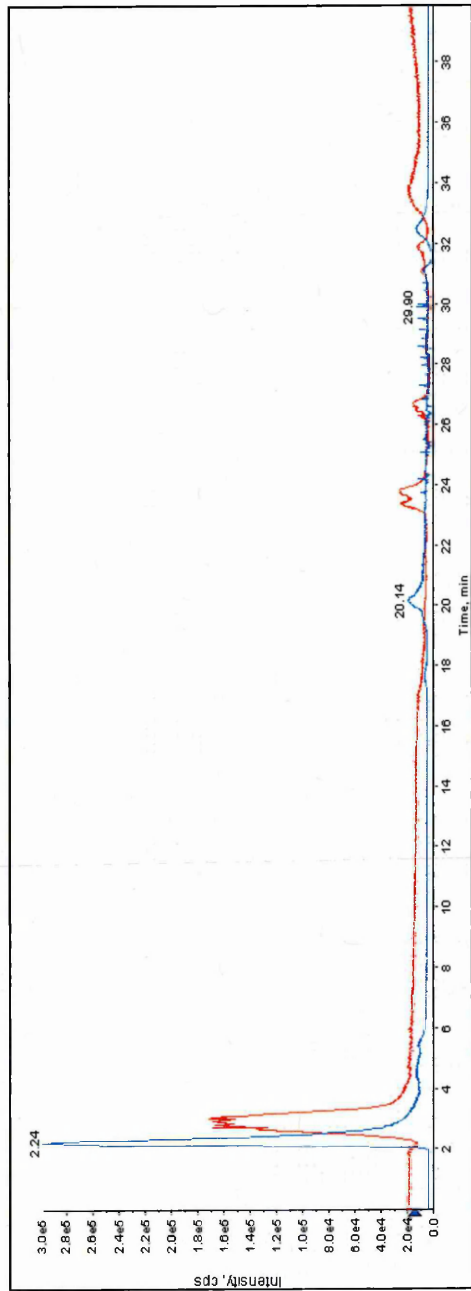
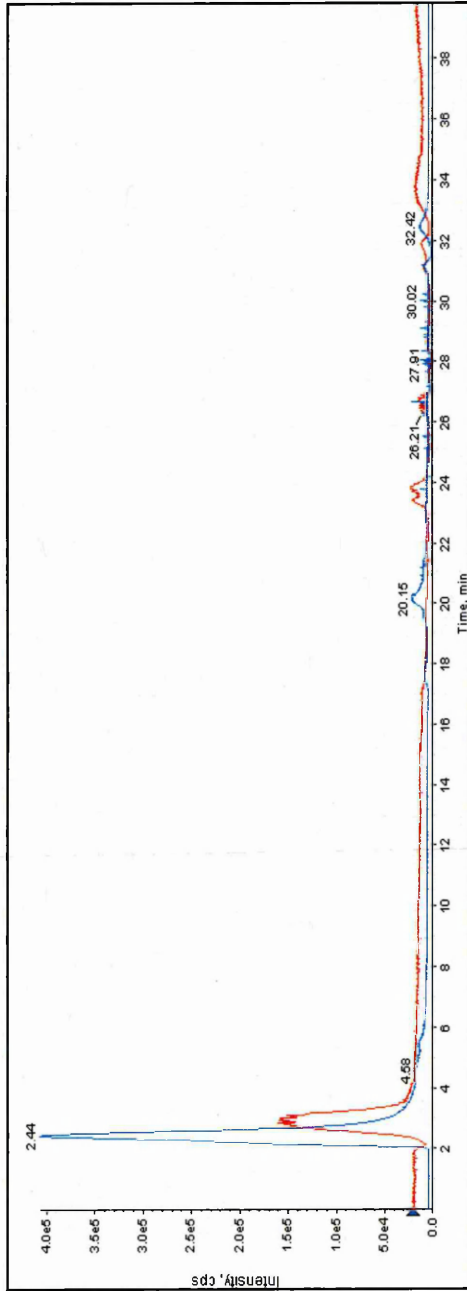


**Figure 3.7** Mean variation of the amount of TDA ( $\mu\text{mol}$ ) in a culture of HaCaT cells and blank media formed over time following addition of 100  $\mu\text{mol}$  TDI (n=4)



a



b

**Figure 3.8** Chromatograph showing the rapid elution of TDA at m/z 123 (blue trace) and EDA at m/z 213 (red trace) from 10 $\mu$ mol spike of TDI (a) and 100 $\mu$ mol spike of TDI (b). Note: even with the 10-fold increase in TDI concentration only a relatively small increase in TDA [M+H]<sup>+</sup> peak area is observed.

### 3.4 Conclusion

LC-MS analysis and a media extraction method incorporating a triple DCM rinse procedure has been developed as a quantitative method for the analysis of TDA. The method produced calibration data showing good linearity. However, the test samples analysed did not contain TDA in the expected concentration ranges following spiking with TDI. Several reasons have been proposed for this including possible reactions occurring between peptides and proteins.

Improvements and changes in the method increased the precision and accuracy of the extraction and analytical process. However, despite these improvements similar results were observed to the first experiment. The experiment is believed to have been unsuccessful due to the isocyanate – peptide conjugation. As peptides and FCS are essential media components for cell maintenance and proliferation it appears the experiment is not viable in its present form, except as a method for measuring the unconjugated diamine metabolite.

Conducting a lengthy acid hydrolysis as demonstrated by Skarping et al <sup>[17]</sup> may have increased the yield of TDA obtained but as this will hydrolyse any TDI or TDA conjugates or similar species present in the media it would be impossible to determine whether the diamine was pre-formed by reactions occurring within the cells as opposed to the hydrolysis of any remaining TDI or toluene monoamine in

the media during the extraction process. Another reason for the low yield of TDA could be that the TDI was conjugated to proteins within the cells and was not released back into the media as TDA. As only the media matrix surrounding the cells was extracted the conjugate may have remained in the well plate.

Alternative analytical methodologies need to be investigated. One method would be the identification and subsequent quantitation of a TDI conjugate biomarker. Another would be to assess and quantitatively measure increases in cytokine expression following exposure of the HaCaT cells to TDI. This could be conducted using immunological methods such as ELISA assays.

### 3.5 References

- [1] Bosch, E., Bou, P., Allemann, H., Roses, M., Retention of Ionizable Compounds on HPLC. pH Scale in Methanol-Water and the pK and pH Values of Buffers. *Anal. Chem.* 1996 68 p3651-3657
- [2] Liu, G., The effect of buffer salt concentration on the HPLC retention of nucleic acid components. *Chromatographia.* 1989 28 p493-496
- [3] Majors, R.E., Carr, P.J., Freeman, P.H., High performance liquid chromatography (HPLC). *Proc. Anal. Div. Chem. Soc.* 1975 12 p25-31
- [4] Cole, R.B., Some tenets pertaining to electrospray ionization mass spectrometry. *J. Mass. Spectrom.* 2000 35 p763-772
- [5] Iribarne, J.V., Thompson, B.A., On the evaporation of small ions from charged droplets. *J. Chem. Phys.* 1976 64 p2287-2294
- [6] Schmelzeisen-Redeker, G., Bütfering, L., Röllgen, F.W., Desolvation of Ions and Molecules in Thermospray-MS. *Int. J. Mass Spectrom. Ion Processes.* 1989 90 p139-150
- [7] Kless, J.E., Ott, M.G., Diisocyanates in polyurethane plastics applications. *Occup. Med.* 1999 14 p759-776
- [8] Bernstein, I.L., Isocyanate-induced pulmonary disease: A current perspective. *J. Allergy. Clin. Immunol.* 1982 70 p24-31
- [9] Koschier, F.J., Burden, J.A., Brunkhorst, C.S., Friedman, M.A., Concentration-dependent elicitation of dermal sensitization in guinea pigs treated with 2,4-toluene diisocyanate. *Toxicol. Appl. Pharamcol.* 1983 67 p401-407

[10] Nakashima, K., Takeshita, T., Morimoto, K., Review of the occupational exposure to isocyanates: Mechanisms of action. *Environ. Health Prev. Med.* 2002 7 p1-6

[11] Raulf, M., Baur, X., Pathomechanisms and pathophysiology of isocyanate induced diseases – summary of present knowledge. *Am. J. Ind. Med.* 1998 34 p137-143

[12] Timchalk, C., Smith, F.A., Bartels, M.J., Route-dependant comparative metabolism of [<sup>14</sup>C] toluene 2,4-diisocyanate and [<sup>14</sup>C]toluene 2,4-diamine in fischer 344 rats. *Toxicol. Appl. Pharmacol.* 1994 124 p181-190

[13] Sakai, T., Morita, Y., Roh, J., Kim, H., Kim, Y., Improvement in the GC-MS method for determining urinary toluene-diamine and its application to the biological monitoring of workers exposed to toluene-diisocyanate. *Int. Arch. Occup. Health* 2005 76 p459-467

[14] Sakai, T., Morita, Y., Kim, Y., Tao, Y.X., LCMS determination of urinary toluenediamine in workers exposed to toluene diisocyanate. *Toxicol. Lett.* 2002 134 p259-264

[15] Skarping, G., Dalene, M., Lind, P., Determination of toluenediamine isomers using capillary gas chromatography. *J. Chromatogr. A.* 1994 663 p199-210

[16] Dalene, M., Skarping, G., Lind, P., Workers exposed to thermal degradation products of TDI and MDI based polyurethane. *Am. Ind. Hyg. Ass. J.* 1997 58 p587-591

[17] Dalene, M., Skarping, G., Brorson, T., Chromatographic determination of amines in biological fluid with special reference to the biological monitoring of isocyanates and amines.4.Determination of 1,6-hexamethylene diamine in human urine using capillary gas chromatography and selective ion monitoring. J. Chromatogr. 1990 516 p405-413

[18] Liu, Y., Berode, M., Stowe, M.H., Holm, C.T., Walsh, F.X., Slade, M., Boeniger, M.F., Redlich, C.A., Urinary hexane diamine to assess respiratory exposure to hexamethylene diisocyanate aerosol: a human inhalation study. Int. J. Occup. Environ. Health. 2004 10 p262-271

[19] Persson, P., Dalene, M., Skarping, G., Adamsson, M., Hagmar, L., Biological monitoring of occupational exposure to toluene diisocyanate: measurement of toluene diamine in hydrolysed urine and plasma by gas chromatography mass spectrometry. Brit. J. Indus. Med. 1993 50 p1111-1118

[20] Lind, P., Dalene, M., Skarping, G., Hagmar, L., Toxicokinetics of 2,4- and 2,6-toluenediamine in hydrolysed urine and plasma after occupational exposure to 2,4- and 2,6-toluene diisocyanate. Occup. Environ. Med. 1996 53 p94-99

[21] RTI. Disposition of 2,6-toluene diisocyanate in fischer 344 rats. Report RTI/2227/ 00-06P In research triangle report to the NTP. 1985

[22] Kennedy, A.L., Alarie, Y., Brown, W.E., Comparative analysis of the uptake and distribution of inhaled <sup>14</sup>C labeled isocyanates in blood. Toxicologist. 1990 10 p236-242

[23] Rosenberg, C., Savolainen, H., Detection of urinary amine metabolites in toluene diisocyanate exposed rats. J. Chromatogr. 1985 323 p429-433

- [24] Karlsson, D., Spanne, M., Dalene, M., Skarping, G. Determination of complex mixtures of airborne isocyanates and amines. Part 4. Determination of aliphatic isocyanates as dibutylamine derivatives using liquid chromatography and mass spectrometry. *Analyst*. 1998 123 p117-23
- [25] Friedmann, P.S., Contact sensitization and allergic contact dermatitis: Immunobiological mechanisms. *Toxicol. Lett*. 2006 162 p49-54
- [26] Enk, A.H., Katz, S.I., Early molecular events in the induction phase of contact sensitivity. *Proc. Natl. Acad. Sci. USA*. 1992 89 p1398-1402
- [27] Kimber, I., Cumberbatch, M., Langerhans cell migration: initiation and regulation. In Moll, H., *The immune functions of epidermal langerhans cells*. 1995 R.G Landes Co. Austin p103-117
- [28] Cumberbatch, M., Kimber, I., Dermal tumor necrosis factor- $\alpha$  induces dendritic cell migration to draining lymph nodes and possibly provides one stimulus for Langerhans cell migration. *Immunology*. 1992 75 p257-263
- [29] Ban, D., Hettich, M., Goutet Bonnet, P., TDI inhalation in guinea-pigs involves migration of dendritic cells. *Toxicol. Lett* 1997 93 p185-194

## **4.0 Sample Preparation and Data Interpretation Procedures for the Examination of Xenobiotic Compounds in Skin by Indirect Imaging MALDI-MS**

## 4.1 Introduction

### 4.1.1 Introduction to Chlorpyrifos

Chlorpyrifos (*O,O*-diethyl-*O*-(3,5,6-trichloro-2-pyridyl) phosphorothioate (figure 4.1) is an insecticide in common use worldwide. It is classified as an organophosphate (OP) pesticide. Its structure consists of a phosphorothioate attached to a pyrimidine ring containing three chlorines, which makes the compound very hydrophobic in nature. Chlorpyrifos has many metabolites, primarily the chlorpyrifos-oxon intermediate (CPO) and metabolites: 3,5,6-trichloro-2 pyridinol (TCP) and 3,5,6-trichloro-2 methoxy pyridine (TMP) [1].

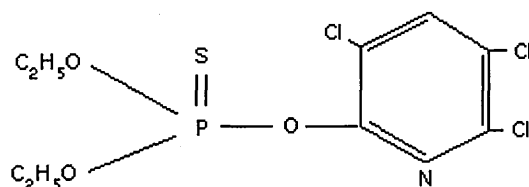


**Figure 4.1** The structure of Chlorpyrifos

Chlorpyrifos is commercially prepared by several methods, the most common of which includes reacting TCP with 0,0-diethyl phosphorochloridothioate under basic conditions with dimethyl formamide, as the final synthetic step. The synthesis of chlorpyrifos was first described by Rigterink in 1966 <sup>[2]</sup>.

The most common formulations of chlorpyrifos include: emulsifiable concentrates, granulers, and wettable powders, but other formulations available are dust, microcapsule, pellet, and sprays <sup>[3]</sup>. The purpose of each formulation is based on delivery and pest control in order to maximize product stability and availability to the target pest with a minimum of human exposure.

#### **4.1.2 Exposure**

Chlorpyrifos is mostly used as a foliar pesticide which can be applied by ground or aerial equipment, depending on crop type, to primarily control a variety of surface-feeding insects.

Chlorpyrifos is a component of many branded agricultural insecticide products. One of the most common of these is Dursban 4. Dursban 4 contains chlorpyrifos at a concentration of 480g/l in a registered solvent and is in liquid form at room temperature. It is applied to the crop as a suspension in water at concentrations ranging from 0.1-2% depending upon the severity of insect infestation.

Chlorpyrifos can be absorbed via skin contact, inhalation and ingestion, with the dermal route usually the most significant with occupational exposure <sup>[4]</sup>. Dermal exposure to chlorpyrifos has been measured by applying solutions to human volunteer skin and quantifying primary chlorpyrifos metabolites extracted from the volunteer's urine samples <sup>[5]</sup>. Until recently chlorpyrifos has been included in formulations used for domestic infestation control and concerns have been raised concerning infant and neonatal exposure resulting from household exposure <sup>[6]</sup>.

#### **4.1.3 Toxicity of Chlorpyrifos**

Acute exposure to Chlorpyrifos causes inhibition of acetylcholinesterase (AChE, EC 3.1.1.7) in the brain, neuromuscular junction and peripheral nerves. AChE activity hydrolyzes acetylcholine to choline and acetate at cholinergic synapses. Inhibition of AChE results in excessive accumulation of synaptic acetylcholine which continually stimulates cholinergic receptors in the central nervous system (CNS), autonomic nervous system and neuromuscular junction <sup>[7]</sup>. In vivo chlorpyrifos toxicity is primarily due to the P450 mono-oxygenase-mediated metabolism of chlorpyrifos to chlorpyrifos-oxon (CPO), which is a more potent acetylcholinesterase inhibitor than chlorpyrifos <sup>[8]</sup>. The toxic effects of organophosphates are largely associated with short-term exposures to high concentrations of pesticide, during the manufacture, formulation, mixing and application of these chemicals. In these cases, death may occur from respiratory

failure due to the paralysis of respiratory muscles, increased bronchial secretions and depression of the respiratory centre in the brainstem <sup>[9]</sup>. Long-term damage to the nervous system can also be caused by prolonged exposure to lower doses of chlorpyrifos. This is usually observed as poor mental health in patients as well as a reduction in memory capability and attention span <sup>[10]</sup>.

#### **4.1.4 Methods of Measuring Chlorpyrifos Exposure**

Exposure to chlorpyrifos is usually measured by recording metabolites such as TCP and TMP in urine or plasma <sup>[11]</sup>. The analysis may be conducted by mass spectrometric methods such as Gas Chromatography – Mass Spectrometry (GC-MS) <sup>[12]</sup> or more frequently LC-MS <sup>[13, 14]</sup>. HPLC methods have also been presented without the use of MS detection <sup>[15]</sup>. A urine extraction and clean-up method has been described by Koch et al 2001 using an automatic steam distillation process <sup>[16]</sup>. The use of this method allows limits of detection as low as 0.05µg per litre to be recorded when combined with GC-MS analysis.

## **4.1.5 Introduction to Isocyanates**

A detailed introduction to isocyanates has been presented in chapter two of this thesis. Isocyanates are commonly used in industry in the manufacture of polyurethane products such as foams, paints and plastics. They are highly reactive compounds, known to produce adverse effects in humans after exposure. Dermal exposure is of particular concern although the mechanisms of this are poorly understood.

### **4.1.5.1 Isocyanate Reactivity**

A comprehensive review of the reactive nature of diisocyanates has been previously presented in chapter 2 of this thesis. A derivatisation method incorporating the use of an alcohol to form a stable substituted isocyanate urea has been demonstrated and the reaction mechanism discussed. A range of derivatising compounds have been described and demonstrated for stabilising isocyanates for transportation and analysis including tryptamine <sup>[17]</sup>, 1-(2-methoxyphenyl) piperazine <sup>[18]</sup> and ferrocenoyl piperazide <sup>[19]</sup>.

#### **4.1.6 Aims**

Mass spectrometric imaging (MSI) analysis of isocyanate distribution on skin has not, thus far, been presented. Localizing the compound on the dermal surface could provide useful information concerning exposure parameters i.e. revealing routes of dermal exposure to areas of skin not fully covered by workers personal protective equipment (PPE). The aim of the investigation was to develop an imaging MALDI-MS method for measuring the distribution of the chlorpyrifos and isocyanates both on the surface of skin and as a dermal absorption profile.

#### **4.2 Method**

##### **4.2.1 Materials**

1-(2-methoxyphenyl) piperazine derivatised 1,6-hexamethylene diisocyanate (HDI-2MP) and Dursban 4 (Dow Agrochemicals) were provided by the Health and Safety Laboratory, Buxton. Chlorpyrifos standards were purchased from GMX.  $\alpha$ -Cyano-4-Hydroxy Cinnamic Acid ( $\alpha$ -CHCA) was purchased from Sigma-Aldrich (Dorset, U.K). Trifluoroacetic acid (TFA) and HPLC grade ethanol and acetone were purchased from Fisher (Leicester, U.K). Cellulose and carbon conductive membranes (0.08mm thickness) were obtained from Goodfellow, UK.

#### **4.2.2 Analysis of Chlorpyrifos on Porcine Epidermal Surface**

Porcine ear skin was used as a model of human skin for the investigation. 5µl of suspensions containing Dursban in water at dilutions of 1:10, 1:50, 1:100 and 1:500 were applied to separate areas of a 2cm x 2cm piece of tissue. The tissue was incubated at 37°C for 1 hour. A cellulose membrane was saturated in methanol and air dried for a period of 60 seconds prior to blotting. The membrane was applied to the tissue surface for 60 seconds. 5 ml of the matrix  $\alpha$ -Cyano-4-Hydroxy Cinnamic Acid ( $\alpha$ -CHCA), in acetone containing 0.1% TFA, was applied to the membrane by airspray at a distance of 10cm. The experiment was repeated using a carbon filled conductive membrane (0.08mm thickness, Goodfellow, UK). Dursban exposed tissue was blotted directly onto the carbon membrane without the use of methanol. Matrix was applied as for the previous experiment.

#### **4.2.3 Depth Profiling of Chlorpyrifos Absorption**

Suspensions of 200µl of Dursban in water (1:10 dilution) were applied to 2cm x 2cm pieces of tissue. The tissue was incubated at 37°C for 1 hour. Surface bound Dursban was lightly rinsed from the tissue with water for 5 seconds. The tissue was sectioned and blots of the tissue cross-sections performed onto cellulose (saturated in methanol and air dried for 60 seconds) and carbon

conductive membranes. 5ml of  $\alpha$ -CHCA, at 25mg/ml in acetone / 0.1% TFA, was applied to the membranes by airspray at a distance of 10cm.

#### **4.2.4 Analysis of HDI-2MP on Porcine Epidermal Surface**

Porcine ear skin was used as a model for human skin. 5  $\mu$ l of 1mg/ml HDI-2MP in methanol was applied to the surface of two pieces of porcine ear tissue (2 x 2cm). A commercially available plastic ring binder enforcer was used to maintain the circular distribution of the isocyanate on the skin. The tissue samples were incubated at 37°C for a period of one hour. Each piece of skin was rinsed with water and allowed to dry for 60 seconds before being blotted on the carbon filled membrane or the dry cellulose paper membrane. Both membranes were prepared for imaging analysis by applying 5ml of  $\alpha$ -CHCA (25mgml<sup>-1</sup>) by airspray to each respective membrane at a distance of 10cm.

#### **4.2.5 On-Membrane Ethanol-Derivatisation of HDI**

In order to evaluate the alcohol - isocyanate derivatisation/extraction approach, 1 $\mu$ l of neat HDI was pipetted onto the surface of a 2cm x 2cm piece of porcine skin. The tissue was incubated at 37°C for 1 hour. A cellulose membrane was saturated in ethanol and allowed to air-dry for a period of 60 seconds. The

membrane was applied to the tissue surface for 60 seconds. 5ml of the matrix  $\alpha$ -Cyano-4-Hydroxy Cinnamic Acid ( $\alpha$ -CHCA), in ethanol containing 0.1% TFA, was applied to the membrane by airspray at a distance of 10 cm. The experiment was repeated using porcine skin spiked with HDI in the same manner. In the subsequent experiment the ethanol saturated cellulose membrane was only allowed to air dry for a period of 30 seconds before being blotted onto the tissue.

#### **4.2.6 Mass Spectrometric Analysis**

All analyses were performed using an Applied Biosystems/MDS Sciex API "Q-Star" Pulsar I hybrid quadrupole time of flight instrument, fitted with an orthogonal MALDI ion source and "O-MALDI Server 4.0" ion imaging software. The Nd:YAG laser used has an elliptical laser spot size of 150 $\mu$ m x 100 $\mu$ m. The laser was used at an energy setting of 30% (3.2 $\mu$ J) and a repetition rate of 1 kHz. The laser was rastered over the membrane surface and mass spectra were acquired at 0.2mm increments, the laser firing for approximately 2 seconds per spot.

## 4.3 Results

### 4.3.1 MALDI-MS Spot Analysis of Chlorpyrifos Standard and Dursban 4

From the recorded spectra from the chlorpyrifos standard (figure 4.2a) a clear ion pattern is observed for chlorpyrifos showing two peaks of approximate equal intensity at  $m/z$  349.9 and  $m/z$  351.9. The distinct spectra are due to the chlorine isotope distribution of the chlorpyrifos molecule. A high intensity signal was recorded for the protonated molecule  $[M+H]^+$  at  $m/z$  351.87 and sodium adducts were observed a  $m/z$  373.84 for both the chlorpyrifos standard and the Dursban 4 formulation (figure 4.2b).

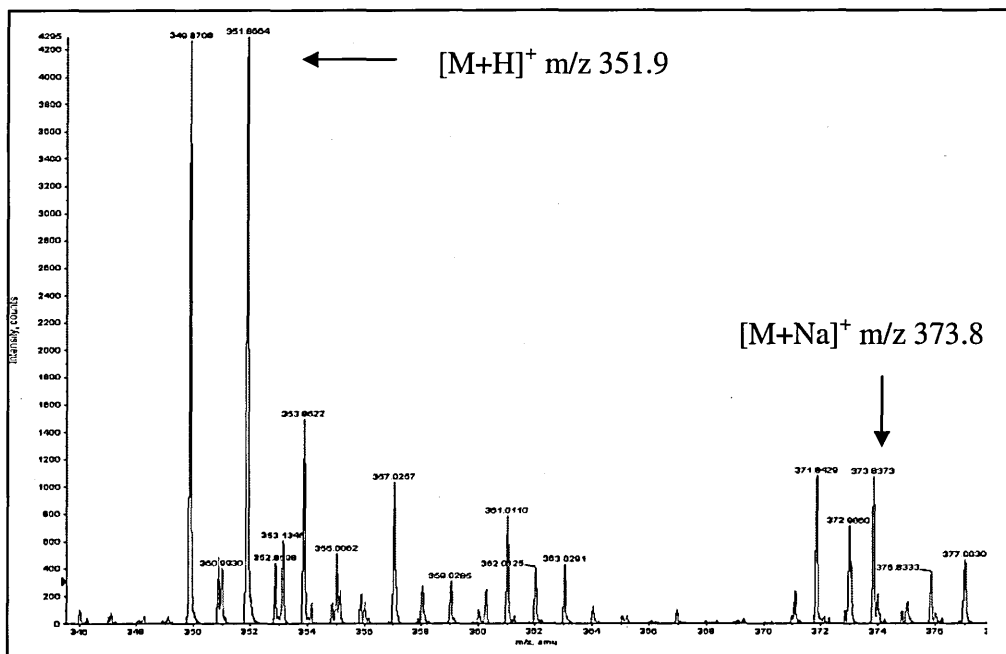


**Figure 4.2a** MALDI-MS spectrum showing the presence of the chlorpyrifos protonated molecule isotope pattern and sodium adducts from chlorpyrifos standard

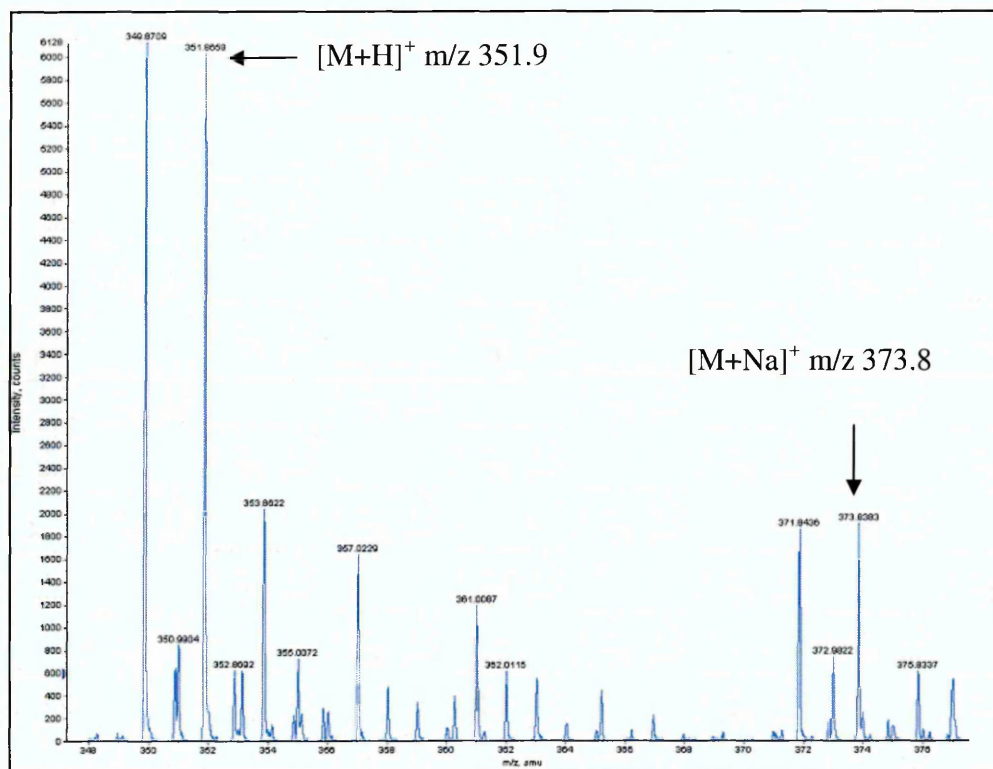


**Figure 4.2b** MALDI-MS spectrum showing the presence of the chlorpyrifos protonated molecular isotope pattern and sodium adducts from Dursban 4.

### 4.3.2 Profiling Chlorpyrifos Absorption on Skin Surface

A relatively homogeneous coverage of  $\alpha$ -CHCA matrix was observed on both the cellulose and carbon membranes. The images included show the distribution of the  $\alpha$ -CHCA molecular ion over the surface of the blotting membrane (figures 4.3a and 4.3b). A lower intensity of matrix ions is observed in the regions of the membrane blotted directly onto the Dursban; this may be due to matrix suppression by the chlorpyrifos.

Figures 4.4 and 4.5 show a comparison of two different approaches for surface blotting techniques for the imaging of chlorpyrifos on skin. Whilst both approaches proved successful as can be seen, the use of carbon membranes yielded higher quality images. In addition analyte spreading was minimised during the blotting process since there was no requirement for a transfer solvent.

Chlorpyrifos has been extracted from the surface of the porcine epidermal tissue at the 1:10, 1:50 and 1:100 dilutions by utilising a methanol saturated cellulose membrane (figure 4.4). At the highest concentration analyte spreading has occurred and the intensity of ions observed at the 1:50 and 1:100 dilutions is low (barely visible in the image at the 100 fold dilution). The lowest concentration at 1:500 was not observed on the membrane indicating the use of cellulose membranes in this method could not extract sufficient chlorpyrifos from the Dursban exposed tissue to be detected by the current instrumentation. The use of the extraction solvent in this blot is the most likely reason for the analyte spreading observed at the higher concentrations of Dursban.

Chlorpyrifos was observed at all the tested concentrations by imaging MALDI-MS analysis of the carbon membrane (figure 4.5). Spatial resolution had been retained at the higher concentration ranges and a good intensity of chlorpyrifos molecular ions is observed for the entire dilution range examined. Using carbon membranes the presence of chlorpyrifos was detected even at the 1:500 dilution, although the ion intensity observed is low.

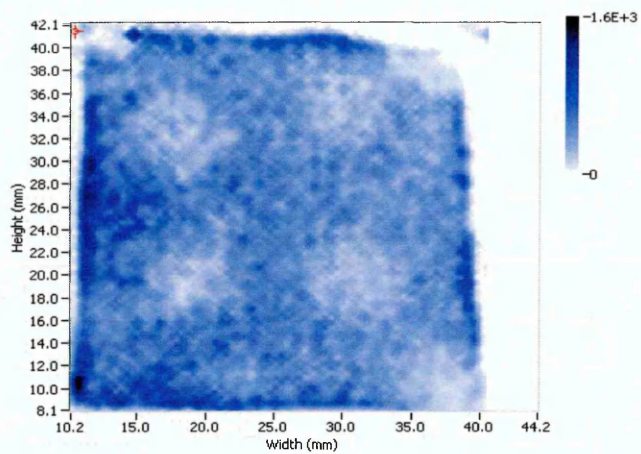


**Figure 4.3a** MALDI Image showing the homogeneous coverage of the protonated molecule of  $\alpha$ -CHCA ( $m/z$  190) over the cellulose membrane surface

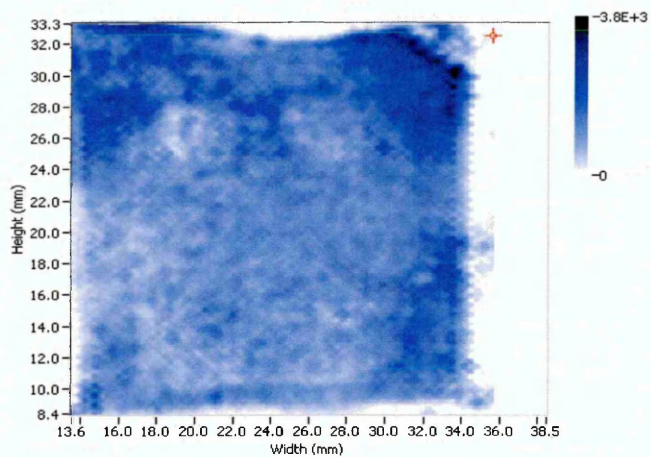


**Figure 4.3b** MALDI Image showing the homogeneous coverage of the protonated molecule of  $\alpha$ -CHCA ( $m/z$  190) over the carbon membrane surface

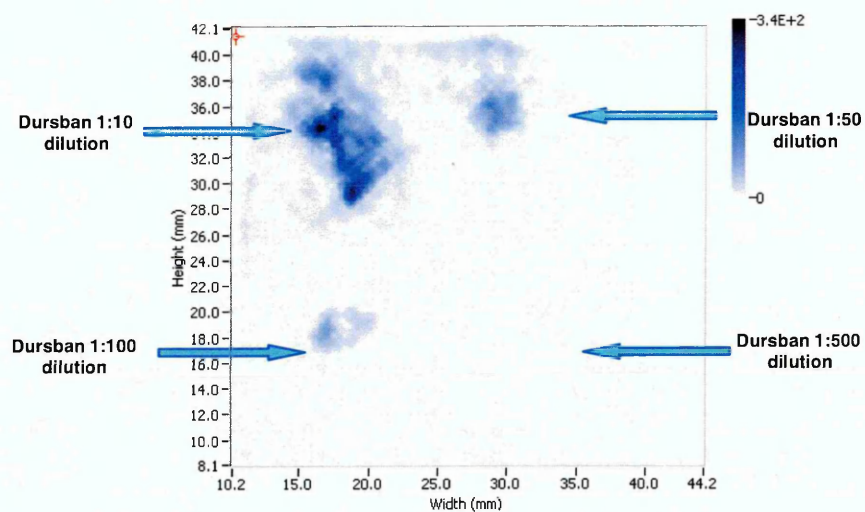


**Figure 4.4** MALDI image showing distribution of the chlorpyrifos protonated molecule (m/z 351.9) on the cellulose membrane surface

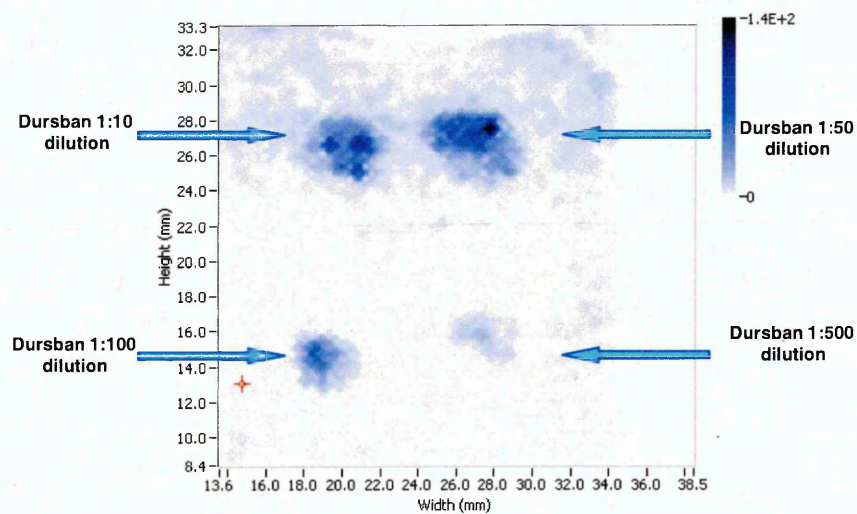


**Figure 4.5** MALDI image showing distribution of the chlorpyrifos protonated molecule (m/z 351.9) on the carbon membrane surface

### 4.3.3 Profiling Chlorpyrifos Absorption into Skin

The protonated molecule of chlorpyrifos was observed from the cellulose blot of the Dursban exposed porcine tissue (figure 4.6). However it was not seen across the entire exposed area, but only in a small localised pocket. Chlorpyrifos ions were detected down to a depth of 1.7mm in the tissue indicating chlorpyrifos had penetrated through the stratum corneum. One reason for the poor extraction of chlorpyrifos from the cross section of tissue could be due to the choice of a volatile extraction solvent. The majority of ethanol had evaporated from the membrane before the blotting took place (this was to minimise analyte spreading), which was vital as maintaining spatial resolution was paramount for this experiment. However, if the ethanol did not evaporate uniformly from the membrane, this would leave pockets of the membrane that contained more ethanol than others. This may explain why only localised areas of chlorpyrifos were seen from the blot, i.e. the areas where chlorpyrifos is seen in the image is where the membrane contained the most ethanol and thus more chlorpyrifos was extracted from the surface.

The carbon blotting medium was also the most successful for imaging of the vertical section. Chlorpyrifos was observed to reach a penetration depth of 1.7 mm (Figures 4.7 & 4.8). Chlorpyrifos was observed to penetrate through the epidermis and dermis within the 1 hour exposure time with the highest concentration being observed in the dermis. This can be clearly seen when the

chlorpyrifos  $[M+H]^+$  distribution image is placed next to a subsequent skin tissue section (figure 4.8). A small amount remains on the surface and the chlorpyrifos concentration increases with depth until it reaches a peak amount in the dermis. The prevalence of ions decreases in the lower dermis and hypodermis regions. The possibility of chlorpyrifos being removed from the uppermost layers of the skin during the light rinsing process is low due to the high hydrophobicity of the compound.

Complete absorption of chlorpyrifos through skin is well documented with chlorpyrifos being detectable in the urine of exposed workers (J. Cocker *personal communication*). A proposed reason for the improved performance of carbon membranes is due to the relative non-polar and highly hydrophobic properties of the analyte. From this limited study it would appear that the choice of membrane is related to the hydrophobicity of the compound. However, the blotting procedure is not 100% reproducible with satisfactory images only produced from approximately 50% of the blots. The process also appears to be dependent upon the physical properties of the tissue. Fat and endogenous liquids including blood may be transferred during the blotting process causing analyte suppression and resulting in the production of a poor quality image.

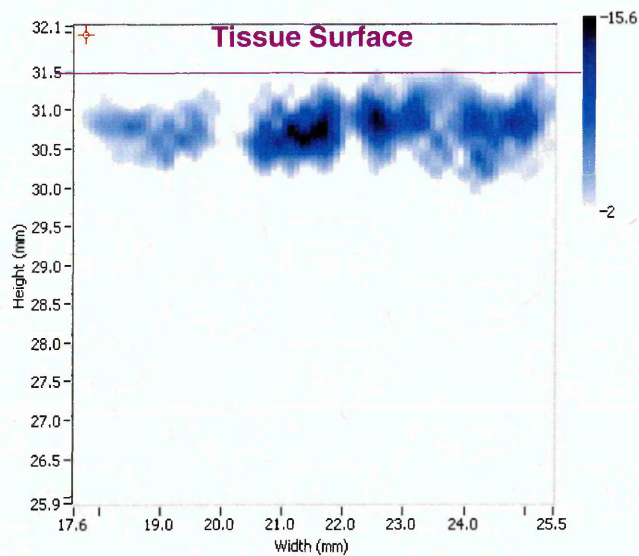


**Figure 4.6** Image showing the distribution of Chlorpyrifos (m/z 351.9) within a vertical cross section of skin blotted onto a carbon membrane. A penetration depth of 1.7mm is observed.

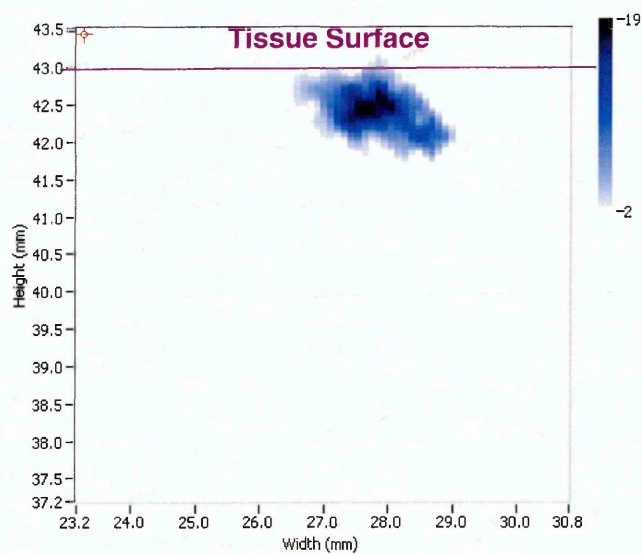


**Figure 4.7** Image showing the distribution of Chlorpyrifos (m/z 351.9) within a vertical cross section of skin blotted onto a cellulose membrane. A penetration depth of 1.5mm is observed.

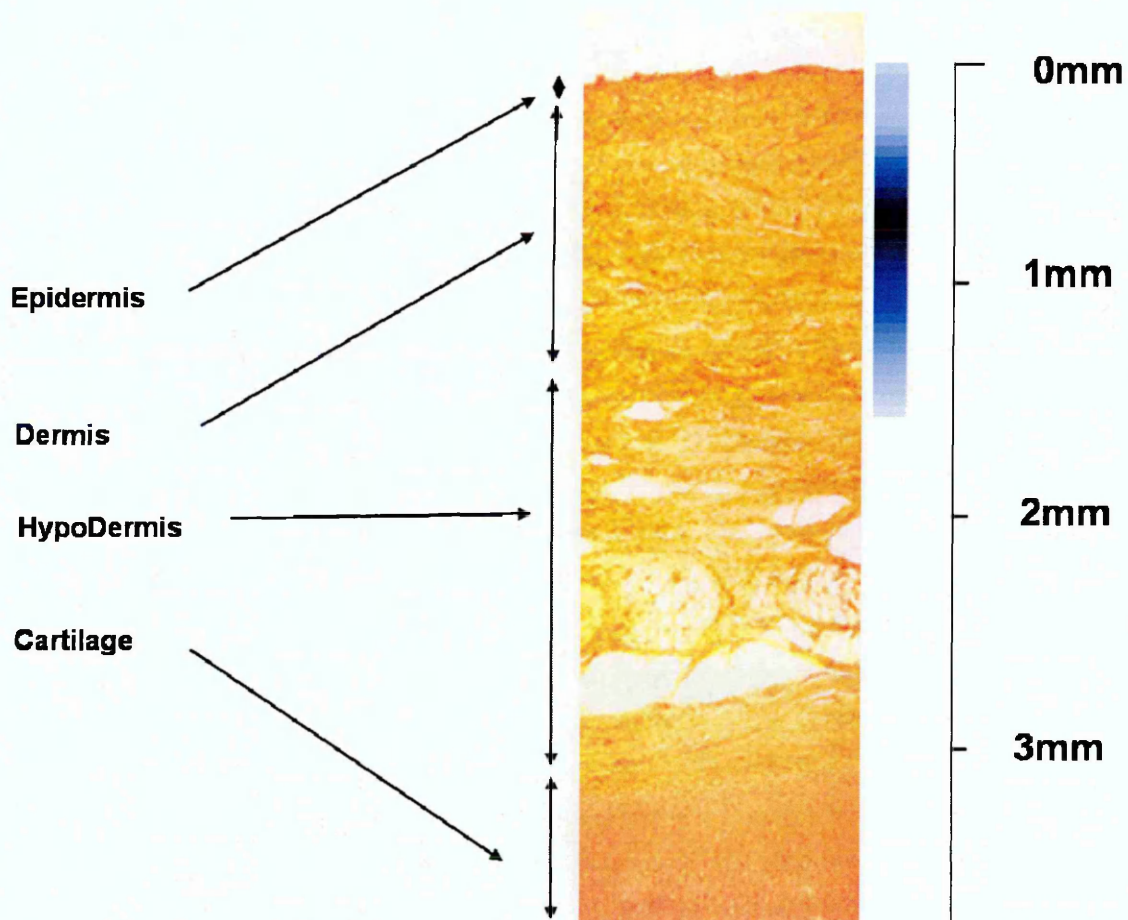


**Figure 4.8** Comparison of the histological image obtained from a skin section and the corresponding MALDI image taken from an adjacent section blotted onto a carbon membrane. The chlorpyrifos appears to have penetrated through the epidermis, dermis and into the hypodermis tissue. However after the one hour exposure time used in this experiment the highest concentration of chlorpyrifos is in the dermis.

#### 4.3.4 Analysis of HDI-2MP on Porcine Epidermal Surface

The images show homogeneous matrix coverage over both the cellulose and carbon membranes. A high intensity of matrix is observed on the surface of both membranes as indicated by the coverage of the  $[M+H]^+$  for CHCA at  $m/z$  190 for the cellulose (figure 4.9a) and the carbon membrane (figure 4.9b).

The distribution of the derivatising agent methoxy piperazine (MP) on the surface of the carbon filled membrane shows that some analyte spreading has occurred (figure 4.9d). The image from the cellulose blotting retains the circular exposure shape although there appears to be an excess of isocyanate that has formed part of an outer ring (figure 4.9c). This is likely to be due to the isocyanate spreading over the top of the ring enforcer during incubation rather than spreading during the blotting process as the circular shape has been clearly maintained. The analyte appears to have travelled over the plastic shape retainer before the blotting as opposed to diffusion during blotting as in the case of the carbon filled membrane. The carbon membrane produced a slightly higher maximum intensity of MP  $[M+H]^+$  ions at  $m/z$  193 ( $1.6 \times 10^3$  in comparison to  $1.3 \times 10^3$ ) this may be directly related to the slightly higher abundance of matrix ions observed on the surface of the carbon membrane.

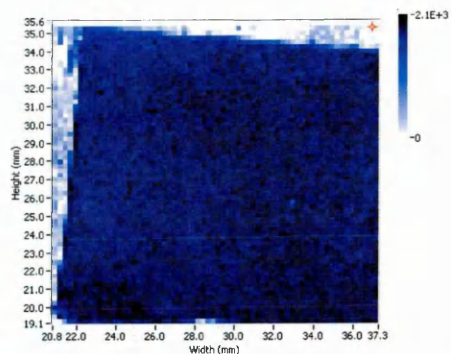


**Figure 4.9a** Distribution of a-CHCA  $[M+H]^+$  at  $m/z$  190 over cellulose membrane

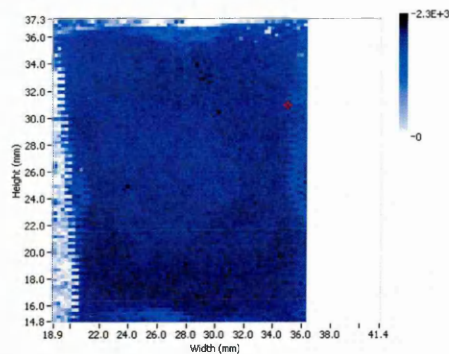


**Figure 4.9b** Distribution of a-CHCA  $[M+H]^+$  at  $m/z$  190 over carbon membrane

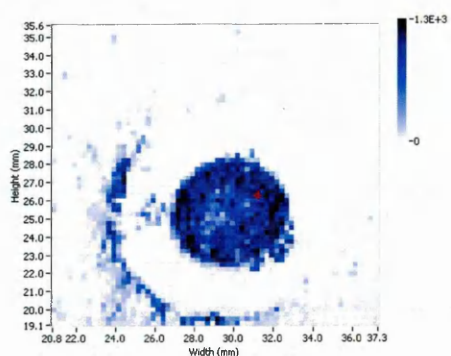


**Figure 4.9c** Distribution of MP derivatising agent  $[M+H]^+$  at  $m/z$  193 over cellulose membrane

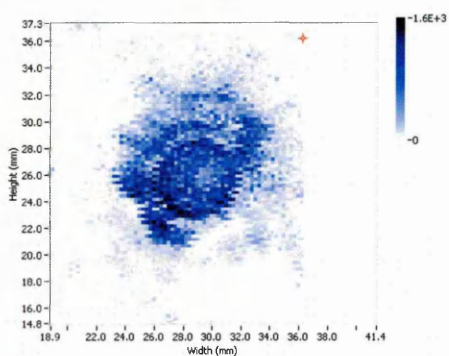


**Figure 4.9d** Distribution of MP derivatising agent  $[M+H]^+$  at  $m/z$  193 over carbon membrane

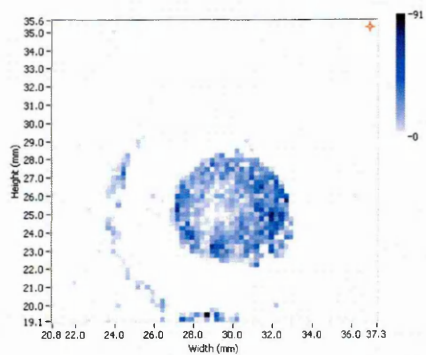


**Figure 4.9e** Distribution of HDI-2MP  $[M+H]^+$  at  $m/z$  553 over cellulose membrane

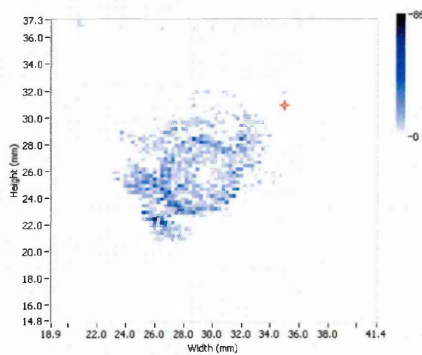


**Figure 4.9f** Distribution of HDI-2MP  $[M+H]^+$  at  $m/z$  553 over carbon membrane

The molecular ion of HDI-2MP was observed from blots performed using both types of blotting media (figures 4.9e & 4.9f). A higher degree of analyte spreading occurred during the extraction of the isocyanate from the skin using the carbon membrane.

HDI-2MP  $[M+H]^+$  maximum ion intensities were very similar for both blotting media although the ions seem more highly concentrated within the 'ring' on the cellulose membrane. The spreading which occurred during the carbon blot resulted in the ions being distributed over a wider surface area. From comparison of the images 4.9c with 4.9e and 4.9d with 4.9f, a higher intensity of HDI-2MP molecular ions is observed in the same locations as the higher intensities of MP ions.

One reason for the loss of spatial information occurring during the carbon blots is the hydrophilic nature of the compound. The HDI-2MP has a greater polarity than the previously investigated chlorpyrifos and thus hydrophobic interactions between the compound and the carbon surface are weaker. Hence the physical and chemical nature of the analyte will influence the most suitable choice of blotting media. The moisture content of the tissue is also a factor. Increased moisture content will aid the transfer of a water soluble analyte into the absorbent cellulose membrane whereas an excess of liquid results in 'spreading' of the analyte over the shiny, non absorbent carbon surface during the blotting process.

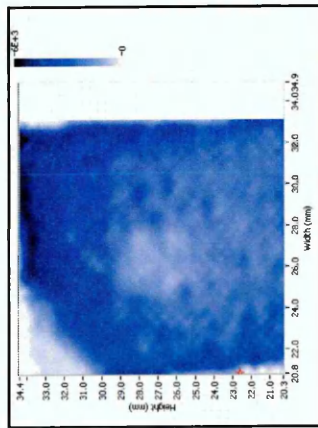
### 4.3.5 On-Membrane Ethanol-Derivatisation of HDI

Ethanol derivatised HDI was observed in the skin as monomer and dimer species (figure 4.10 b&c). Underivatised HDI species were also present (figure 4.10 d-f) and these were observed at higher intensities than ethanol-derivatised HDI. Figure 4.10b shows the distribution of the ethanol derivatised HDI. Spatial information has been clearly maintained during the blotting process and a high intensity of the derivatised  $[M+H]^+$  ion is recorded (<1000 counts). The HDI dimer is also derivatised by ethanol and this is observed from the same blot at an  $m/z$  value of 403 (figure 4.10c). Again spatial resolution is maintained throughout the blotting process and the ion intensity observed is approximately half that of the derivatised monomer.

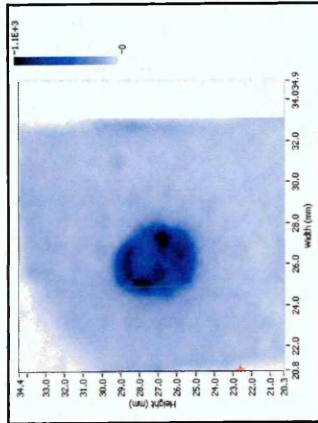
From experiments previously conducted at Sheffield Hallam University (and reported in chapter 2 of this thesis) it is known that the reaction between an alcohol and a diisocyanate is time-dependent. Therefore it would be expected that the HDI would not be fully derivatised during the relatively short blotting (and thus short ethanol exposure) time period. This is clearly observed from the results obtained. Underivatised HDI is observed in monoamine (figure 4.10d), dimer (figure 4.10e) and trimer (figure 4.10f) form from the analysed blot. In all cases the underivatised species was observed at far higher abundance than the derivatised counterpart. In a direct comparison between the HDI dimer species a

maximum ion intensity of 8500 was observed for the underivatised isocyanate, showing an approximate 14-fold increase on the derivatised species (max ion intensity of 590).

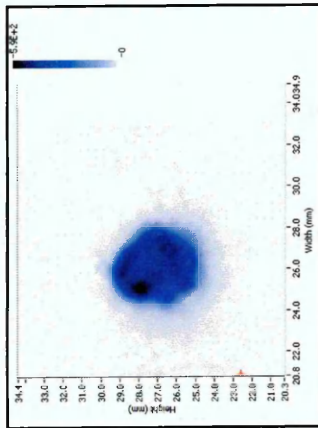
No derivatised trimer of HDI was observed from the blots. However, an underivatised trimer was recorded at a relatively high intensity. As lower intensities of HDI derivatised dimers were recorded than monomers it is believed that the derivatisation kinetics decrease in relation to isocyanate polymer length. This is supported by previous research that indicates isocyanate reactivity decreases with polymer chain length <sup>[20]</sup>. Underivatised HDI monomer ( $[M+H]^+$  expected at  $m/z$  169) was not observed in any of the blots. It is believed that the diisocyanate had hydrolysed to the monoamine (observed at  $m/z$  143) or the diamine 1,6-hexamethylene diamine (1,6-HDA) of which the protonated molecule was observed at  $m/z$  117.



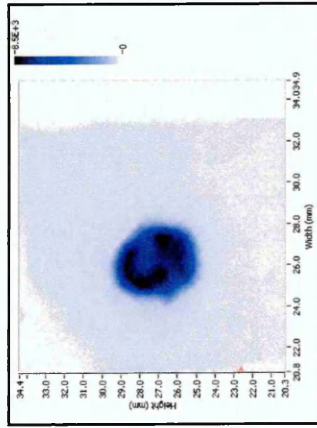
a)  $\alpha$ -CHCA [M+H]<sup>+</sup>  
m/z 190.1



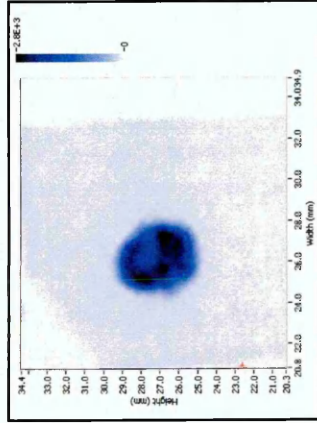
b) Ethanol-Derivatised HDI  
m/z 261.2



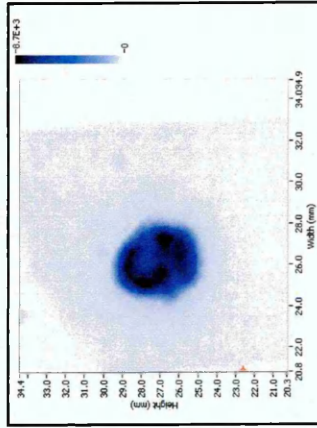
c) Ethanol-Derivatised HDI  
Dimer m/z 403.3



d) Underderivatised HDI  
monoamine m/z 143.1

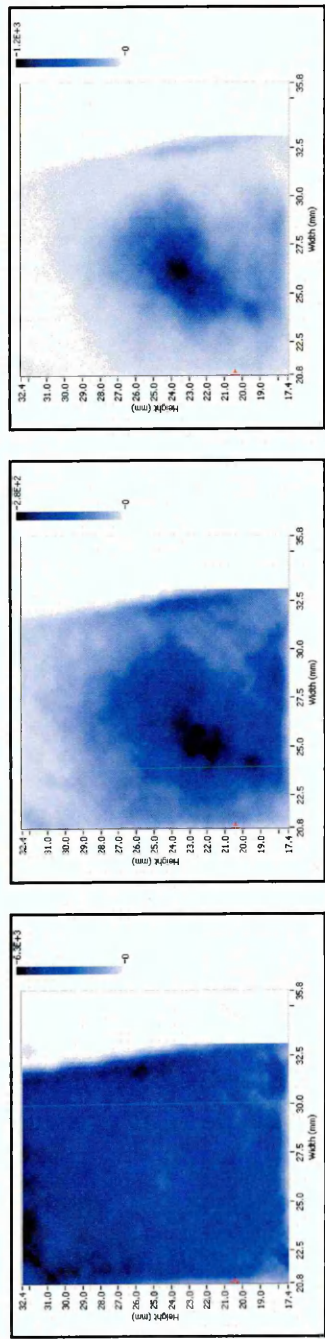


e) Underderivatised HDI Dimer  
m/z 311.2

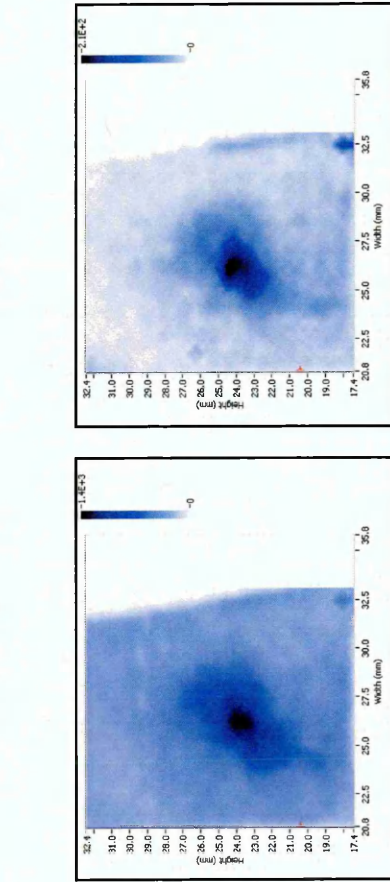


f) Underderivatised HDI Trimer  
m/z 453.2

**Figure 4.10** – MALDI-MS images showing the distribution of ethanol-derivatised HDI (b&c) and underderivatised HDI (d-f) from a blot taken from porcine skin surface utilising an ethanol saturated cellulose membrane



b) Ethanol-Derivatised HDI  
m/z 261.2



d) Underivatised HDI Dimer  
m/z 311.2



f) Underivatised HDI Trimer  
m/z 453.2

**Figure 4.11** – MALDI-MS images showing the distribution of ethanol-derivatised HDI (b&c) and underivatised HDI (d-f) from a blot taken from porcine skin surface utilising an ethanol super-saturated cellulose membrane

Increasing the ethanol saturation on the membrane led to increased intensity of ethanol-derivatised HDI ions observed (figure 4.11 b&c). However, spreading and thus loss of spatial information occurred. Underivatised ions were still observed at much higher intensities than the derivatised isocyanates (figure 4.11 d-f). Even with the increased amount of ethanol on the membrane a derivatised HDI trimer was not observed. As the underivatised trimer was still present (figure 4.11f) it is believed the derivatisation of the trimer did not occur before complete evaporation of the ethanol from the membrane.

#### **4.4 Conclusion**

Solvent assisted blotting proved to be previously successful for determining the xenobiotic distribution of compounds in biological tissue. Loss of spatial resolution was observed but by manipulation of experimental parameters it could be minimised. In contrast this procedure has not been found suitable for the analysis of the absorption of chlorpyrifos into skin. Here, the loss in spatial resolution caused by use of an extraction solvent was unacceptable and the use of a hydrophobic membrane was found to be more appropriate.

The use of a dry cellulose membrane as a blotting medium for the determination of derivatised HDI from skin proved successful. HDI-2MP was extracted from the

skin surface and spatial resolution was maintained. The carbon membrane proved less successful in this instance. It is believed this is due, in part, to the moisture content of the porcine tissue which is variable dependent on the tissue section used. Increased moisture content aids the transfer of water soluble compounds to the absorbant cellulose membrane whereas the higher moisture content could lead to increased analyte spreading during the blotting process using carbon membranes.

Preliminary work carried out on the incorporation of a derivatisation step into indirect MALDI imaging by blotting isocyanate treated skin onto ethanol soaked membranes has indicated the potential of such an approach for stabilising reactive analytes and enhancing sensitivity. However significant loss in spatial information occurred with the increasing ethanol saturation of the cellulose membrane indicating this method would be unacceptable for occasions where such margins are paramount i.e depth profiling of compounds.

From the investigation it may be concluded that successful extraction and imaging of an analyte from the skin is dependent upon optimisation of the blotting parameters. Of paramount importance is the choice of blotting media whose suitability is determined by the physical and chemical properties of the analyte.

## 4.5 References

- [1] Nolan, R.J., Rick, D.L., Freshour, N.L., Saunders, J.H., Chlorpyrifos: Pharmacokinetics in human volunteers. *Toxicol. Appl. Pharmacol.* 1984 73 p8-15
- [2] Rigterink R.H., O-Pyridyl Phosphates and Phosphorothiorates. U.S Patent No. 3,244,586
- [3] Yamashita, M., Tanaka, J., Ando, Y., Human mortality in organophosphate poisonings. *Vet. Hum. Toxicol.* 1997 39 p84-85
- [4] Griffin P., Mason H., . Heywood K., Cocker J., Oral and dermal absorption of chlorpyrifos: a human volunteer study. *Occup. Environ. Med.* 1999, 56, p 10–13.
- [5] Drevenkar, V., Vasilik, Z., Stengl, B., Frobe, Z., Rumenjak, V., Chlorpyrifos metabolites in serum and urine of poisoned persons. *Chem. Biol. Interact.* 1993 87 p315-322
- [6] Costa, L.G., Current issues in organophosphate toxicology. *Clin. Chem. Acta.* 2006 399 p1-13
- [7] Amitai, G., Moorad, D., Adani, R., Doctor, B.P., Inhibition of acetylcholinesterase and butyrylcholinesterase by chlorpyrifos-oxon. *Biochem. Pharmacol.* 1998 56 p293-299
- [8] Tang, J., Cao, Y., Rose, R.L., Brimfield, A.A., Dai, D., Goldstein, J.A., Hodgson, E., Metabolism of chlorpyrifos by human cytochrome P450 isoforms and human, mouse and rat liver microsomes. 2001 29 p1201-1204

- [9] Minton N.A., Murray V.S.G., A review of organophosphate poisoning. *Med. Toxicol.* 1988, 3 , p.350–375
- [10] Mearns J., Dunn J., Lees-Haley P.R., Psychological effects of organophosphate pesticides: a review and call for research by psychologists. *J. Clin. Psychol.* 1994, 50, p.286–294
- [11] Timchalk, C., Nolan, R.J., Mendrala, A.L., Dittenber, D.A., Brazk, K.A., Mattsson, J.L., A physiologically based pharmacokinetic and pharmacodynamic (PBPK/PD) model for the organophosphate insecticide chlorpyrifos in rats and humans. 2002 66 p34-53
- [12] Thompson, T.S., Treble, R.G., Solid phase extraction and GCMS techniques for the confirmation of chlorpyrifos contamination of surface water supplies. *Bull. Environ. Contam. Toxicol.* 1996 57 p525-531
- [13] Bicker, W., Lammerhofer, M., Genser, D., Kiss, H., Lindner, W., A case study of acute human chlorpyrifos poisoning: Novel aspects on metabolism and toxicokinetics derived from liquid-chromatography tandem mass spectrometry analysis of urine samples. *Toxicol. Lett.* 2005 159 p235-251
- [14] Hernandez, F., Sancho, J.V., Pozo, O.J., Direct determination of alkyl phosphates in human urine by liquid chromatography/electrospray tandem mass spectrometry. *Rapid Commun. Mass Spectrom.* 2002 16 p1766-1773
- [15] Abu-Quare, A.W., Abou-Donia, M.B., Quantification of nicotine, chlorpyrifos and their metabolites in rat plasma and urine using high-performance liquid chromatography. *J. Chromatogr. B.* 2001 757 p295-300
- [16] Koch, H.M., Angerer, J., Analysis of 3,5,6-trichloro-2-pyridinol in urine samples from the general population using gas chromatography mass

spectrometry after steam distillation and solid phase extraction. J. Chromatogr. B. 2001 759 p43-49

[17] Wu, W.S., Stoyanoff, R.E., Szklar, R.S., Gai, V.S., Rakanovic, M., Application of tryptamine as a derivatising agent for airborne isocyanate determination. Part 3. Evaluation of total isocyanates analysis by high-performance liquid chromatography with fluorescence and amperometric detection. Analyst. 1990, 115 p801-807

[18] Creely, K.S., Hughson, G.W., Cocker, J., Jones, K., Assessing Isocyanate Exposures in Polyurethane Industry Sectors Using Biological and Air Monitoring Methods. Ann. Occup. Hyg. 2006, 50 p609-621

[19] Seiwert, B., Henneken, H., Karst, U., Ferrocenoyl piperazide as derivatizing agent for the analysis of isocyanates and related compounds using liquid chromatography/electrochemistry/mass spectrometry (LC/EC/MS) : Focus: Electrochemistry and cleavage combined with MS. J. Am. Soc. Mass Spectrom. 2004, 15 p1727-1736

[20] Krol, P., Wojturska, J., Kinetic study on the reaction of 2,4- and 2,6-tolylene diisocyanate with 1-butanol in the presence of styrene, as a model reaction for the process that yields interpenetrating polyurethane-polyester networks. J. Appl. Polym. Sci. 2003, 88 p327-336

## **5.0 Indirect Blotting and Direct Skin Analysis by Imaging MALDI-MS to Determine the Dermal Absorption of Hexamethylene Diisocyanate**

## **5.1 Introduction**

### **5.1.1 Introduction to HDI**

The reactivity of HDI was discussed in detail in Chapter 1 of this thesis. The mechanism for the rapid initial hydrolysis of one isocyanate group to an amine was presented as an intermediate product in the hydrolysis of diisocyanates.

### **5.1.2 HDI Exposure**

Monomeric HDI vapourizes fairly rapidly, leading to the inhalation and dermal exposure of workers who come into contact with the air containing the HDI vapours. Polymeric and biuret forms typically have a very low vapour pressure and therefore little or none is vapourized at room or paint shop ambient temperatures <sup>[1]</sup>. Exposure to polymeric forms occurs primarily via the inhalation or dermal route, when the paint / lacquer component is sprayed onto a metal surface. During the spraying process, small droplets of the mixture (containing both the monomeric and polymeric forms) suspended in the surrounding air is inadvertently inhaled or lands on the exposed skin of a worker.

The majority of studies concerning occupational exposure to HDI investigate the inhalation exposure route. However dermal, oral and ocular exposure routes for both monomeric and polymeric HDI have been reported <sup>[2]</sup>. The potential for significant exposure of workers' skin to HDI in paints has been demonstrated in autobody shops <sup>[3]</sup>.

### **5.1.3 Dermal Toxicology of HDI**

#### **5.1.3.1 Irritation**

Acute toxic cutaneous responses to HDI have been observed in a range of exposed animal models. The earliest data concerning the ability of HDI to act as a direct skin irritant was published by Haskell in 1961 <sup>[4]</sup>. HDI was applied to the non-occluded intact skin of adult male albino guinea pigs either undiluted (100%) or in solutions of 0.05, 0.5, 5 and 25% in 1:1 acetone-dioxane containing 13% guinea pig fat. Applications of the neat compound resulted in actual skin necrosis and guinea pigs exposed to concentrations as low as 5% displayed severe erythema and edema. Less severe irritation was noted at the 0.5% exposure and no irritation response was observed at the 0.05% concentration.

A further investigation into primary irritation by HDI conducted by Dupont (1977) reported slight dermal irritation of guinea pigs 24 hours after exposure to a 0.1%

solution of HDI in acetone. No irritation response was detected in animals exposed to a lower 0.01% HDI solution [5].

Toxic cutaneous responses have been demonstrated in rabbit models [6]. Male New Zealand Rabbits were topically exposed to HDI by covering shaved skin with 2.5 x 2.5cm cloths saturated with 500µl of undiluted HDI and covered with an inert PVC film. After 4 hours exposure the patches were removed and irritation of the skin was immediately observed, presenting as moderate to severe erythema and slight corrosion in all the animal test population. Severe cutaneous edema was observed in all but one animal. Upon investigations at subsequent time points, dry surface necrosis was observed. However, by the final time point (8 days after exposure) no further gross cutaneous changes were reported.

#### **5.1.3.2 Sensitization**

In addition to producing acute dermal irritation responses, HDI has also been reported to induce skin sensitization after dermal exposure to laboratory animals. Stadler and Karol (1985) investigated the dose-response relationship for dermal sensitization to HDI in guinea pigs [6]. This was proposed as a simulation model for human occupational exposure. Male guinea pigs were initially exposed to a sensitizing dose of HDI. Seven days after the initial dose, a further topical dose of either 0, 0.01, 0.1, 1 or 10mg was placed on the skin and examined for erythema.

Initial reactions were reported after 8 hours and erythema reached a maximum severity at 24 hours following exposure. The severity of erythema was observed to follow the dose-response relationship. The 0.1mg exposed group displaying the lowest severity and the 10mg group exhibiting the highest. The relationship between dose and response was found to be statistically significant ( $p < 0.05$ ).

A BALB/cBy mouse model has also been investigated <sup>[6]</sup>. Sensitizing doses of HDI were topically applied to mouse ear skin. Five days after the initial dose, HDI in the dose range 1, 10, 100 and 1000 $\mu$ g was placed on the ear and the skin was examined for an immune response (increase in skin thickness) after 24 hours. Sensitization was shown to follow a dose-response curve in the region of 1 – 100 $\mu$ g HDI. However, as doses were increased above 100mg, a reduction in ear thickness was observed. The chemical dose threshold required to sensitize 50% of the tested mouse population ( $SD_{50}$ ) was calculated as approximately 0.20mg/kg.

Thorne et al (1987) conducted a study to investigate the potential for cross-sensitization between HDI and other diisocyanates, notably dicyclohexylmethane-4,4'-diisocyanate (HMDI), diphenylmethane-4,4'-diisocyanate (MDI) and Toluene diisocyanate (TDI) <sup>[7]</sup>. Groups of male mice were exposed to dermal doses of HDI and other diisocyanates (separately) in acetone. A control model of animals exposed only to topical doses of acetone was utilised and no adverse dermal reactions were observed in this test group. Mouse ear

skin was used for the exposure study and the dermal reactivity of each dose of HDI was determined by observing changes in dermal thickness. A dose-dependant relationship was observed with an increase in ear swelling occurring as the dose of HDI increased. Of the diisocyanates investigated, HDI was reported as being the most potent dermal sensitizer with TDI being the weakest. HDI was calculated as having an SD<sub>50</sub> value of 0.088mg/kg which was more than 60 times greater than TDI. The diisocyanates were observed to elicit cross-reactivity. Mice sensitized to a specific isocyanate demonstrated cross-reactions with all dermally applied aromatic (MDI and TDI) or aliphatic (HDI and HMDI) isocyanates. However, the greatest immune response was observed when the skin was exposed to the same isocyanate used to induce sensitization. Interestingly the study noted that aliphatic isocyanates induced a more severe dermal response than aromatic isocyanates (which are most frequently associated with respiratory sensitization). Lethal doses were reported as 2,800mg/kg applied topically in acetone. A topical dose of HDI at this concentration resulted in a 100% mortality rate of the mouse test population within 16 hours of exposure.

### **5.1.3.3 Toxicity of HDI Pre-Polymers**

Polymeric HDI has been reported to induce an immune response in male guinea pigs previously sensitized to the HDI monomer <sup>[8]</sup>. In this investigation initial

sensitization was induced by four direct intradermal injections of dilute HDI monomer (0.1ml of 1% HDI in dimethyl phthalate) once a week over a three week period. A pre-sensitized test group exposed to the HDI polymer Desmodur N-75, which contained 74% 1,3,5-tris(normal-hexylisocyanate)-biuret and 0.45% free HDI monomer, elicited a more severe immune response (erythema and erythema plus edema) and in a greater number of the test population than a pre-sensitized group exposed to HDI monomer only. No further studies on dermal sensitization to polymeric HDI have yet been published. However, further studies have been conducted on respiratory sensitization to pre-polymer HDI biurets. Dose-related pulmonary immune responses <sup>[9]</sup> and increased expression of stress-induced markers <sup>[10]</sup> were observed following HDI biuret exposure in animal models.

#### **5.1.4 Aim**

Indirect and direct methods of tissue analysis by imaging mass spectrometry have been discussed in the introduction to this thesis. Both cellulose blotting (indirect) and direct skin approaches, combined with imaging MALDI-MS analysis, were utilised to investigate the dermal absorption of the diisocyanate HDI using excised porcine ear skin.

## 5.2 Method

### 5.2.1 Materials

$\alpha$ -Cyano-4-Hydroxy Cinnamic Acid ( $\alpha$ -CHCA) was purchased from Sigma-Aldrich (Dorset, U.K). 1.6-hexamethylene diisocyanate (HDI), trifluoroacetic acid (TFA) and HPLC grade ethanol and acetone were purchased from Fischer (Leicester, U.K). Cellulose membranes were obtained from Goodfellow, (Cambridge, UK.)

### 5.2.2 Indirect Blotting Approach

1 $\mu$ l of neat HDI was spotted onto the surface of a 2cm x 2cm piece of porcine ear skin and incubated at 37°C for 1 hour. The tissue was sectioned and blots of the tissue cross section were performed on dry cellulose membranes. 5 ml of  $\alpha$ -Cyano-4-Hydroxy Cinnamic Acid ( $\alpha$ -CHCA) at 25mg/ml in acetone containing 0.1% TFA, was applied to the membrane by airspray at a distance of 10cm. Image analysis was performed using BioMap software. The mass spectrometric image was superimposed over a light microscope image (4x magnification) of a corresponding histological section sectioned at 14 $\mu$ m thickness using a cryostat. The skin section was stained using standard haematoxylin and eosin (H&E) stain protocols.

### **5.2.3 Direct Tissue Analysis**

Porcine ear skin was spiked with HDI and incubated as above. Sections were taken at 12 $\mu$ m increments by cryostat and placed onto aluminium backing. 5 ml of  $\alpha$ -CHCA matrix (25mg/ml in acetone containing 0.1% TFA) was applied by airspray at a distance of 10cm from the tissue. The experiment was repeated with the addition of a sputter coating of gold (~5nm) applied directly after the matrix to the surface of a 12 $\mu$ m section of tissue using an Emitech SC7620 Mini Sputter Coater.

### **5.2.4 Mass Spectromeric Analysis**

All analyses were performed using an Applied Biosystems/MDS Sciex API "Q-Star" Pulsar I hybrid quadrupole time of flight instrument, fitted with an orthogonal MALDI ion source and "O-MALDI Server 4.0" ion imaging software. The Nd:YAG laser used has an elliptical laser spot size of 150  $\mu$ m x 100  $\mu$ m. The laser was used at an energy setting of 30% (3.2  $\mu$ J) and a repetition rate of 1 kHz. The laser was rastered over the membrane surface and mass spectra were acquired at 0.2mm increments, the laser firing for approximately 2 seconds per spot.

## 5.3 Results

### 5.3.1 Indirect Blotting Approach to Profile the Dermal Absorption of HDI

Intact HDI was not observed from the blot. As HDI is known to be highly reactive, hydrolysis of the diisocyanate to the monoamine may have occurred upon exposure to water content in the air during the process of application of HDI onto the skin. Hydrolysis may also have occurred during absorption into the skin upon exposure to the high water content of the porcine skin. The HDI monoamine (molecular mass 142) was observed from the blot as the protonated molecule at  $m/z$  143.

The distribution of the monoamine of HDI at  $m/z$  143 was mapped from the tissue blot using BioMap software. By superimposing the resulting image over a histological image acquired from the H&E stained porcine skin tissue, an absorption profile was obtained (figure 5.1). HDI was observed to have penetrated through the epidermis and into the hypodermis. The highest concentration of HDI was observed in the dermis. The maximum penetration depth of HDI observed was 2.6mm.

Hexamethylene diisocyanate has been previously reported to penetrate through skin and be excreted as the diamine derivative, hexamethylene diamine (HDA),

in the urine <sup>[2]</sup>. The presence of the HDI monoamine in the dermis indicates that penetration readily occurs across the stratum corneum within the 1 hour exposure time. However the absence of any protonated HDA molecules indicates that full hydrolysis may only occur in vivo, possibly upon conjugation with proteins in the circulatory system.

Due to the high fat content of the skin and the presence of endogenous liquids such as blood and lipids, analyte spreading and poor matrix crystallization may occur. Successful blots were only achieved from approximately 50% of the sample population.

### **5.3.2 Direct Skin Analysis to Profile Dermal Absorption of HDI**

An optical image showing the structure of the porcine ear tissue investigated is presented in figure 5.2.

Inhomogeneous matrix coverage was observed over the porcine skin section. Figure 5.3 shows the distribution of the protonated molecule of  $\alpha$ -CHCA at m/z 190. Matrix ion intensities are very low over the tissue, most likely due to poor crystallization of the matrix as a result of the waxy nature of the skin tissue.

The phosphatidyl choline (PC) head group is commonly observed as a fragment ion in the MS analysis of various lipids <sup>[11]</sup> and tissues <sup>[12]</sup>. In figure 4a the distribution of the PC head group at m/z 184 appears to be inhomogeneous throughout the tissue. However, one main cause of this inhomogeneity is the inhomogeneous coverage of the matrix on the tissue. When the intensity of the PC head group at m/z 184 is normalized against the protonated molecule of the matrix (m/z 190) a more homogenous distribution of the PC head group is observed throughout the porcine ear skin (figure 5.4b). A clear distinction can be observed between the skin layers and the cartilage running through the centre of the ear. Only a very low intensity of m/z 184 ions is observed in the cartilage whereas vastly greater intensities are observed in the skin tissue. This is as would be expected due to the high lipid content (and thus high PC content) of the skin.

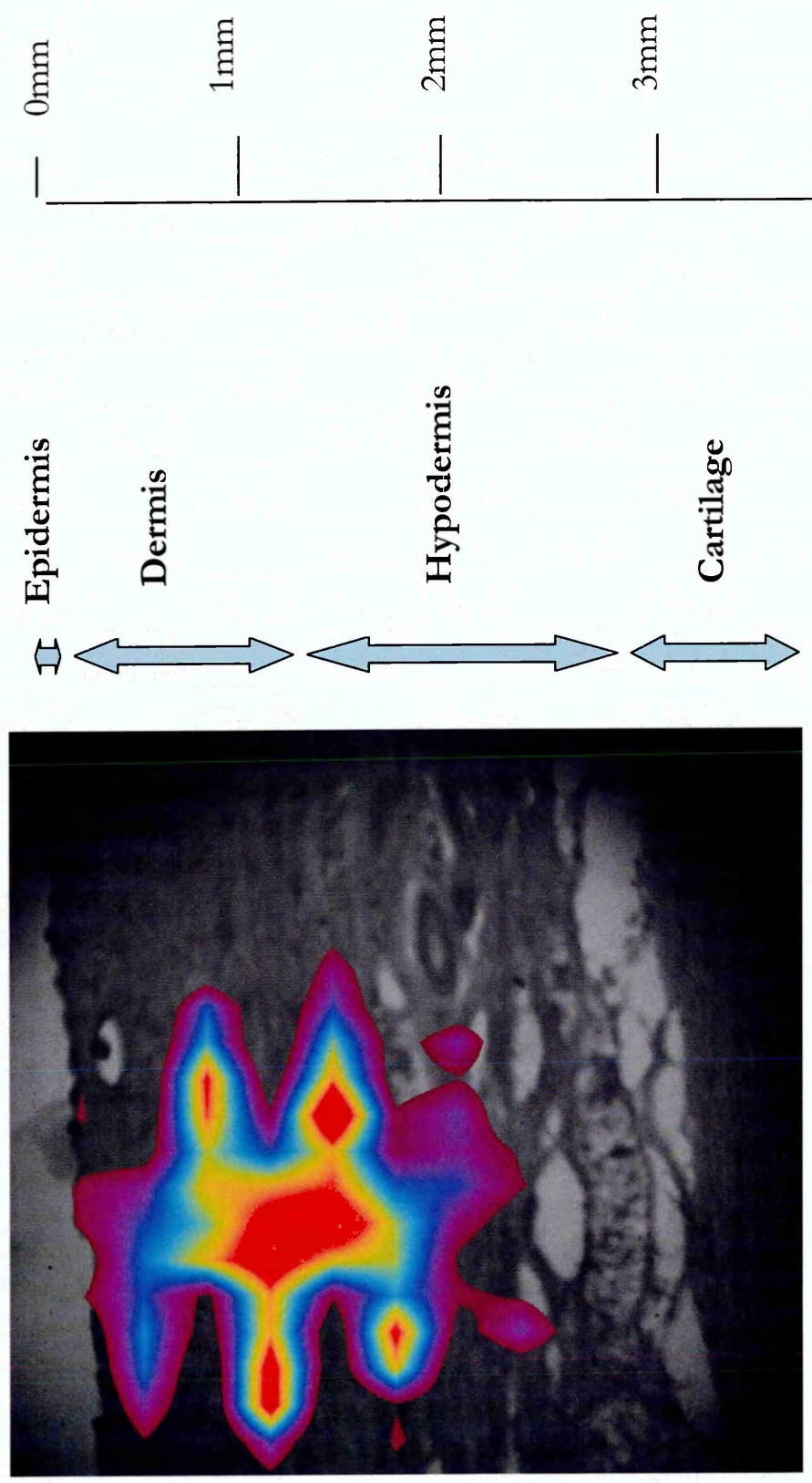


**Figure 5.1** MALDI-MS image showing the distribution of  $m/z$  143 (HDI monoamine) from porcine skin vertical section blot superimposed over H+E stained corresponding tissue. HDI appears to have penetrated through the epidermis, dermis and into the hypodermis tissue. However after the one hour exposure time used in this experiment the highest concentration of HDI is located in the dermis

Intact HDI ( $[M+H]^+$  expected at  $m/z$  189) was not observed on the skin surface following normalization against the matrix at  $m/z$  190. However, the hydrolysed monoamine at  $m/z$  143 was clearly observed following normalization and its distribution is shown in figure 5.1. The explanation for the absence of intact HDI is again believed to be due to the diisocyanate being hydrolysed to the monoamine upon exposure to water either; during application to and absorption in the skin, or during the cryostat tissue sectioning process. As occurred with the indirect blotting method, HDA was not detected on the tissue.

The relatively homogeneous nature of the distribution of the PC head group through the porcine skin enabled it to be used as a reference for dermal penetration. The image of HDI monoamine distribution in the skin section was superimposed over the distribution of the PC head group enabling the location of the monoamine in the skin to be determined (figure 5.6). From this image HDI was observed to penetrate through all layers of the skin, ultimately reaching the cartilage. Upon penetrating thus far it appears to spread horizontally along the cartilage as further absorption isn't possible due to the impermeability of the cartilage. The highest intensity of HDI monoamine is observed in the dermis and a penetration depth of 2.3mm was observed in this sample. However HDI monoamine was not detected in the upper skin layers, with the  $m/z$  143 ion initially being observed at a depth of 0.6mm into the skin.

HDI has been reported to readily penetrate through the skin and so it would be expected that the highest concentration of HDI monoamine to be located in the dermis. However, small quantities of HDI monoamine would be expected to remain on the surface and in the epidermal skin layers (as was observed from the indirect blots). The absence of the HDI monoamine in this region may be a result of analyte suppression caused by a high quantity of matrix accumulating around the edges of the tissue section during airspray application. Normalization against the matrix would however be expected to minimise this effect. Another proposed reason is curling or folding of the skin section on the aluminium plate. Due to the waxy and fragile nature of the skin sections adhesion to the aluminium plate was relatively low, leading (in some sections) to notable raising of the section edges upon removal from the cryostat and thus probable dehydration of the tissue.

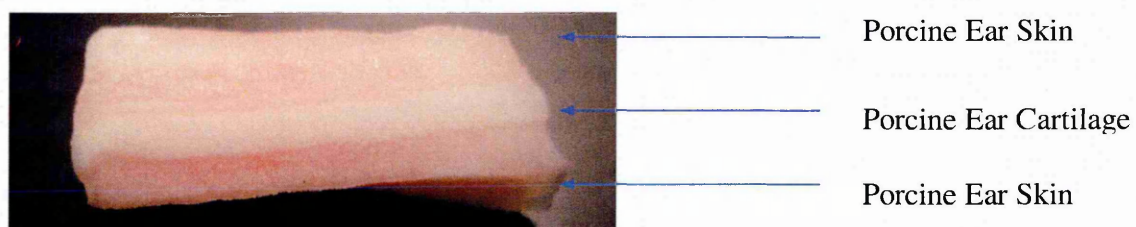


**Figure 5.2** Optical image of HDI-spiked porcine ear prior to sectioning

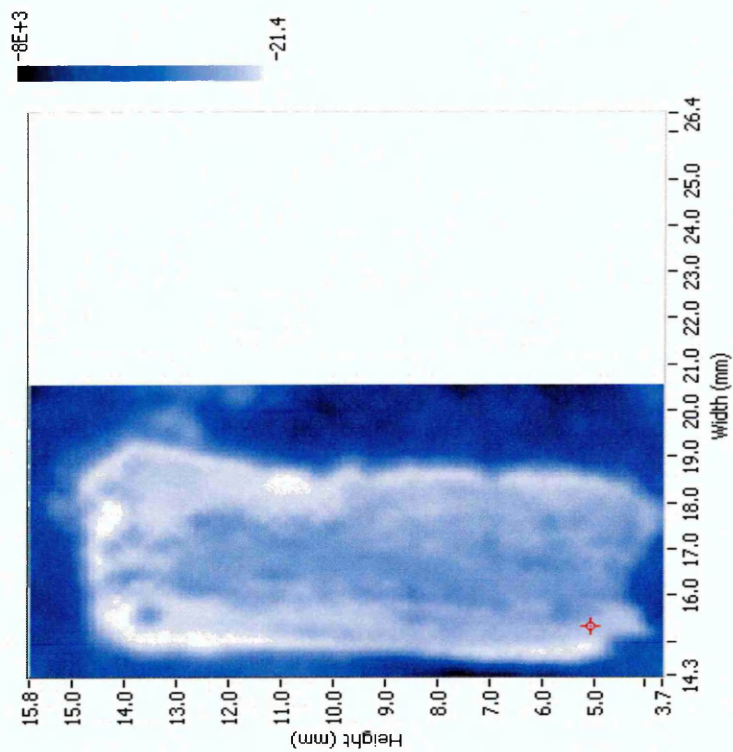
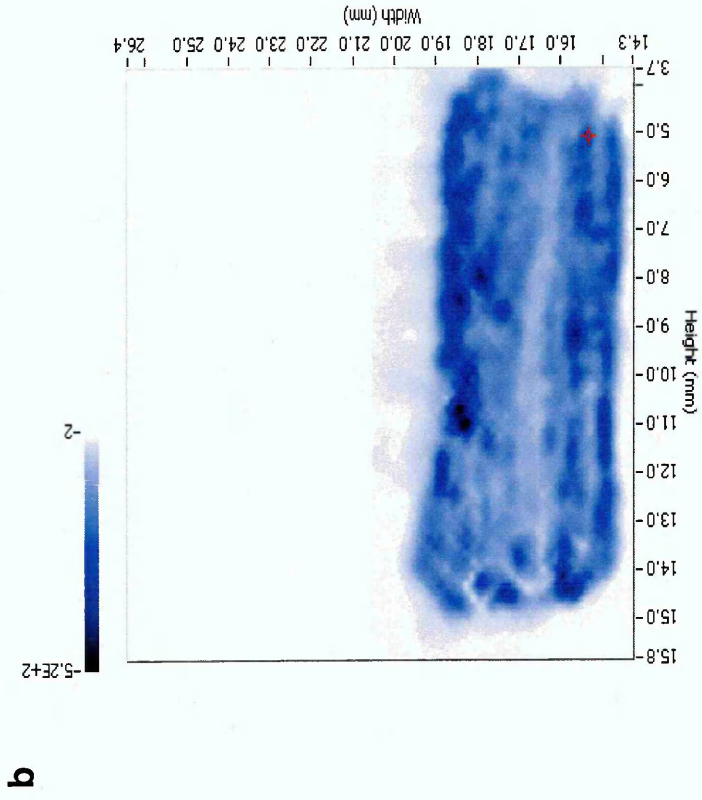
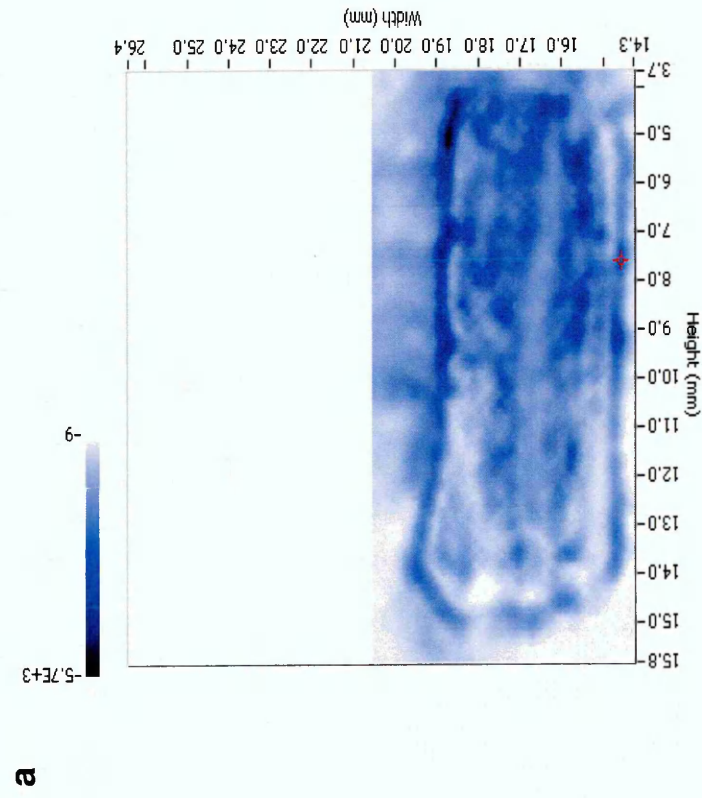


**Figure 5.3** MALDI Image showing the inhomogeneous distribution of the molecular ion of  $\alpha$ -CHCA ( $m/z$  190) over the porcine ear section surface



**Figures 5.4a & 5.4b** MALDI images showing the distribution of the PC head group ( $m/z$  184) in porcine ear skin section without normalisation (**a**) and following normalisation against the  $\alpha$ -CHCA  $[M+H]^+$  ion at  $m/z$  190 (**b**)

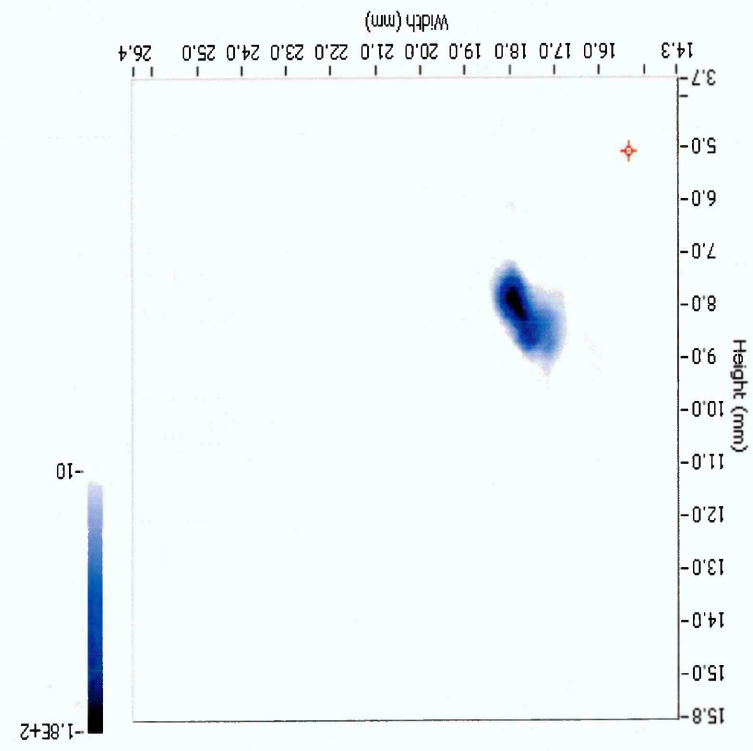


**Fig5. 5** MALDI image showing the distribution of HDI monoamine in the porcine skin section normalised against  $\alpha$ -CHCA  $[M+H]^+$

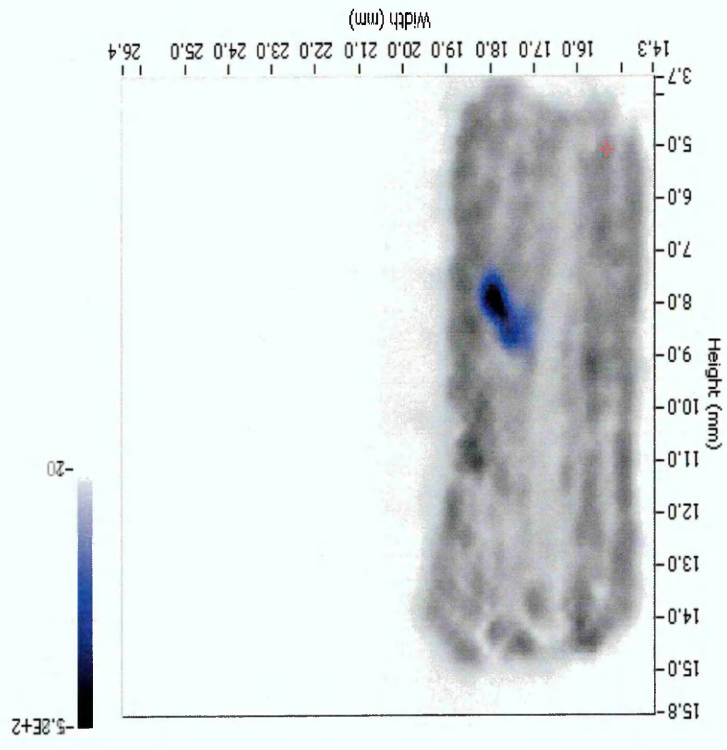


**Fig 5.6** Distribution of HDI monoamine ( $m/z$  143) normalised against  $\alpha$ -CHCA  $[M+H]^+$  superimposed over distribution of PC head group seen in figure 4b

### 5.3.3 Use of Gold Coating to Enhance Sensitivity of HDI Species from Tissue

Coating biological tissue sections with gold has been shown to increase sensitivity of mass spectrometric analysis of certain compounds for MALDI <sup>[13]</sup> and SIMS <sup>[14]</sup> analysis. In this investigation porcine ear skin sections (pre-spiked with HDI) were sputter-coated with a thin layer of gold after the application of  $\alpha$ -CHCA by airspray deposition with the aim of observing any enhancement in detected sensitivity of HDI species on the tissue.

Inhomogeneous  $\alpha$ -CHCA coverage was again observed over the tissue section surface with a very low intensity of protonated molecular ions being detected (fig 7). The PC head group was observed but was also apparently inhomogeneously distributed throughout the skin (figure 5.8a). Normalization against the matrix at  $m/z$  190 resulted in a clearly more homogeneous distribution of the PC head group (figure 5.8b) enabling the skin and cartilage tissue layers to be clearly distinguished.

The HDI monoamine at  $m/z$  143 was not observed in the porcine ear section without normalization (figure 5.9). When normalized against the matrix at  $m/z$  190, the HDI monoamine was observed at very low intensities (figure 5.10). As in previous results, the isocyanate penetrated into the lower layers of the skin

although an accurate penetration profile and depth cannot be determined from this image due to the very low intensity of isocyanate ions observed (<15).

Very low signals for HDI monoamine were obtained from all gold-coated samples in comparison to samples where  $\alpha$ -CHCA matrix was used without the gold sputter coating. The gold coating appeared to result in suppression of HDI monoamine  $[M+H]^+$  ionization. However, the PC head group was observed at equal or greater intensities than by use of  $\alpha$ -CHCA alone.

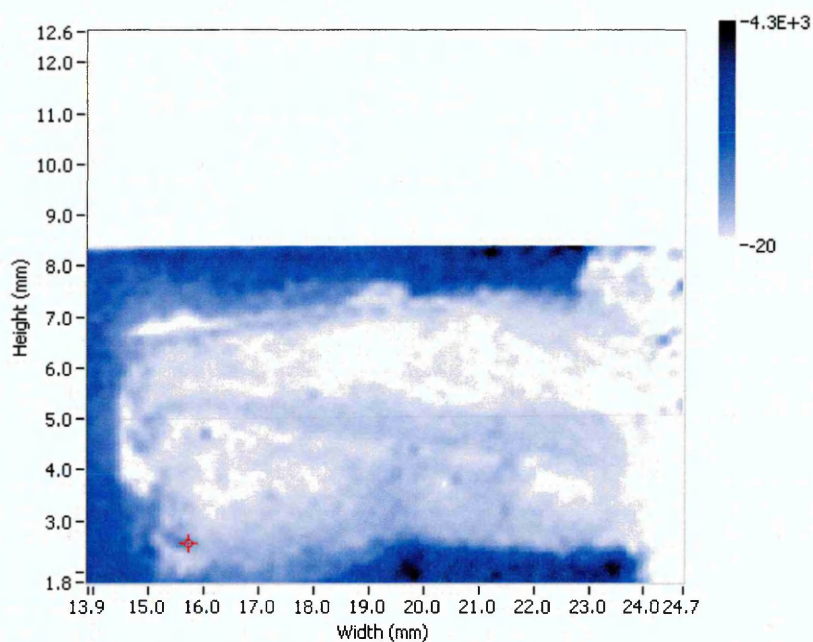
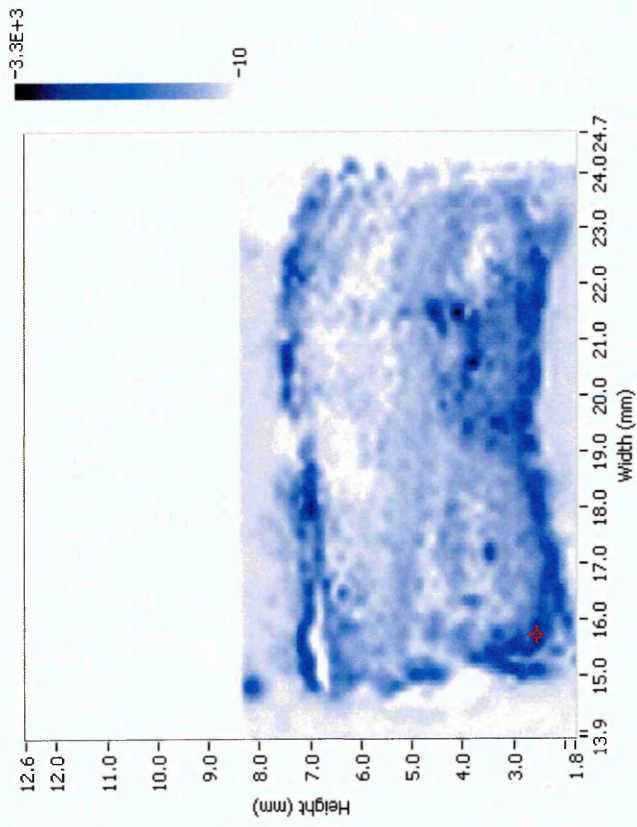


**Figure 5.7** MALDI image showing the distribution of  $\alpha$ -CHCA  $[M+H]^+$  (m/z 190) over porcine ear section sputter-coated with gold

**a**



**b**

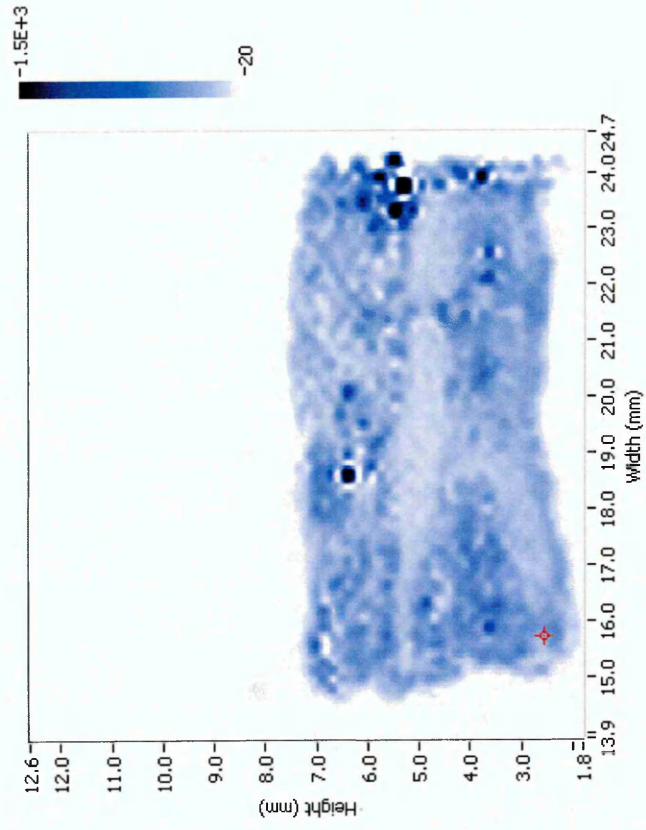


**Figure 5.8** MALDI images showing the distribution of the PC head group (m/z 184) in gold sputter-coated porcine ear skin section without normalisation (**a**) and following normalisation against the CHCA [M+H]<sup>+</sup> ion at m/z 190 (**b**)

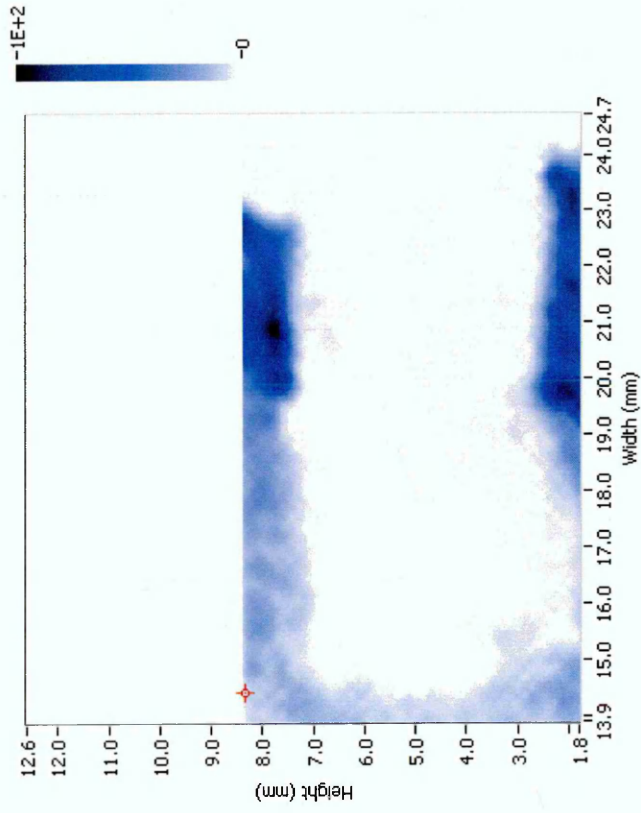


**Figure 5.9** MALDI image showing the distribution of HDI monoamine in the porcine skin section without normalisation against  $\alpha$ -CHCA  $[M+H]^+$ . Note HDI monoamine is not detected on the tissue section

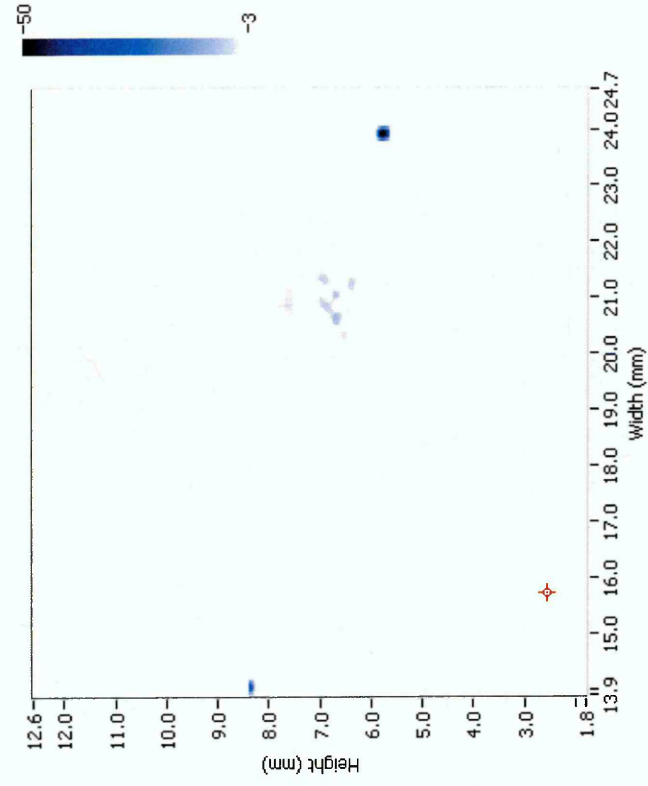


**Figure 5.10** Distribution of HDI monoamine ( $m/z$  143) normalised against the  $\alpha$ -CHCA  $[M+H]^+$  ion ( $m/z$  190). Note very low ion intensity is observed.

## 5.4 Conclusion

The indirect and direct methods for imaging MALDI-MS analysis of the dermal absorption of HDI proved successful. In both the direct and indirect investigations the distribution of the protonated HDI monoamine at  $m/z$  143 was mapped in skin. Similar absorption profiles were obtained by both methods. Penetration of HDI-derived monoamine through the stratum corneum occurred readily with the highest amounts of HDI monoamine observed in the dermis after the 1 hour exposure period.

Both imaging methodologies have advantages and disadvantages. The use of indirect blotting increased the potential for spreading of the isocyanate during the blotting process and the success of the blot was dependent upon the composition of the tissue. High fat levels and the presence of endogenous liquids such as blood resulted in a successful blot being achieved in only approximately 50% of cases. A homogeneous matrix coverage was achieved over the membrane surface thus negating the requirement for normalization against the matrix.

Direct skin analysis eliminated the risk of analyte spreading during blotting but difficulties occurred in sectioning the porcine ear tissue. 'Curling' of the tissue edges also proved to be a problem and it is believed this may have resulted in suppression of the HDI monoamine signal in the upper layers of the skin section.

By normalizing the HDI monoamine ion intensity against the  $\alpha$ -CHCA  $[M+H]^+$  the location of HDI within the tissue section was determined. However, it must be noted that normalizing against the matrix intensity will not compensate for analyte suppression effects (ASE) or matrix suppression effects (MSE) <sup>[15]</sup> which may be occurring. The use of an independent internal standard incorporated in the matrix mixture would be ideal, although due to the highly reactive nature HDI and its cross reactivity with other isocyanates a deuterated isocyanate internal standard would not be suitable.

The application of a gold layer above the matrix did appear to improve the sensitivity of endogenous lipids in the porcine skin. However, the HDI monoamine was only observed at low intensities in the tissue resulting in a poor quality image which was not suitable for penetration studies.

## 5.5 References

- [1] Lesage, J., Goyer, N., Desjardins, F., Vincent, J.Y., Perrault, G. Workers' exposure to isocyanates. *Am. Ind. Hyg. Assoc. J.* 1992 53 p146-153
- [2] Pronk, A., Yu, F., Vlaanderen, J., Tielemans, E., Preller, L., Bobeldijk, I., Deddens, J.A., Latza, U., Baur, X., Heederik, D. Dermal, inhalation, and internal exposure to 1,6-HDI and its oligomers in car body repair shop workers and industrial spray painters. *Occup. Environ. Med.* 2006 63 p624-631
- [3] Liu, Y., Sparer, J., Woskie, S.R., Cullen, M.R., Chung, J.S., Holm, C.T., Qualitative assessment of isocyanate skin exposure in auto body shops: A pilot study. *Am. J. Ind. Med.* 2000 37 p265-274
- [3] Haskell Laboratory, Evaluation of the toxicity of hexamethylene diisocyanate relative to that of toluene-2,4-diisocyanate. 1961 EPA/OTS Dot #86-870001008
- [4] E.I. Dupont de Nemours. Special primary skin irritation and sensitization on guinea pigs. 1977 EPA/OTS Dot #86-870001005
- [5] Mowbay Corporation. The evaluation of hexamethylene-1,6-diisocyanate for primary skin irritation in rabbits. 1981 EPA/OTS Dot #86-870001242
- [6] Stadler, J.C., Karol, M.H., Use of dose-response data to compare the skin sensitizing abilities of dicyclohexylmethane-4,4-diisocyanate and picryl chloride in two animal species. *Toxicol. Appl. Pharmacol.* 1985 78 p445-450
- [7] Thorne, P.S., Hillebrand, J.A., Lewis, G.R. Contact sensitivity by diisocyanates potencies and cross-reactivities. *Toxicol. Appl. Pharmacol.* 1987 87 p155-165

- [8] E.I. Dupont de Nemours. Primary skin irritation and sensitization testing on guinea pigs. 1977 EPA/OTS Dot #86-870001118
- [9] Lee, C.T., Friedman, M., Poovey, H.G., Ie, S.R., Rando, R.J., Hoyle, G.W. Pulmonary toxicity of polymeric hexamethylene diisocyanate aerosols in mice. *Toxicol. Appl. Pharmacol.* 2003 188 p154-164
- [10] Lee, C.T., Ylostalo, L., Friedman, M., Hoyle, G.W. Gene expression profiling in mouse lung following polymeric hexamethylene diisocyanate exposure. *Toxicol. Appl. Pharmacol.* 2005 205 p53-64
- [11] Al-Saad, K.A., Siems, W.F., Hill, H.H., Zabrouskov, V., Knowles, R.N. Structural analysis of phosphatidylcholines by post-source decay matrix-assisted laser desorption/ionization time-of-flight mass spectrometry. *J. Am. Soc. Mass Spectrom.* 2003 14 p373-382
- [12] Taguchi, R., Houjou, T., Nakanishi, H., Yamazaki, T., Ishida, M., Imagawa, M., Shimizu, T. Focused lipidomics by tandem mass spectrometry. *J. Chromatogr. B.* 2005 823 p26-36
- [13] McCombie, G., Knochenmuss, J., Enhanced MALDI ionization efficiency at the metal matrix interface: Practical and mechanistic consequences of sample thickness and preparation method. *Am. Soc. Mass Spectrom.* 2006, 17 p.737-746
- [14] Delcorte, A., Bertrand, P. Interest of silver and gold metallization for molecular SIMS and SIMS imaging. *Appl Sur. Sci.* 2004 232 p250-255

[15] Knochenmuss, R., A quantitative model of ultraviolet matrix-assisted laser desorption/ionization including analyte ion generation. *Anal. Chem.* 2003 75 p2199-2207

## 6.1 Conclusion and Future Work

Occupational hygiene monitoring is of vital importance for the protection of the health and wellbeing of workers. Health and Safety governing bodies are constantly searching to optimise analytical methods for determining occupational exposure levels to hazardous compounds.

Mass spectrometric methods have previously been applied to the analysis of occupationally sampled hazardous compounds. The most common MS techniques used are LC-MS and GC-MS. The aim of this thesis was to apply MALDI-MS and specifically the relatively new technique of MALDI-MS imaging (MALDI-MSI) to the characterization and localization of occupational compounds of interest in skin.

The application of MALDI-MS and MALDI-MS/MS for the initial stability testing of an aliphatic and an aromatic isocyanate resulted in the observation of a reaction occurring where one isocyanate group hydrolysed to an amine. This was observed to form rapidly upon exposure to water vapour in the laboratory atmosphere. The diamine hydrolysis products of many diisocyanates in biological fluids are reported in the current literature (listed in chapter 3 of this thesis) but direct measurement of a diisocyanate derived monoamine has yet to be reported. The monoamine intermediate product may hold a vital role in sensitization

reactions. Immunological methods could be applied to obtain further information concerning this.

Due to the highly reactive nature of isocyanates, a derivatisation step is incorporated into most analysis. An ethanol-derivatisation step to stabilize the HDI monomer and related monoamine species is reported in chapter 2 of this thesis. The ethanol-derivatised HDI (HDI urethane) proved to be stable over a 14 day experimental period. A surface swabbing method incorporating the ethanol derivatisation step was introduced and was shown to be reproducible for the extraction of HDI (as the ethanol derivatised urethane) from both personal protective equipment and a sample aluminium surface.

The MALDI-MS technique provided a rapid method of analyzing many samples of monomeric and pre-polymeric HDI species in comparison to standard GC-MS and LC-MS methods. However, further work is recommended to identify and characterize larger polymer forms of isocyanates which would be expected to occur in the workplace during the application of the diisocyanate. MALDI-MS would be viable for this due to the large mass range covered and would provide further vital information relating to the types of HDI species to which workers are exposed.

Occupational exposure monitoring via direct sampling of diisocyanates from workers skin has inherent difficulties. Most analytical methods require

diisocyanates to be derivatised for transport and analysis. Due to the toxic nature of the derivatising agents, direct sampling via impregnated swabs or wipes of workers skin is impossible. The ethanol-saturated cellulose blotting method described in chapter 4 of this thesis proved to be successful for the extraction and derivatisation of HDI from porcine ear skin. However, not all of the HDI present on the membrane reacted with the ethanol. Increasing the amount of ethanol on the membrane did increase the amount of derivatised HDI monomer observed although this occurred at the expense of spatial information retention.

A similar method was used for the analysis of the insecticide chlorpyrifos, for both skin surface sampling and permeation studies. Due to the hydrophobic nature of the compound, carbon membranes appeared to be a more suitable blotting medium and produced images at higher intensities which retained a higher degree of spatial information than the ethanol-saturated cellulose membranes. From the images obtained, chlorpyrifos was observed to readily penetrate through the stratum corneum and the greatest amount was located in the dermis after the 1 hour exposure time.

The mechanisms by which diisocyanates react within the body are not yet fully understood. Diisocyanates have been observed to penetrate through the skin and to be excreted in the urine (usually in protein-conjugate form). A method for the determination of free TDA monomer formed by reactions (hydrolysis) of the TDI monomer when applied to HaCaT Cells by LC-MS was described in chapter

3 of this thesis. The method incorporated the use of a novel extraction procedure to extract TDA from the cell media and water control and this extraction proved to be precise. Only small amounts of free TDA were observed in the cell media extracts, however, even after the spiking of a 100 $\mu$ mol concentration of TDI. The TDI appeared to remain conjugated to proteins and/or peptides in the cells and culture media.

The monoamine of HDI proved to be relatively stable for imaging MALDI analysis. As described in chapter 5 of this thesis, the monoamine was mapped through the excised porcine ear section by both indirect blotting and direct skin approaches. A similar absorption profile was observed for both methods showing that HDI penetrated readily through the stratum corneum and that the highest concentration was located in the dermis. These are the first data describing direct MALDI-MS analysis of skin as the waxy nature of the surface has been reported previously to lead to poor matrix crystallization and homogeneity <sup>[1]</sup>. By normalizing the protonated molecule of the HDI monoamine against the protonated molecule of  $\alpha$ -Cyano-4-Hydroxy Cinnamic Acid ( $\alpha$ -CHCA) matrix, the location of HDI (in monoamine form) in the skin was clearly observed. It would be interesting to determine whether the HDI was hydrolyzing to the monoamine in the skin or whether the reaction had already occurred during the pipetting and skin incubation procedure. Again this could be further investigated by use of an immunological technique (i.e. monitoring cytokine expression) preferably using live tissue as (from the evidence determined during direct exposure of TDI to

keratinocyte cells) conjugation of the isocyanate would occur with proteins in the HaCaT cells.

It must be noted that all the results obtained for the dermal extraction or permeation experiments were dependent upon the properties of the excised (and snap frozen) porcine ear skin that was used as the model for human skin. It would be realistic to assume that the snap freezing procedure may compromise the integrity of the stratum corneum to some extent, resulting in greater penetration of compounds. Ideally excised human skin or artificial skin constructs would be used for these investigations. However, due to ethical constraints this was not possible during the experimental duration.

Methods for sampling and MALDI-MS analysis of isocyanates and chlorpyrifos have been developed. Future work will involve testing both the MALDI-MS analysis and alcohol derivatisation method via field sampling of workplaces (specifically autobody spray shops and adhesive manufacturers) where large quantities of HDI pre-polymers are used. The data obtained will provide more information on the isocyanate species present under these conditions and may result in the development of new and/or improved Health and Safety Executive methods for the determination of hazardous substances (MDHS) for diisocyanates.

## 6.1 References

- [1] Bunch, J., Clench M. R., Richards D.S., Determination of Pharmaceutical Compounds in Skin by Imaging Matrix Assisted Laser Desorption Ionisation Mass Spectrometry, *Rapid Comm. Mass Spec.*, 2004, 18, p.3051-3060

## Appendix

### Oral Presentations

Winner of the Barber- Bordoli prize for best postgraduate oral presentation, **'Imaging Matrix Assisted Laser Desorption Ionisation—Mass Spectrometry for the Investigation of Dermal Absorption of Chlorpyrifos'** presented at the British Mass Spectrometry Annual Conference, York, UK (September 2005).

**'Applications of Imaging Matrix Assisted Laser Desorption Ionisation - Mass Spectrometry to the Study of Dermal Absorption of Isocyanates'** presented at 3<sup>rd</sup> National Conference on Environmental Mass Spectrometry, Chester, UK (April 2006)

Selected for the Journal of Mass Spectrometry award for an oral presentation titled **'Applications of Imaging MALDI-MS to the Dermal Absorption of Isocyanates'** presented at the International Mass Spectrometry Conference, Prague, Czech Republic (September 2006)

**'Investigation of the Dermal Absorption and Surface Sampling of Isocyanates using Novel Methodology'** presented at British Occupational Hygiene Conference, Glasgow, UK (April 2007)

## Appendix 2

### Poster Presentations

**'Applications of Matrix Assisted Laser Desorption Ionisation - Mass Spectrometry to the Study of Dermal Absorption of Isocyanates for Occupational Hygiene Interests'** presented at American Society of Mass Spectrometry Annual Conference, Nashville, US (June 2004), the 2nd Environmental Mass Spectrometry Meeting, Chester, UK (April 2004), Royal Society of Chemistry Research Forum, Preston, UK (July 2004), and the British Mass Spectrometry Annual Conference, Derby, UK (September 2004).

**'Applications of Matrix Assisted Laser Desorption Ionisation - Mass Spectrometry to the Study of Dermal Absorption of Chlorpyrifos for Occupational Hygiene Interests'** presented at American Society of Mass Spectrometry Annual Conference, San Antonio, Texas, US (June 2005) and the Royal Society of Chemistry Research Forum, Plymouth, UK (July 2005),

**'Applications of Imaging MALDI-MS to the Study of Dermal Absorption of Isocyanates'** presented at American Society of Mass Spectrometry Annual Conference, Seattle, Washington, US (June 2006) and the Royal Society of Chemistry Research Forum, Cork, Ireland (July 2006)

## Appendix 3

### Publications

Prideaux, B., Atkinson, S.J., Carolan, V.A, Morton, J., Clench, M.R. **Sample preparation and data interpretation procedures for the examination of xenobiotic compounds in skin by indirect imaging MALDI-MS.** *International Journal of Mass Spectrometry*, 2007 **260** p243-251

Atkinson S.J. , Prideaux B. , Bunch J. , Warburton K.E. , Clench M.R. , **Imaging Matrix assisted laser desorption ionisation mass spectrometry - New technique for drug distribution studies**, *Chemistry Today*, 2005 **23** p5-8